University of Alberta

Physical Hydrogeological Characterization and Three-Dimensional Numerical Modelling of Groundwater Flow in Till at a Central Alberta Site

by

Trevor Richard Butterfield

A thesis submitted to the Faculty of Graduate Studies and Research in partial fulfillment of the requirements for the degree of Master of Science

Department of Earth and Atmospheric Sciences

Edmonton, Alberta
Spring 2003

National Library of Canada
Acquisitions and Bibliographic Services
395 Wellington Street
Ottawa ON K1A 0N4
Canada

Bibliothèque nationale du Canada
Acquisitions et services bibliographiques
395, rue Wellington
Ottawa ON K1A 0N4
Canada

Your file Votre référence

Our file Notre référence

The author has granted a non-exclusive licence allowing the National Library of Canada to reproduce, loan, distribute or sell copies of this thesis in microform, paper or electronic formats.

L'auteur a accordé une licence non exclusive permettant à la Bibliothèque nationale du Canada de reproduire, prêter, distribuer ou vendre des copies de cette thèse sous la forme de microfiche/film, de reproduction sur papier ou sur format électronique.

The author retains ownership of the copyright in this thesis. Neither the thesis nor substantial extracts from it may be printed or otherwise reproduced without the author's permission.

L'auteur conserve la propriété du droit d'auteur qui protège cette thèse. Ni la thèse ni des extraits substantiels de celle-ci ne doivent être imprimés ou autrement reproduits sans son autorisation.

0-612-82255-9

Canada

University of Alberta

Library Release Form

Name of Author: Trevor Richard Butterfield

Title of Thesis: Physical Hydrogeological Characterization and Three-Dimensional Numerical Modelling of Groundwater Flow in Till at a Central Alberta Site

Degree: Master of Science

Year this Degree Granted: 2003

Permission is hereby granted to the University of Alberta Library to reproduce single copies of this thesis and to lend or sell such copies for private, scholarly or scientific research purposes only.

The author reserves all other publication and other rights in association with the copyright in the thesis, and except as herein before provided, neither the thesis nor any substantial portion thereof may be printed or otherwise reproduced in any material form whatever without the author's prior written permission.

.....

Trevor Richard Butterfield
11155-38 Avenue
Edmonton, Alberta, Canada
T6J 0K8

Date: January 30, 2003

University of Alberta

Faculty of Graduate Studies and Research

The undersigned certify that they have read, and recommend to the Faculty of Graduate Studies and Research for acceptance, a thesis entitled **Physical Hydrogeological Characterization and Three-Dimensional Numerical Modelling of Groundwater Flow in Till at a Central Alberta Site** submitted by Trevor Richard Butterfield in partial fulfillment of the requirements for the degree of Master of Science.

.....
Dr. Carl A. Mendoza (Supervisor)

.....
Dr. Benjamin J. Rostron (Committee)

.....
Dr. Kevin W. Biggar (External)

Date: January 30, 2003

ABSTRACT

The physical hydrogeology of till at a central Alberta site is described as part of a remediation research project at a decommissioned gas treatment site. Field investigations reveal seasonally dynamic groundwater flow in the upper 4 m of weathered, fractured till, but not below in unweathered, sparsely fractured till. The water budget is dominated by the vertical fluxes of precipitation (494 mm) and evapotranspiration (545-575 mm). Upward vertical hydraulic gradients of up to 2.5 are strongly indicative of perched water table conditions. Horizontal flow is not found to be important due to low horizontal hydraulic gradients, low permeability, and lack of geologic continuity.

To confirm field interpretations, numerical models of groundwater flow are created with FRAC3DVS, a finite-element simulator. Model calibration to water level measurements is achieved primarily through modification of the timing and magnitude of the net surface boundary flux, and the magnitudes of hydraulic conductivity and specific storage. Model validation and sensitivity analyses reveal the difficulties in modelling fractured domains with a continuum approach.

ACKNOWLEDGEMENTS

Sincere thanks to my supervisor, Carl Mendoza, for accepting me as part of his research group and for all of the guidance he provided throughout the project. I learned a great deal in my time here. Ben Rostron and Kevin Biggar provided excellent reviews of the thesis. Brian Smerdon accepted the unenviable task of reading the first draft of each chapter and made several helpful suggestions as well.

The talented collaborators on the Gas Plant Remediation Project were a pleasure to work with. Field visits and discussions with, in particular, Larry Bentley, Angus Chu, Mehran Gharibi, Michelle Laplante, Stuart Lunn, and Ole Mrklas were important to the development of the hydrogeological interpretation. Thanks also to James Armstrong of Komex International Ltd. for providing data and interpretations. Rob McLaren of the University of Waterloo graciously (and rapidly) answered several of my questions about FRAC3DVS.

I am indebted to my fellow students in the hydrogeology group at the University of Alberta for many reasons. Many of the field visits would not have been possible without the accompaniment of a fellow student. The hydrogeology group was a great bunch to bounce ideas off of, or to hang out with for "just one pint". I feel that many of us have developed friendships that will last for a long time. So, thanks to Jennifer Adams, Arif Alkalali, Dan Born, Kristine Haug, Sarah Hill, Heather Iampen, Dan Khan, Jim Letourneau, Zsolt Margitai, Adrienne Price, Tannis Sharp, Brian Smerdon and Heather von Hauff. Special thanks to Sarah Hill for her "extra" field visits and help with the evapotranspiration data, and to Dan Born for being an excellent office-mate.

Imperial Oil Resources provided funding, personnel, a site for the study and allowed the publication of results. Funding was also provided by the Department of Earth and Atmospheric Sciences, through scholarships and teaching

assistantships, and by NSERC grants to the Gas Plant Remediation Project and Carl Mendoza.

Finally, thank you to my parents, Rick and Jean. You have continued to provide me with countless types of support throughout my time at the University, be it encouragement to pursue what I am interested in, or a roof over my head. Thank you for tolerating my insolence for these extra couple of years and for understanding why I never knew the answer to the question, 'When are you going to be done?'.

TABLE OF CONTENTS

CHAPTER 1 INTRODUCTION 1
1.1 Project Objectives 2
1.2 Purpose and Scope 4
1.3 Previous Research on Groundwater Flow in Shallow, Low Hydraulic Conductivity Environments 5
1.3.1 Till Groundwater Systems 5
1.3.2 Hydraulic Testing of Tills 8
1.3.3 Simulation of Flow and Transport in Low Hydraulic Conductivity Environments 10

CHAPTER 2 REGIONAL AND SITE CHARACTERIZATION 13
2.1 Regional Characterization 13
2.1.1 Topography, Drainage and Climate 13
2.1.2 Bedrock Geology 13
2.1.3 Surficial Geology 15
2.1.4 Regional Hydrogeology 17
2.2 Site Characterization 18
2.2.1 Local Physical Environment 18
2.2.2 Operational History and Target Processing Chemicals 19
2.2.3 Previous Site Investigations and Remediation Projects 20

CHAPTER 3 FIELD AND LABORATORY METHODS 25
3.1 Timeline of Field Instrumentation 25
3.2 Data Acquisition 25
3.3 Meteorological Monitoring 26
3.3.1 Monitoring at the GPRS 26
3.3.2 Other Meteorological Data 29
3.4 Variably-Saturated Zone Monitoring and Testing 29
3.4.1 Neutron Probe 29
3.4.2 Soil-Water Characteristics 32
3.4.3 Guelph Permeameter 34
3.5 Groundwater Monitoring and Testing 36
3.5.1 1999 Piezometer Installations 36
3.5.2 Other Piezometer Installations 37
3.5.3 Water Level Measurements 39
3.5.3.1 Manual Water Level Measurements 39
3.5.3.2 Automated Water Level Measurements 40
3.5.4 Hydraulic Conductivity Determinations 42
3.5.4.1 2000 Bail (Slug) Testing 42
3.5.4.2 Bail (Slug) Testing Conducted by Others 43
3.5.5 Dewatering Operations/ Hydraulic Testing 43
3.6 Other Installations 44
3.6.1 Multi-Level Vapour Monitoring 44
3.6.2 Thermistor Strings 46

CHAPTER 4 FIELD AND LABORATORY RESULTS AND DISCUSSION: METEOROLOGICAL AND VARIABLY-SATURATED ZONE CONDITIONS 47
4.1 Meteorological Conditions 47
4.1.1 Data Analysis and Selection 48
4.1.2 Historical and Spatial Comparison 51
4.2 Water Budget Components 53
4.2.1 Precipitation and Groundwater Recharge 53
4.2.2 Evapotranspiration 54
4.3 Calculation of Evapotranspiration at the GPRS 55
4.3.1 Reference Evapotranspiration (ET_o) Calculation Methods 55
4.3.2 Reference Evapotranspiration (ET_o) Results 56
4.3.3 Actual Evapotranspiration (ET_c) Calculation Methods 59
4.3.3.1 Crop Coefficient Method 60
4.3.4 Actual Evapotranspiration (ET_c) Results 60
4.4 Variably-Saturated Zone Conditions 63
4.4.1 Soil Moisture 63
4.4.2 Soil-Water Characteristic Curve Fitting 67
4.4.3 Variably-Saturated Zone Material Properties 70
4.4.3.1 Dry Bulk Density 70
4.4.3.2 Unsaturated Hydraulic Conductivity from Guelph Permeameter 72
4.4.3.3 Grain Size Distribution and Other Soil Properties 73
4.5 Summary of Key Points for Conceptual Model Development 74

CHAPTER 5 FIELD RESULTS AND DISCUSSION: GROUNDWATER CONDITIONS 76
5.1 Site Hydrostratigraphy 76
5.2 Hydraulic Conductivity Results 82
5.2.1 2000 Bail Test Results 82
5.2.2 Other Bail Test Results and Other Hydraulic Conductivity Results 88
5.3 Water Level Measurements: Results and Analysis 89
5.4 Groundwater Recharge From Precipitation 100
5.5 Barometric Efficiency of Till Deposits 104
5.5.1 Barometric Pressure Effects 104
5.5.2 Clark's Method 106
5.5.3 Correction of Measured Water Levels 111
5.6 Horizontal Groundwater Fluxes 113
5.6.1 Relation of Water Table to Topography 113
5.6.2 Contour Maps of Hydraulic Head 114
5.6.3 Horizontal Groundwater Gradients and Velocities 120
5.7 Summary of Key Points for Conceptual Model Development 123

CHAPTER 6 NUMERICAL GROUNDWATER MODELS OF THE GPRS 126
6.1 Objectives and Strategy 126
6.2 Conceptual Model 127
6.3 Model Design 128
6.3.1 Code Selection 128
6.3.2 Model Construction 130

6.3.2.1 Domain and Grid 130
6.3.2.2 Temporal Discretization 133
6.3.2.3 Material Properties 134
6.3.2.4 Boundary Conditions 134
6.3.2.5 Initial Conditions 137
6.3.2.6 Internal Stresses 138
6.3.2.7 Convergence Criteria 139
6.4 Results and Discussion 139
6.4.1 Calibration Description 139
6.4.2 Calibration Evaluation 140
6.4.2.1 Period of Net Recharge 141
6.4.2.2 Period of Net Discharge 147
6.4.2.3 Additional Measures of Calibration 151
6.4.3 Verification 157
6.4.4 Sensitivity Analysis 162
6.5 Summary and Conclusions 170

CHAPTER 7 CONCLUSIONS 172

REFERENCES 176

APPENDIX A COLLECTED DATA AND MODEL INPUT FILES 189

APPENDIX B EVAPOTRANSPIRATION CALCULATION METHODS 190
B.1 Reference Evapotranspiration Calculation Methods 190
B.1.1 Temperature-Based Method 191
B.1.2 Radiation-Based Method 192
B.1.3 Penman-Combination Methods 192
B.2 Actual Evapotranspiration Calculation Methods 195
B.2.1 Crop Coefficient Method 195

LIST OF TABLES

Table 2-1 Degree of connectivity between piezometers in the area of the horizontal well 23

Table 3-1 Deployment schedule of instrumentation 25

Table 3-2 Meteorological instrumentation installed 28

Table 3-3 Summary of 1999 piezometer installations 38

Table 3-4 Pressure transducer installation locations 41

Table 3-5 Summary of groundwater extraction since 1998 45

Table 4-1 Mean annual meteorological parameters 50

Table 4-2 Fitting parameters to laboratory measured P_c-S data 69

Table 4-3 Dry bulk density determinations for each neutron probe access tube location 71

Table 4-4 GPRS soil properties determined by Wong and Alfaro (2001) 73

Table 5-1 Hydraulic conductivity results for single well bail tests 85

Table 5-2 Hydraulic conductivity results in glaciated till plain settings 87

Table 5-3 Linear decline rates for instrumented piezometers 98

Table 5-4 Recharge estimates for instrumented piezometers 102

Table 5-5 Calculated barometric efficiencies and correlation coefficients .. 109

Table 5-6 Differences between measured and corrected hydraulic heads during the barometric efficiency study. 112

Table 5-7 Horizontal hydraulic gradient estimates 122

Table 5-8 Average linear groundwater velocity estimates 123

Table 6-1 Initial porous medium parameter estimates for numerical modelling 135

Table 6-2 Initial Type II boundary constant flux estimates for numerical modelling 137

Table 6-3 Final porous medium parameter estimates for numerical modelling 141

Table 6-4 Final Type II boundary flux estimates for numerical modelling .. 141

Table 6-5 Mean absolute errors between observed and modelled heads . 154

Table 6-6 Description of parameter and boundary condition modifications for the sensitivity analysis simulations. 163

LIST OF FIGURES

Figure 1-1 The groundwater regions of North America 6

Figure 2-1 Physiographic regions of Alberta 8

Figure 2-2 Surficial geology of the Western Alberta High Plains 16

Figure 2-3 Aerial photograph of the site from 1987 18

Figure 2-4 Site schematic with configuration of spring 1999..... 21

Figure 3-1 The automated meteorological station..... 27

Figure 3-2 Field measurement scenario for a neutron probe 31

Figure 3-3 The components of a pressure plate extractor 33

Figure 3-4 A field setup of the Guelph permeameter. 35

Figure 3-5 A schematic of a H_2OFX Model H-310 Submersible Pressure Transducer 41

Figure 4-1 Hourly barometric pressure from the GPRS and the Edmonton International Airport 49

Figure 4-2 Average daily incoming solar radiation at the GPRS 50

Figure 4-3 Monthly mean air temperatures recorded at the Breton Plots and the Edmonton International Airport 52

Figure 4-4 Monthly precipitation (rainfall) recorded at the Breton Plots and the GPRS 52

Figure 4-5 Average daily ET_o estimates in monthly increments and 6 month sum of ET_o during the 2000 growing season 57

Figure 4-6 Daily ET_o estimates for June 2000 57

Figure 4-7 Daily ET_c estimates for vegetated and bare soil conditions during the 2000 growing season 61

Figure 4-8 Daily ET_c estimates for vegetated and bare soil conditions during April 2000 62

Figure 4-9 Soil moisture profiles at (a) N99-1, (b) N99-2, and (c) N99-3 64

Figure 4-10 Pressure-saturation data and curve fit 69

Figure 5-1 Cross-section A-A' 78

Figure 5-2 Cross-section B-B' 79

Figure 5-3 Semi-logarithmic plot of water level displacement versus time for P99-1A 83

Figure 5-4 Semi-logarithmic plot of water level displacement versus time for P99-7 84

Figure 5-5 Hydrographs for (a) P97-1, (b) P97-3 and (c) rainfall 90

Figure 5-6 Hydrographs for (a) P97-9, (b) P97-10 and (c) rainfall 91

Figure 5-7 Hydrographs for (a) HP-N, (b) HP-W and (c) rainfall 92

Figure 5-8 Hydrographs for (a) P99-1, (b) P99-5 and (c) rainfall 93

Figure 5-9 Hydrographs from a multi-level piezometer installation in clay till in Saskatchewan 96

Figure 5-10 Hydraulic heads determined by pressure transducers at a shallow and a deeper piezometer during a snowmelt period 97

Figure 5-11 Barometric pressure and pressure head fluctuations at HP-W .. 105

Figure 5-12 Calculation of barometric efficiency 108

Figure 5-13 Water level corrections for HP-W 112

Figure 5-14 Water table map from December 21, 1999 116

Figure 5-15 Water table map from May 18, 2000 117

Figure 5-16 Water table map from September 1, 2000 118

Figure 6-1 Hypothetical N-S cross-section representing the conceptual model under consideration 128

Figure 6-2 Numerical grid representing the modelled domain 131

Figure 6-3 Plan view of the modelled domain 132

Figure 6-4 Observed and modelled heads during the period of net recharge for shallow piezometers near the horizontal well 143

Figure 6-5 Observed and modelled heads during the period of net recharge for raised pad area piezometers 145

Figure 6-6 Observed and modelled heads during the period of net recharge for outer piezometers 146

Figure 6-7 Observed and modelled heads during the period of net discharge for shallow piezometers near the horizontal well 149

Figure 6-8 Observed and modelled heads during the period of net discharge for raised pad area piezometers 150

Figure 6-9 Observed and modelled heads during the period of net discharge for outer piezometers 152

Figure 6-10 Scatterplots of observed heads versus modelled heads 153

Figure 6-11 Plan view of the modelled hydraulic head distribution on September 8, 2000 156

Figure 6-12 Observed and verification heads during the period of net recharge in all areas 160

Figure 6-13 Observed and verification heads during the period of net decline in all areas 161

Figure 6-14 Sensitivity analysis results for (a) shallow and (b) deeper monitoring points in the area of the horizontal well 166

Figure 6-15 Sensitivity analysis results for (a) raised pad area and (b) outer piezometers 167

CHAPTER 1

INTRODUCTION

Subsurface contamination is ubiquitous throughout the industrialized world. This largely stems from the wide-scale production and mishandling of chemicals in the fabrication of various products. There are approximately 65 000 chemicals in commercial use today, with over 10 000 of them being produced at more than 450 000 kg per year each (Freeze 2000). Two of the largest culprits of subsurface contamination are leaky underground fuel storage tanks and chlorinated solvents used in degreasing operations from the early 1960's to the late 1980's (Ward et al. 1997). In jurisdictions heavily dependent on oil production, for example Alberta, there is increased potential for the introduction of process-related fluids to the subsurface.

An area of environmental management that has been misunderstood, wasteful and expensive is subsurface remediation. This is due to ignorance of the magnitude of the problem, and the complexity and relative inaccessibility of the subsurface environment (Ward et al. 1997). Groundwater issues have traditionally been quantity issues, until the 1970's when water quality issues expanded the scope of investigations (Bedient et al. 1994). Thus far, most remedial efforts have focused on groundwater extraction, or "pump and treat", and landfilling (Suthersan 1997). These technologies relocate contamination, but do little to completely remove potentially hazardous materials from the environment.

The Gas Plant Remediation Site (GPRS), the site under consideration in this thesis, is similar to many upstream gas operations in Alberta and Canada, both in terms of the processes and chemicals used and the geological setting of the site. The plant was in operation for 15 years until 1993, and impacted a portion of the subsurface with amines and glycols, compounds that were used to sweeten and dehydrate natural gas. The introduction of processing chemicals to the

subsurface at natural gas sites is a common problem in Canada and the United States. There are approximately 90 sites in Canada using amines for gas sweetening, while many thousands perform glycol dehydration (Sorensen et al. 1997).

Many of these sites are similar to the GPRS in that they are situated on low permeability silt and clay tills deposited by ice sheets during the Late Wisconsinan glacial advance. Typically, groundwater flow rates in clay till matrices are very low, thus making dissolved solute relatively inaccessible in a traditional remediation scenario. These low flow rates have often necessitated the excavation and subsequent ex-situ treatment of impacted tills (Bowles 1998).

The textural heterogeneity of these tills limits the viability of groundwater extraction as a remediation mechanism due to the development of preferential flow paths along more highly permeable conduits such as sand lenses. Groundwater extraction has not proven to be economical in tills because the small capture zones require closely spaced extraction wells over often large areas (Bowles et al. 2000). In-situ treatments, such as hydraulic fracturing of the contaminated medium to enhance permeability (Frank and Barkley 1995) and vacuum enhanced recovery (Nyer 1996), are emerging technologies. There is an obvious need for the development of practical and effective in-situ remedial techniques for low permeability sedimentary environments containing amine and glycol processing chemicals.

1.1 Project Objectives

The primary goal of the Gas Plant Remediation Project (GPRP) was to develop cost effective methods for the in-situ remediation of amine and glycol impacted soil and groundwater at hydrocarbon processing sites as alternative methods to excavation and landfilling. To achieve this goal, a multi-disciplinary approach was undertaken, which required the cooperation of several research groups from distinct areas of expertise. This approach was necessary given the complex

nature of the contamination problem. Each research group conducted their own field and laboratory studies; however, each relied on the results and participation of the other groups to plan and execute future experimental and remedial work.

The main areas of GPRP research were as follows:

1. *Laboratory studies for chemistry and biochemistry* (Mrklas et al. 2001; Mrklas 2002). The primary goal of this research was to establish the potential for in-situ microorganisms to degrade amine and glycol compounds under different aeration regimes. Also important was the quantification of physical and chemical transformation processes, and degradation kinetics. This research also assisted in the calibration of the geophysical resistivity measurements (Bentley et al. 2001).

2. *Three-dimensional electrical resistivity tomography* (Bentley et al. 2001). The objective of the geophysical program was to develop a non-invasive, cost efficient method to monitor the progress of remediation. Petrophysical properties of the site were monitored and correlated to changes in pore water chemistry, thus alleviating the need for comprehensive borehole sampling in latter stages of the project.

3. *Physical hydrogeological characterization and numerical modelling* (Butterfield, this thesis). The hydrogeological program was initiated to gain a site-specific understanding of the physical processes controlling groundwater flow. The program consisted of field characterization followed by the development of numerical groundwater models for further interpretation. The detailed objectives and scope of this research are presented in section 1.2.

1.2 Purpose and Scope

Initial site characterization and remedial efforts could not characterize the hydrogeology in enough detail to be of use for further investigative and remedial designs (Komex 2000b). The lack of knowledge of site-specific groundwater characteristics obtained from previous remedial efforts at the GPRS provided the necessary impetus for the research in this thesis.

Thus, the objectives of the hydrogeological research program for the GPRP were as follows:

1. Conduct a field and laboratory program to improve site characterization. Although there was some legacy information, the site geology needed to be refined, including better hydrogeological characterization of near-surface till units, the location and character of the bedrock-till interface and the distribution of fractured porous media.

2. Collect sufficient relevant hydrologic and hydrogeologic data to characterize the physical hydrogeological regime of the GPRS. The characterization of flow at the site lies within the scope of describing groundwater flow and transport in shallow, low hydraulic conductivity sedimentary environments, an area of research that has been emerging over the past 25 years. This will be described further in section 1.3.

3. Construct numerical models that adequately describe the behaviour of groundwater flow at the site. Numerical models were developed to test conceptual flow models and to help interpret field observations, not only from the hydrogeological study, but also from the geochemical and geophysical studies.

1.3 Previous Research on Groundwater Flow in Shallow, Low Hydraulic Conductivity Environments

1.3.1 Till Groundwater Systems

As a result of the advance and subsequent retreat of continental glaciers approximately 10 000 years ago, much of the bedrock of Canada, the United States and northern Europe is covered by a veneer of clay-rich glacial sediment. The deposits were formed by direct glacial deposition and by indirect deposition by large glacial lakes and rivers (Cherry 1989). In North America, the Western Glaciated Plains (WGP) region (Figure 1-1) occupies nearly 2 million km^2, 60% of which is covered by till, while the other 40% consists of lacustrine and glacio-fluvial deposits (Lennox et al. 1988).

Given the areal extent and geological diversity of the WGP, numerous types of hydrogeological flow systems exist, ranging from local flow systems in discontinuous glacial deposits to regional flow systems that extend to the Precambrian basement. In general, the WGP are flat with locally elevated (30 m to 60 m) topography arising from glacial landforms. The till can be up to 300 m thick in the WGP, usually increasing in thickness with distance from the Rocky Mountains. Field and modelling studies have shown that the distribution of flow systems in the region largely depends on the surface topography and the heterogeneity of geologic materials (Lennox et al. 1988).

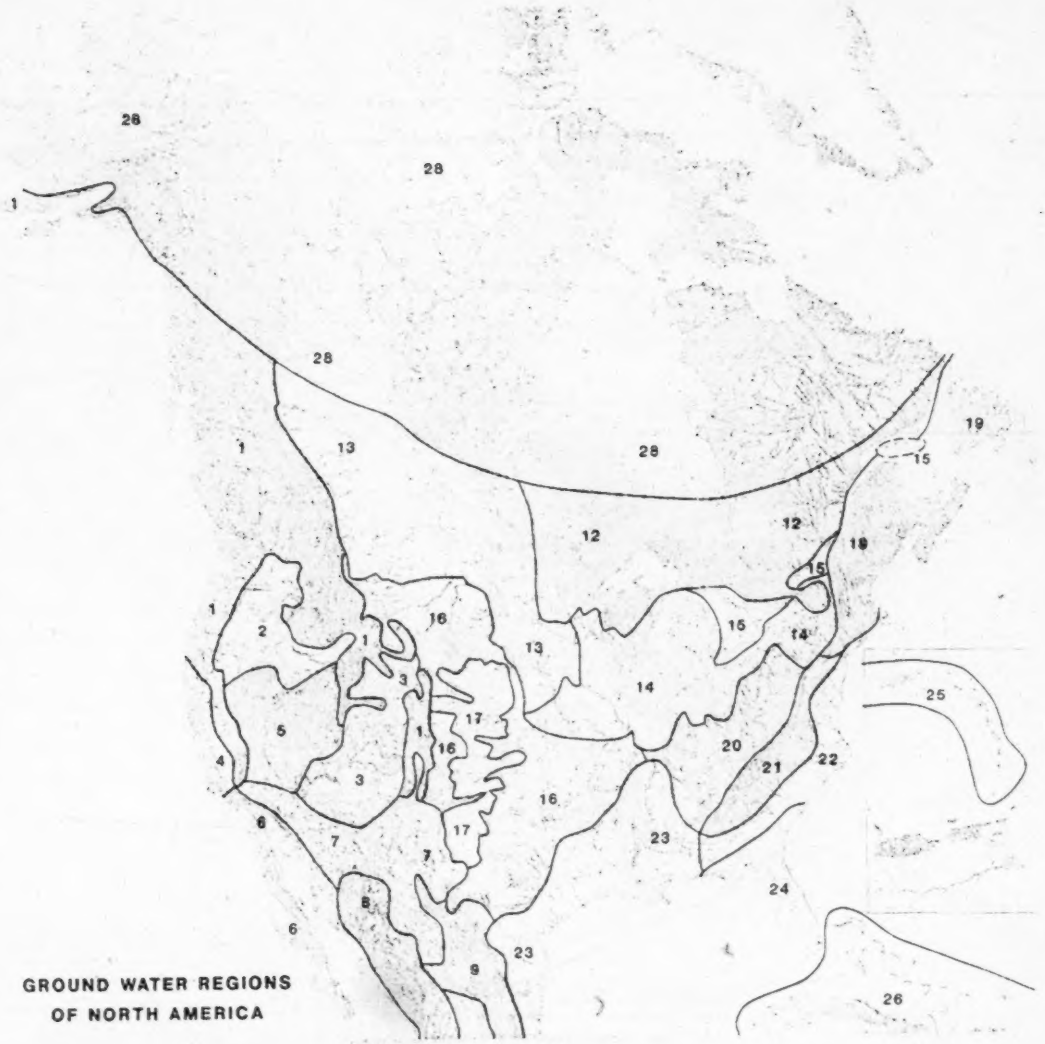

Figure 1-1 The groundwater regions of North America. The Western Glaciated Plains are represented by region 13 (modified from Heath 1988).

Surface tills were long regarded as low-permeability aquitards having little hydraulic connection with lower aquifers (Gerber et al. 2001), but research over the past 35 years has shown that tills can contain active groundwater flow systems. Therefore, for many aquifers that are overlain by till deposits, the management of water supply and the protection of water quality may be highly dependent on determining the groundwater flow characteristics of the till

deposits. For example, it was thought that tills limited aquifer recharge; however, sustainable pumping rates have indicated that, in some cases, recharge has been higher than previously expected (van der Kamp 2001). Also, landfills and other industrial sites have been placed in regionally extensive glacial deposits with leachates and chemical spills breaking through to aquifers much sooner than previously expected (Cherry 1989). Reliable determinations of groundwater flow characteristics in glacial deposits have aided in explaining these observations.

Investigations into the hydraulic behaviour of clayey glacial deposits was begun by Canadian hydrogeologists in the 1960's (Cherry 1989), such as the study reported by Meyboom (1966) which described groundwater flow and landscape characteristics (head, salinity, vegetation) in hummocky moraine deposits. The impact of fractures on the hydraulic behaviour of weathered till was studied by Williams and Farvolden (1967). Since that time, research into shallow groundwater flow systems has endeavoured to resolve whether till deposits were fractured or not, given the ability of fracture permeability to control groundwater flow in these materials. Mechanisms and physical controls on groundwater flow in till remain poorly understood, and thus a major problem in remediation studies remains to characterize field-scale flow pathways and fluxes (Gerber et al. 2001).

Field studies extending from Alberta in the west, to Ontario in the east, have uncovered some similarities in the material properties and hydraulic characteristics of tills. In general, there are two distinct till types that sometimes form part of the same stratigraphic unit (Grisak et al. 1976; Hendry 1982, 1989; Keller et al. 1986, 1988, 1989; Cravens and Ruedisili 1987; D'Astous et al. 1989; Ruland et al. 1991; Shaw and Hendry 1998; others). The uppermost till unit is often highly weathered and fractured, has a distinct brown colour, and has a greater sand fraction than the lower till. The brown colour indicates a zone of clay mineral oxidation with the formation of iron sesquioxide compounds (Rodvang and Simpkins 2001). The lowermost till unit is sometimes sparsely

fractured, has a grey colour, is discontinuous and contains a higher silt and clay fraction than the uppermost till unit. Bedrock fragments are more prevalent in the lower than the upper till. The grey colour indicates the weathering history and reducing conditions currently present in the till (Rodvang and Simpkins 2001). The colour change between the upper and lower units coincides with, or is proximal to, the change from oxidized to reduced conditions.

1.3.2 Hydraulic Testing of Tills

The determination of the hydraulic properties of tills is highly dependent upon the scale of measurement, both temporally and spatially. As long as tills are not too thick or impermeable, they are amenable to transient flow analysis, such as pumping tests (van der Kamp 2001). The measurement of till permeability from the laboratory, to the site, to the regional scale often results in permeabilities ranging over several orders of magnitude. However, the measurements at different scales have allowed the characterization of secondary permeability structures, most often fractures (van der Kamp 2001).

Several researchers in Canada (Grisak and Cherry 1975; Hendry 1982, 1988; Keller et al. 1988, 1989; Ruland et al. 1991, others) have reported on the permeability of clay tills at two scales, where there are clearly two permeability populations indicated by testing results. Often, this is from laboratory testing and field-scale testing with slug tests, pumping tests, and monitoring flow into excavations. The two populations reflect both the scale of measurement and the location that the measurement was acquired in relation to the interface between oxidized and non-oxidized deposits. Smaller-scale laboratory tests often determine the till matrix permeability, while larger scale tests tend to intercept fractures, sand lenses or other zones of enhanced permeability that raise the bulk permeability of the samples by at least two orders of magnitude (van der Kamp 2001). These results have been reflected by other researchers from elsewhere in North America and around the world (e.g., Bradbury and Muldoon

1990; Fredericia 1990; Rudolph et al. 1991). Shaver (1998) reported similar results in the determination of specific storage in till deposits in North Dakota.

Most often, high permeability results from the field-scale tests come from the oxidized till zone. There is then a decrease in the hydraulic conductivity below the transition zone from oxidized to unoxidized material (Shaw and Hendry 1998). As depth increases, the bulk permeability more closely reflects the matrix permeability due to a lesser degree of weathering. This is not always the case, as Keller et al. (1986) determined that the bulk permeability of a deep unweathered till in Saskatchewan exceeded the matrix permeability by two orders of magnitude. It has been previously realized that unoxidized tills could be fractured from stresses during deglaciation (Grisak et al. 1976), but most studies lack hydraulic evidence for it.

There are other methods for measuring the hydraulic conductivities of till formations, but it is important to have measurements at a minimum of two scales to adequately characterize the hydraulics of the formation. For example, Gerber and Howard (2000) compare their determination of hydraulic conductivity from regional flow modelling against laboratory determinations to arrive at the same conclusion as many others: the bulk permeability of the formation exceeds that of the matrix.

It has been shown that fractures may exist in both weathered and unweathered deposits and that the lack of direct observation of fractures does not necessarily mean that they are not present (e.g., Keller et al. 1986). This unpredictability makes it important to ensure that a site-specific study is undertaken for each study of flow in low permeability tills. Of equal importance is to use several different methods for characterization of flow. Conclusions about the nature of flow within till deposits are more readily reached when the results of several different methods are compared (van der Kamp 2001).

The most commonly used methods to characterize till deposits, by means other than hydraulic testing, are solute and isotope tracer methods. The observations of the transient distributions of conservative solutes (usually Cl^-) or isotopes (usually ^3H or ^{18}O) help to determine recharge mechanisms, fluxes and flow pathways in low conductivity materials. Many of the aforementioned researchers (e.g., Hendry 1982, 1988; Keller et al. 1986, 1988; D'Astous et al. 1989; Ruland et al. 1991; Gerber and Howard 2000) employed these methods in their studies, along with several others (e.g., McKay et al. 1993; Remenda et al. 1996).

1.3.3 Simulation of Flow and Transport in Low Hydraulic Conductivity Environments

Numerical methods emerged concomitantly with the field characterizations of flow in shallow till environments. Most of the early work in this area focused on developing mathematical models to explain the bulk movement of groundwater in these shallow deposits, particularly in fractured systems (Gerber et al. 2001). The most important concept recognized by various researchers, regardless of the methods they employed to analyze their systems, is that the coupling of the high transmission, low storage, advection-dispersion dominated fractures, with the low transmission, high storage, diffusion dominated porous medium, is essential to the correct characterization of the system (Rowe and Booker 1990).

There are two basic approaches to mathematically representing flow and transport in shallow fractured systems (Harrison et al. 1992). The first approach is based on semi-analytical and analytical methods. These are often found inadequate in representing field-scale behaviour because of the inherent assumptions involved in the development of the methods (Harrison et al. 1992). For example, fracture aperture, a key control of the hydraulic conductivity of fractures, is held constant in these methods. Therefore, the second approach endeavours to represent more complex systems with numerical models.

The first of three numerical modelling approaches is to explicitly represent the fractures without any interactions with the porous media. Although this may correctly represent processes within the fractures, it does not emulate overall system behaviour (Harrison et al. 1992). In till matrices, higher flow rates and transport processes other than diffusion have been shown to be significant for some scenarios (Sudicky and McLaren 1992). A second approach is to couple the porous medium and fractures as a dual porosity system, representing the fractures as high conductivity and low storage and the porous medium as low conductivity and high storage. This has been found to be appropriate for the weathered zone, where there are ubiquitous, evenly spaced fractures, but more suspect for the unweathered zone where the frequency of fracturing is irregular (Harrison et al. 1992). A final approach is to represent the matrix and fractures as an equivalent porous medium with macroscopic properties defined over a representative elemental volume (Therrien and Sudicky 1996). While not as accurate as explicitly specifying the processes involved, the advantage to this approach is that it reduces the amount of information required on fracture aperture and spacing, of which there are relatively few studies (McKay et al. 1993).

More recent modelling approaches (Therrien and Sudicky 1996) attempt to fully couple all fracture and matrix flow and transport processes in variably saturated environments. This is important, for example, for unsaturated flow in fractures, where the air-filled fractures may become barriers to flow due to a reduction in hydraulic conductivity (Tindall and Kunkel 1999). Fractures are generally preferential flow paths under saturated conditions. The consideration of a full three-dimensional treatment allows for a more realistic representation of fracture connection (Therrien and Sudicky 1996), because at a given site, fracturing may be prevalent in many directions.

The focus of much research has been on defining fracture and matrix properties and how they relate to bulk system behaviour. Field-scale flow regimes and

determining the importance of various pathways to fluxes generally remain poorly understood in these shallow, low conductivity environments (Gerber et al. 2001). Fracture and matrix properties from one site are usually assumed to be typical of a wide variety of glacial terrains. This is not always the case, and the determination of field-scale heterogeneities on a case-by-case basis, along with numerical modelling, can help to define more localized controls on shallow groundwater flow systems. This agrees with the earlier statement that the characterization of these flow systems is best accomplished using a variety of independent methods.

Currently, the number of practitioners who explicitly incorporate fracture flow into their field-scale numerical modelling efforts is limited. If the various parameters relating to the non-linear process of fracture flow (fracture aperture, orientation and spacing) are estimated or poorly defined, the problem is poorly constrained and becomes computationally intensive (van der Kamp 2001).

CHAPTER 2

REGIONAL AND SITE CHARACTERIZATION

2.1 Regional Characterization

2.1.1 Topography, Drainage and Climate

The GPRS lies within the Western Alberta High Plains (WAHP) physiographic region, east of the front ranges of the Rocky Mountains and Foothills (Pupp et al. 1989) (Figure 2-1). The WAHP region is characterized by undulating topography with a gradual rise in elevation towards the southwest. The maximum local relief is approximately 250 m. Most surface water in the WAHP region drains southeast to the Red Deer River system, part of the Nelson River drainage basin which flows into Hudson Bay. Battle Lake, the headwaters of the Battle River, is the lowest topographic point in the WAHP (Tokarsky 1971).

The climate of the WAHP region was classified as a humid, continental climate by Tokarsky (1971), with the southwestern parts more characteristic of an alpine setting (more precipitation and shorter, cooler summers) than the northeastern parts. The daily mean temperature in the WAHP region in the coldest month, January, ranges from -11°C to -14°C, grading from warmer to cooler from southwest to northeast. In the hottest month, July, daily mean temperatures range from 13°C in the southwest to 16°C in the northeast. Rates of potential evapotranspiration exceed precipitation values for much of the year (May to October, excepting September when the reverse is true) while being near zero for the remainder of the year (November to April) (Tokarsky 1971). Mean annual precipitation in the region is approximately 400 to 500 mm (Dzikowski 1990).

2.1.2 Bedrock Geology

In the WAHP, the near surface bedrock formation is the Paleocene Paskapoo Formation. The Paskapoo Formation is a continental unit consisting primarily of

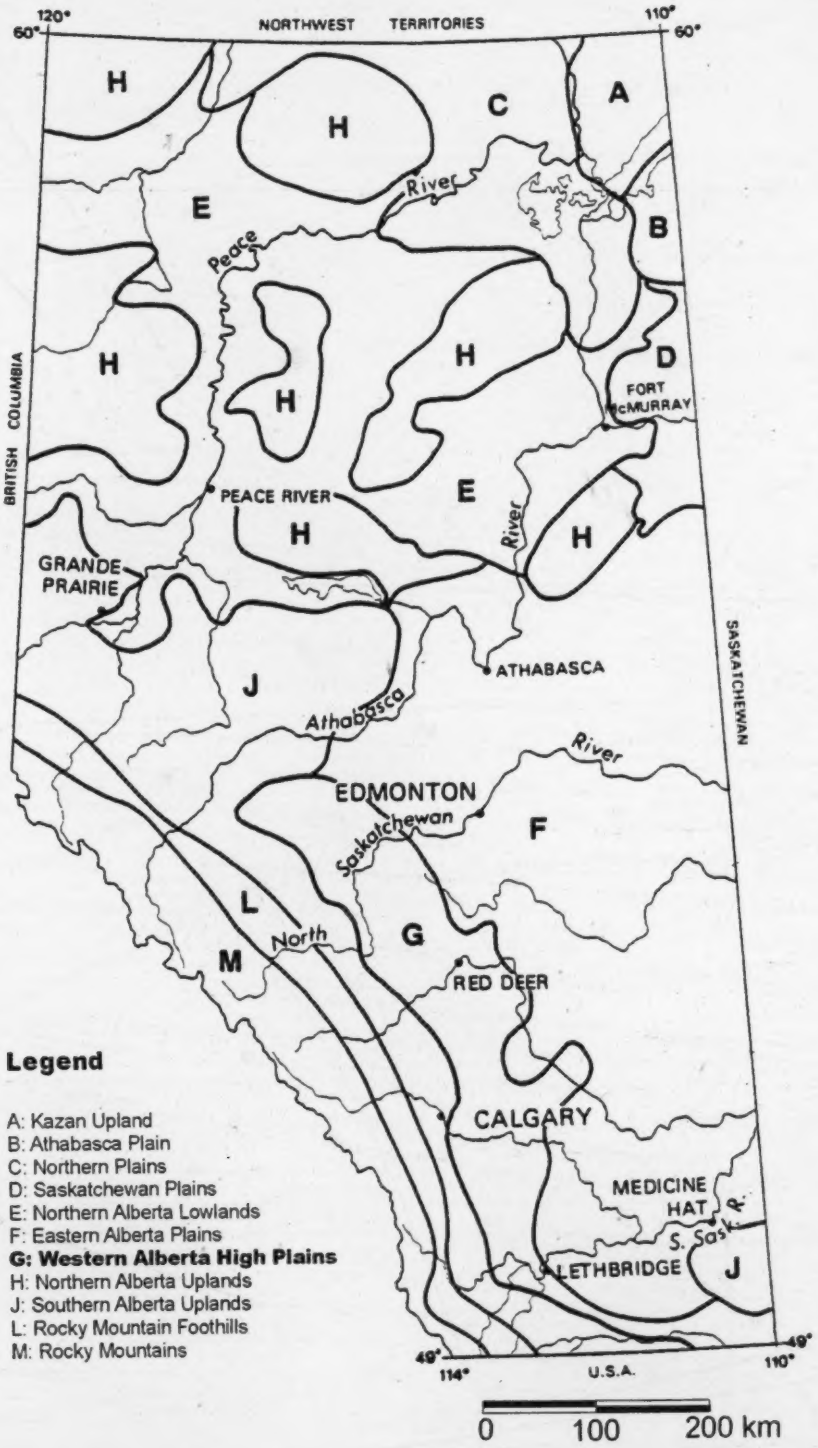

Figure 2-1 Physiographic regions of Alberta (modified from Pettapiece 1986 as referenced in Pupp et al. 1989).

interbedded, soft, grayish-green mudstone and siltstone, although the thickest and most prominent type of sediment is massive, medium to coarse-grained sandstone (Glass 1997). There are minor amounts of limestone, coal, conglomerate and bentonite. There is often a layer of bedrock regolith at the erosional contact with overlying Quaternary sediments (Bowles 1998).

The Paskapoo Formation is sub-horizontal in the WAHP, dipping slightly towards the highly deformed strata of the Foothills and Rocky Mountains (Tokarsky 1971). The formation covers a crescent-shaped area along the Foothills from 50°N to 55°N with its outer erosional contact lying further to the east, at a maximum longitude of 112°W. Reported thicknesses are up to 600 m, with greater thicknesses near the Foothills and Rocky Mountains (Glass 1997).

2.1.3 Surficial Geology

Till is the parent material from which most (70%) of Alberta's soils develop (Pawluk and Bayrock 1969). Repeated glacial and non-glacial intervals throughout the Pleistocene produced a large variety of glacial terranes in the Prairies (Fenton 1984). In central Alberta, six major till units have been identified in stratigraphic studies (Holter 1973). Of these six, four were interpreted to originate from Cordilleran sources, one from Laurentide glaciation and one from a convergence of the two in the Foothills. In the WAHP, the texturally variable surficial sediments originate from the advance and retreat of continental glaciers from the north or northeast (Pawluk and Bayrock 1969).

Till in the WAHP region is referred to as the Sylvan Lake Till (Figure 2-2), deposited as ground moraine and recessional moraine. The Sylvan Lake Till is clayey loam, like most of the other tills of central and southern Alberta (Pawluk and Bayrock 1969). It contains a significant number of Precambrian erratics, reflecting its provenance from the northeast (Boydell et al. 1974). The till is characterized by the transition from oxidized medium brown to unoxidized grey.

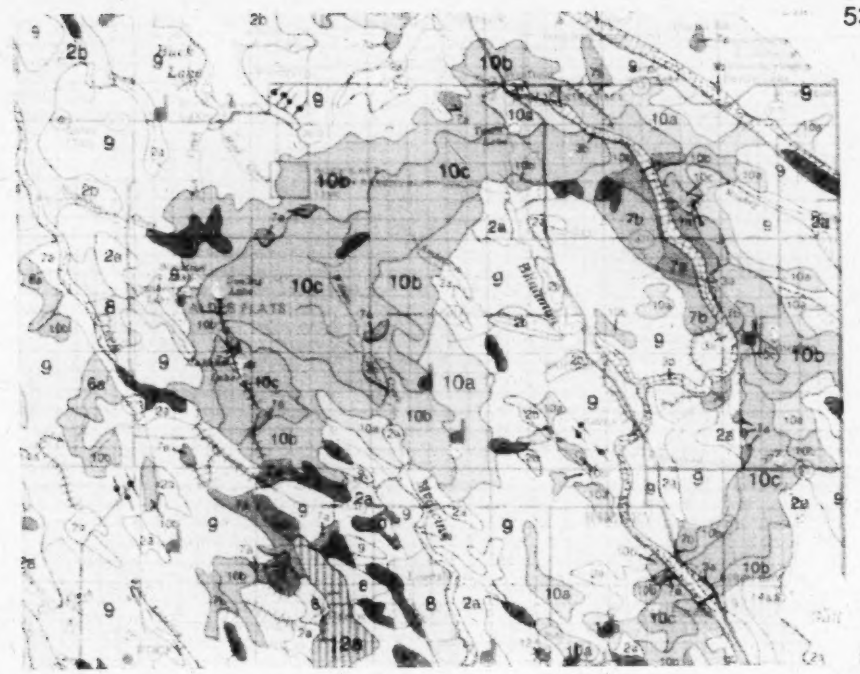

Legend

	organic material	7b	ice contact fluvial silt and clay
1	eolian fine sand and silt	8	ice contact lacustrine and fluvial
2a	lacustrine sand and silt	9	Sylvan Lake ground moraine
2b	lacustrine silt and clay	10a	Sylvan Lake recessional, undulating
3a	fluvial gravel and sand	10b	Sylvan Lake recessional, weakly hummocky
3b	fluvial fine sand, silt and clay	10c	Sylvan Lake recessional, strongly hummocky
	stream and slope eroded	12	ice thrust moraine
6a	ice contact lacustrine sand and silt	12a	ice thrust and recessional moraine
7a	ice contact fluvial gravel and sand	14a	ground moraine on bedrock upland
	meltwater channel		linear feature parallel to ice movement

Figure 2-2 Surficial geology of the Western Alberta High Plains (1:500 000) (modified from Shetsen 1990).

Physically, the particle-size distribution of the till is representative of the composition of the underlying bedrock formation (Pawluk and Bayrock 1969). The principal clay mineral of the tills in the region is montmorillonite, which is characterized by a high cation exchange capacity and the property of doubling its volume by the absorption of water (Prothero and Schwab 1996). Consequently, there is little leaching described for the Sylvan Lake Till (Boydell et al. 1974).

Other surficial deposits in the region, mainly glaciolacustrine deposits, are localized (Figure 2-2). The most recent surficial deposit is alluvium from streams and rivers.

2.1.4 Regional Hydrogeology

Where there are continuous sandstone units, the Paskapoo Formation is a major regional aquifer. The groundwater regime of the Paskapoo is dominated by high groundwater flux and relatively rapid circulation (Pupp et al. 1989). This is attributable to locally elevated relief, permeable (often fractured) sandstone units and recharge of relatively high precipitation through fractured Quaternary units. Data from several wells completed in Paskapoo sandstone in the WAHP show yields of up to 100 to 500 L/min, while averaging 25 to 100 L/min in the Foothills and Rocky Mountains regions (Tokarsky 1971).

Yields can be expected to vary based on topographic position, proximity to surface waters and surrounding geology. Lower yields near the Foothills and Rocky Mountains can be attributed to a decrease in sandstone porosity due to low-grade metamorphism (Pupp et al. 1989). In these areas, flow is structurally, rather than lithologically, controlled due to orogenic deformation.

2.2 Site Characterization

2.2.1 Local Physical Environment

An air photo (Figure 2-3), annotated with significant local features, provides visualization of the GPRS. The site is located on locally elevated topography with steep, natural drainage gullies to the west and east of the site. The gullies are heavily colluviated. Elevation also drops off rapidly to the south in the direction of the access road. The local slope is upward to the north (6-8%), where the gullies converge approximately 200 m away. Streams can be found in the gullies, ephemeral on the west side during heavy precipitation, draining to a lake approximately 500 m to the south.

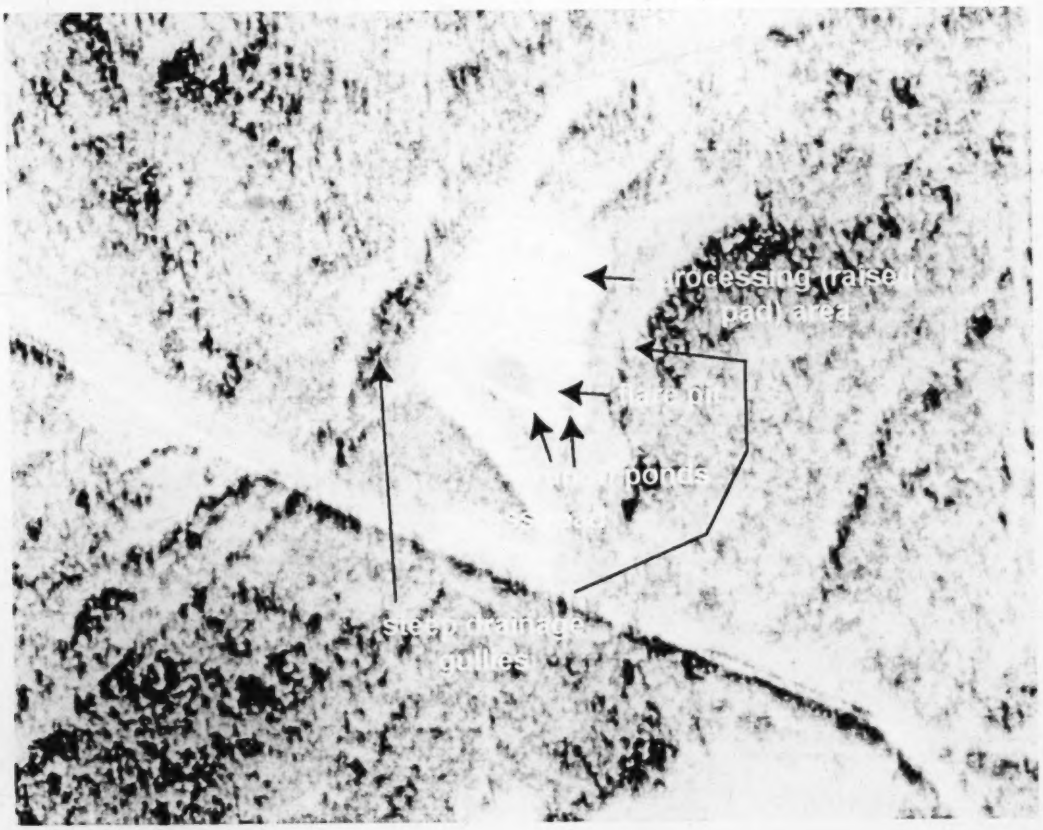

Figure 2-3 Aerial photograph of the site from 1987 with significant local features annotated (1: 4 500).

2.2.2 Operational History and Target Processing Chemicals

The GPRS consisted of a single sour gas well and processing plant, with a capacity of 5.5 million cubic feet per day (MMCFD), in operation from 1978 to 1993 (Komex 2000b). The well was abandoned and all surface infrastructure was removed from the site, except the equipment related to research and remedial efforts. Significant subsurface pipelines also remained after decommissioning.

The chemicals of concern for the GPRP are those related to the processing of sour natural gas, namely alkanolamines and glycols. Alkanolamines are organic derivatives of ammonia (NH_3). They are classified as primary, secondary or tertiary depending on the number of organic substituents bonded to the nitrogen atom (Sorensen et al. 1997). Amines are both basic and nucleophilic, and are therefore highly reactive with acid gases in natural gas such as hydrogen sulphide (H_2S) and carbon dioxide (CO_2) (Komex 2000b). Monoethanolamine (MEA) was used in the greatest volume at the GPRS.

Glycols are alkene derivatives, with alcohol (OH) groups substituted onto each alkene carbon (Komex 2000b). They are hygroscopic, absorbing up to twice their weight of water at 100% humidity (Komex 2000b). Therefore, they are used in natural gas processing to remove water to prevent the formation of hydrates and to reduce corrosion. Ethylene glycol (EG) and triethylene glycol (TEG) were most commonly used at the GPRS.

The environmental fate of the target chemicals is a primary concern of the GPRP. MEA and the glycol compounds have low vapour pressures and are completely miscible with water. Thus, they have a high potential to move advectively with groundwater (Sorensen et al. 1999). The pKa of MEA (9.4) means that it should be protonated at typical background pH levels (6.5-8.5) and, given its relatively high K_d value (2.2-4.9), should be expected to sorb to negatively charged clay soils (Komex 2000b). Both MEA and glycols have been

shown to biodegrade under aerobic and anaerobic scenarios, although field-based studies are complicated by heterogeneous subsurface conditions (Mrklas et al. 2001; Mrklas 2002). Consequently, unless there are significant permeable pathways for the chemicals to move with groundwater, their mobility should be limited at the GPRS, despite their miscibility (Komex 2000b).

2.2.3 Previous Site Investigations and Remediation Projects

Soon after the gas plant was decommissioned, site investigations began to determine source locations and the extent of impacted soils and groundwater. Figure 2-4 illustrates aboveground and subsurface configurations of site installations up until 1999.

Two areas of the site were identified as being impacted by elevated amine and glycol soil concentrations based on field observations and limited preliminary chemical analysis (Komex 2000b). The main source is on top of the raised pad area, just west of the storage building (Figure 2-4), where much of the processing equipment was located. Strong amine and glycol odours were encountered up to 4 m below the ground surface (bgs). Analytical work (Artemis 1997) focused on MEA concentrations in the pad area, finding levels of up to 7 g/kg. Previous investigations of glycol concentrations in the same area found elevated levels of EG and TEG (up to 3 g/kg). The other impacted area of the site was the flare pit (Figure 2-4), although this determination was strictly by detection of odour in the field and not through analytical confirmation.

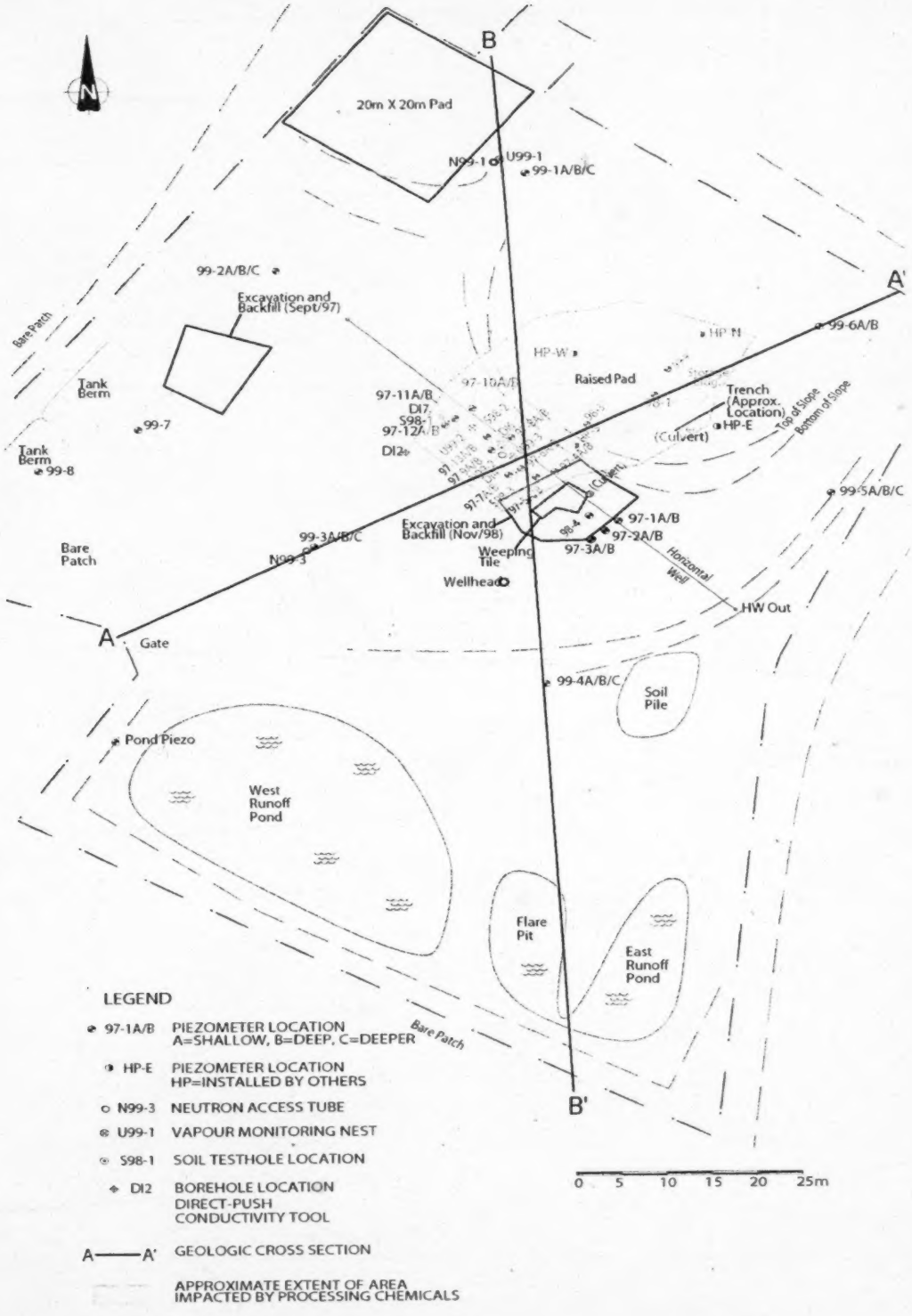

Figure 2-4 Site schematic with configuration of spring 1999.

Subsequent sampling programs reinforced the results of the preliminary investigations and began to reveal the heterogeneity of the processing chemical distribution. A glycol sampling program in the pad area (Figure 2-4) in 1998 encountered TEG levels of up to 7 g/kg in some areas, but did not detect it in other areas. Levels of EG were below 250 mg/kg, while previous sampling programs detected it at higher levels. Just south of the pad area (Figure 2-4), MEA was detected at approximately 16 g/kg, while low glycol levels (< 40 mg/kg) were found (Komex 2000b).

A remediation program involving bioventing was initiated in October 1997 to investigate the in-situ biodegradability of amine and glycol compounds (and their degradation products) in the low permeability soils encountered at the GPRS. Several interpretations were made regarding this program (Komex 2000b):

- The water table was below the impacted soils;
- Oxygen supply limits the biodegradation of the amine and glycol compounds; and,
- Hydraulically fracturing the soil would enhance the permeability sufficiently to make bioventing viable.

The first interpretation was based solely on borehole observations during testhole drilling. The latter two points were based on treatability studies on site soils and reviews of literature involving fracturing methods at other similar sites.

The primary component of the bioventing project was the horizontal well, installed 4 m bgs in a northwest to southeast trend just south of the raised pad area (Figure 2-4). The installation of the horizontal well was not completely successful. A section of slotted PVC pipe ruptured during installation (Komex 2000b), thus reducing the continuity of potential airflow pathways in the subsurface. The soils surrounding the horizontal well were subsequently hydraulically fractured to increase their permeability (Frac Rite Environmental

Ltd. 1997). A second horizontal well was then installed approximately 1 m south of the original. The second well did not appear to intersect many of the fractures induced in the first well. Thus, the second well did not re-establish the air connectivity lost when the first well broke (Komex 2000b).

A detailed piezometer network (Figure 2-4) was installed to monitor the progress of bioventing. Each nest of piezometers 97-1 to 97-13 has completion intervals at two different depths: A at approximately 2 m depth and B at approximately 4 m depth. Borehole logs and piezometer construction details are available in Komex (2000b) and will be discussed further when site geology is described.

Preliminary testing with the application of suction to the horizontal well showed that many of the piezometers had a certain degree of connectivity to the well (Table 2-1); however, a complicating factor was that groundwater invaded the horizontal well and the fractures. Thus, the only way for connectivity to be maintained between the piezometers was for them to be repeatedly bailed or to implement a de-watering program to coincide with the bioventing program.

Degree of air connectivity	Relevant piezometers
Clear connection	97-5B
Moderate connection, if bailed	97-6B, -8A, -8B, -10A, -10B, -11B
Weak connection, if bailed	97-4A, -4B, -6A, -7A, -7B, -9A, -9B, -13A, -13B
Minimal connection	97-1A, -1B, -2A, -2B, -3A, -3B, -11A, -12A, -12B

Table 2-1 Degree of connectivity between piezometers in the area of the horizontal well deduced by applying suction to the horizontal well (Komex 2000b).

During respiration tests, which indirectly measure the potential for aerobic biodegradation, most piezometers showed decreases in headspace O_2 concentrations and increases in headspace CO_2 concentrations that could be described by a first-order expression (Komex 2000b). Such concentration changes are classic indicators of aerobic biodegradation (Bedient et al. 1994). Thus, although the research program appeared to be successful in reducing the processing chemical concentrations, the focus became to monitor biodegradation in a de-watering/bioventing framework to address the invasion of groundwater into the horizontal well/fracture network. This was accomplished by characterizing the transient concentrations of the contaminants and their degradation products in the aqueous phase.

From three major sampling programs up until May 1999, trends in chemical concentration were very much indeterminate. For example, although MEA concentrations in some piezometers were reduced after dewatering, the reduction attributable to either biodegradation or recharge/dilution was unknown (Komex 2000b). Also, MEA concentrations in some piezometers increased in this area following dewatering, suggesting that the dewatering was not impacting the entire source area or that additional leaching was occurring.

Thus, a more comprehensive site characterization was required to evaluate groundwater conditions at the site. Due to the heterogeneity of the subsurface, the distribution and behaviour of groundwater was difficult to characterize. Site activities, such as hydraulically fracturing the medium, exacerbated this difficulty by altering groundwater behaviour in selected areas of the site. Future site investigations had to distinguish between characterizing either the site as a whole or specific areas of the site. For example, of the field methods described in the following chapter, meteorological data was collected to characterize the site as a whole, while dewatering activities were designed specifically to determine the range of hydraulic influence of the area near the horizontal well only.

CHAPTER 3

FIELD AND LABORATORY METHODS

3.1 Timeline of Field Instrumentation

The installation of monitoring infrastructure and data collection equipment began in July 1999 and continued until October 2001. The new installations were designed to answer specific research questions for the GPRP. A schedule of the installations and operations is presented in Table 3-1. The instrumentation is described in further detail in the coming sections.

Instrumentation	Installation Date(s)
6 multi-level and 3 single piezometers	July 1999
3 neutron probe access pipes	July 1999
3 multi-level vapour monitoring installations	July 1999
8 submersible pressure transducers	October 1999
1 sump pump for trench/culvert hydraulic testing	October 1999
1 meteorological station with Handar 555 datalogger	November 1999
1 vacuum pump for dewatering operations	July 2000; June 2001
2 thermistor strings of 6 thermistors each with Campbell Scientific 21-X dataloggers	temporary: July 2001 permanent: October 2001

Table 3-1 Deployment schedule of instrumentation at the GPRS.

3.2 Data Acquisition

The storage frequency of data from the logged instruments depended on the temporal resolution required of the data. There were three general ways in which automated data was acquired:

- A sensor was programmed to give a single measurement at the end of a given time interval. The pressure transducers were programmed this way, logging water pressure values every 15 minutes. This permitted flow transients on 15 minute intervals to be resolved, rather than smoothed if an average was taken over longer time intervals;
- A sensor was programmed to output an hourly averaged value. This was accomplished by taking readings at short time intervals (e.g. 15 s), and then logging the average of these readings at the end of the hour-long interval. The meteorological instruments were programmed this way because the measured parameters were not expected to vary greatly over the hour-long interval. Furthermore, many calculations involving the meteorological data require hourly averages; and,
- A sensor was an event-based sensor. This was the case with the tipping-bucket rain gauge, which recorded 2 mm accumulations of precipitation as they occurred and summed the accumulations hourly.

Many parameters were measured manually, not only to obtain data that were not being recorded automatically, but also to supplement and verify the data collected automatically. The predominant manual measurement obtained was water levels with a sounding tape at each piezometer. Manual measurements, the primary reason for many site visits, were performed approximately weekly, at which times the dataloggers were downloaded.

3.3 Meteorological Monitoring

3.3.1 Monitoring at the GPRS

An automated meteorological station (Figure 3-1) was installed to enable the quantification of site-specific water fluxes between the atmosphere and the subsurface. The station was instrumented to quantify the major input/output of water to/from the system: precipitation and evapotranspiration. Table 3-2 summarizes the instrumentation included with the meteorological station.

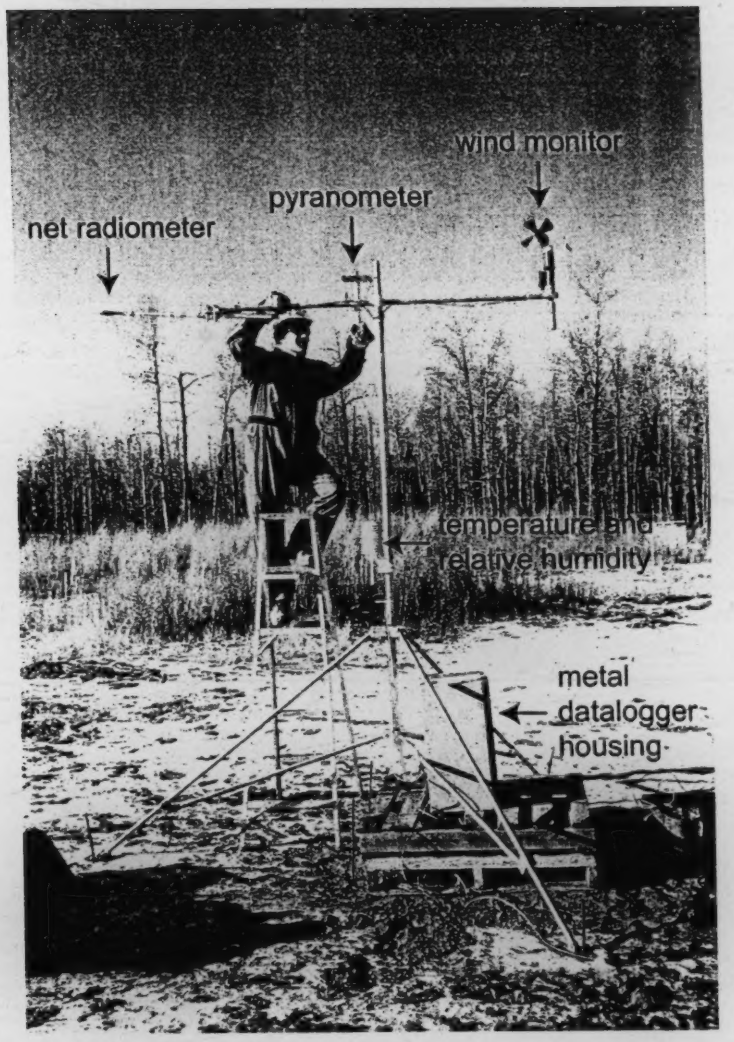

Figure 3-1 The automated meteorological station installed at the GPRS.

The station was installed on level ground at the centre of the site, away from obstructions that might interfere with data acquisition. The sensors were installed at heights suggested to obtain representative measurements (Campbell Scientific 1994). The surrounding ground surface and vegetation shown in Figure 3-1 is typical of much of the site.

Parameter measured	Sensor
Air temperature and relative humidity	Vaisala HMP 35A Relative Humidity and Temperature Probe, in R.M. Young 41004-5 Radiation Shield
Net radiation	REBS Q7.1 Net Radiometer
Incoming solar radiation (global)	Li-Cor 200SZ Pyranometer
Wind speed and direction	R.M. Young Model 05103 Wind Monitor
Precipitation (unfrozen)	Hydrological Services Pty. Ltd. TB-3 Tipping Bucket Rain Gauge
Barometric pressure	Vaisala PTB 100B Analog Barometer

Table 3-2 Meteorological instrumentation installed at the GPRS.

Prior to installation, the instruments were repaired and recalibrated by their respective manufacturers. The barometer was installed on November 17, 1999 while the remaining instruments, except the rain gauge, were installed on November 24, 1999. The rain gauge was installed the following spring.

Most of the instruments were mounted on a 3 m tall Campbell Scientific CM10 tripod (Figure 3-1). The barometer was placed inside the metal box housing the Handar 555 datalogger while the rain gauge was mounted on steel pipe 5 m from the meteorological station approximately 1 m off the ground. The temperature-relative humidity sensor was fastened directly to the tripod, while the wind sensor and the radiation sensors were attached to a Campbell Scientific 019ALU cross-arm sensor mount, with the wind sensor to the north and the radiation sensors to the south (Figure 3-1).

The datalogger housing was mounted on a wooden palette to avoid electrical and data acquisition problems from surface water entering the box. The CM10 tripod and palette were held in place by rebar stakes. The datalogger and the meteorological instruments were powered by a deep-cycle, 12V lead-acid battery

that was housed in the storage shed on-site. A 2A float charger recharged this battery when necessary.

3.3.2 Other Meteorological Data

Other meteorological data were obtained to confirm the quality and to supplement data collected at the GPRS. GPRS data were periodically not available due to equipment malfunction or instruments being sent for repairs and/or recalibration. The additional data were obtained from:

- The Breton Plots Research Station, an agricultural research station operated by the Department of Renewable Resources of the University of Alberta approximately 25 km NW of the GPRS. Data obtained included air temperature, relative humidity, wind speed and direction, precipitation and incoming solar radiation; and,
- The Edmonton International Airport, as acquired by Environment Canada, approximately 50 km NE of the GPRS. Although a variety of data were available, only barometric pressure and air temperature data were acquired from this station.

3.4 Variably-Saturated Zone Monitoring and Testing

Shallow soil is not always saturated. This modifies the effective conducting pore space of the medium, thus modifying the water transmission characteristics of the soil (Tindall and Kunkel 1999). At the GPRS, it was important to describe the spatial and temporal distribution of soil moisture to determine the significance of variably saturated processes in the shallow subsurface.

3.4.1 Neutron Probe

To measure in-situ soil moisture at the GPRS, a neutron probe soil moisture meter was used. To enable this measurement, three 316 grade, Schedule 40

stainless steel tubes of 5 m length, 0.05 m inner diameter (I.D.), supplied by Atlas Alloys of Edmonton, were installed. The bases of the tubes were sealed with a plain steel, beveled cap that provided a watertight base and helped displace soil during installation. The tubes were installed in 3 locations (Figure 2-4):

- N99-1 by the pad near the northwest corner of the site (to 5 m bgs);
- N99-2 in the zone containing the horizontal well (to 4 m bgs); and,
- N99-3, south of N99-2, closer to the west runoff pond (to 4 m bgs).

The access tubes were installed on July 21, 1999 using TerraTest Drilling's (Cochrane, Alberta) direct push rig. The steel pipes were installed to ensure optimal contact with the borehole walls. Boreholes of 0.056 m diameter were drilled, and then the 0.06 m outer diameter (O.D.) pipes were pushed into the hole with the direct push rig's hydraulic jacking system.

The field measurement scenario of the neutron probe is depicted in Figure 3-2. The instrument consists of two main components: a shielded main housing, which hosts the associated electronic assembly, and a probe that contains a radioactive source of high energy neutrons and a detector of low energy (thermal) neutrons. The source is lowered into the cased borehole at user specified depths to take bulk soil moisture measurements.

When the probe is activated, high energy neutrons are emitted into the surrounding soil. These neutrons elastically collide with the surrounding hydrogen nuclei, lose some of their energy, and scatter (Hillel 1982). As the neutrons collide and scatter, the probe detects an amount of low energy neutrons proportional to the soil moisture content. These are counted over measured time intervals and are converted to a measure of moisture content based on laboratory and/or field calibration.

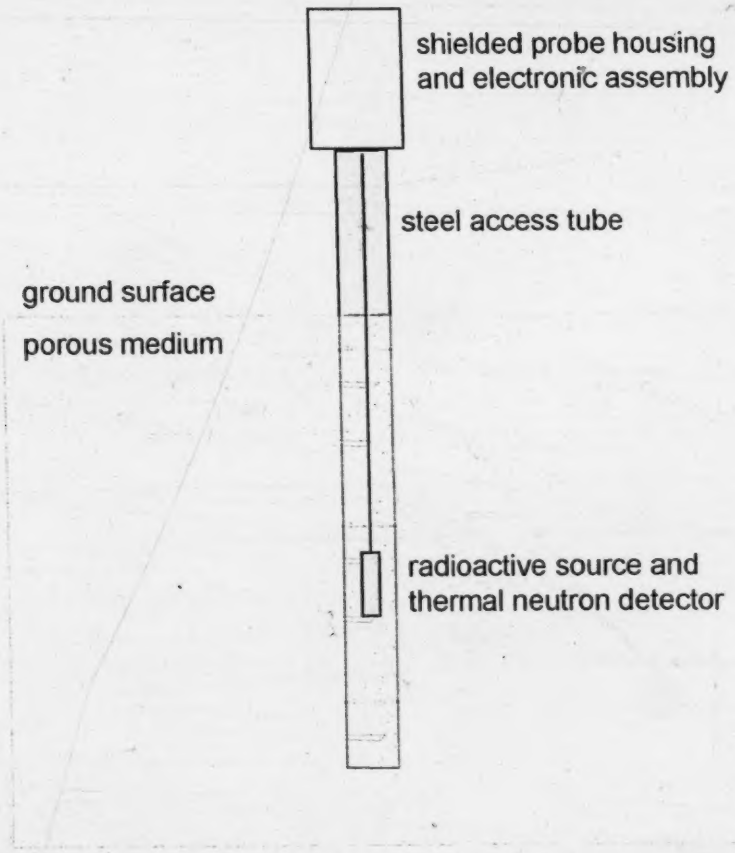

Figure 3-2 Field measurement scenario for a neutron probe soil moisture meter.

The main probe used at the GPRS was a CPN 503 DR Hydroprobe Moisture Depth Gauge, labelled "DSC". Staff in the Department of Renewable Resources at the University of Alberta own and previously experimentally calibrated the probe. The same probe was used each time the soil moisture was measured and at consistent depths in each of the three access tubes (0.1 m intervals, beginning at 0.25 m bgs to the bottom of the tube) to maintain a consistent sampling protocol.

On August 27, 1999, a CPN 501 DR Hydroprobe, labelled "Department 501", capable of measuring soil moisture and in-situ wet bulk density, was used to

verify the moisture measurements of the DSC probe and to collect data allowing the subsequent determination of in-situ dry bulk density. Bulk density is measured by methods similar to soil moisture measurement, except that gamma radiation is emitted and detected by the density probe.

During borehole drilling for the neutron probe access tubes, soil cores were taken and moisture contents were determined by Komex International Ltd. as a means of calibrating the field values collected by the probe (Komex 2000a). There were problems encountered with correlating moisture contents with depth because of sample compaction, borehole flooding when drilling and the interference of woody, organic material in the moisture content determination (Komex 2000a). Therefore, the previous laboratory calibration was used to determine a time-series of soil moisture contents.

3.4.2 Soil-Water Characteristics

The volumetric soil moisture content and the matric potential of soil water for a given soil are functionally related by the soil-moisture characteristic curve, the primary constitutive relationship in describing unsaturated flow (Barbour 1998). Capillary pressure versus saturation relationships were determined for eight samples in the laboratory. Bulk samples were taken from auger flights during the drilling of borehole U99-1 (Figure 2-4) on July 7, 1999. The samples were from regular sampling intervals, the first being from a depth of 0 m to 0.5 m, the second from a depth of 0.5 m to 1 m, and continuing in this manner to a depth of 4 m.

Soil-moisture characteristic drying curves were measured with Soilmoisture Equipment Corporation's 5 and 15 bar Pressure Plate Extractors. The experimental set-up is depicted in Figure 3-3. The principles implemented in these instruments were developed in the early 1900's (Barbour 1998). They bring a thin soil specimen to thermodynamic equilibrium with a known matric potential of water in applied increments.

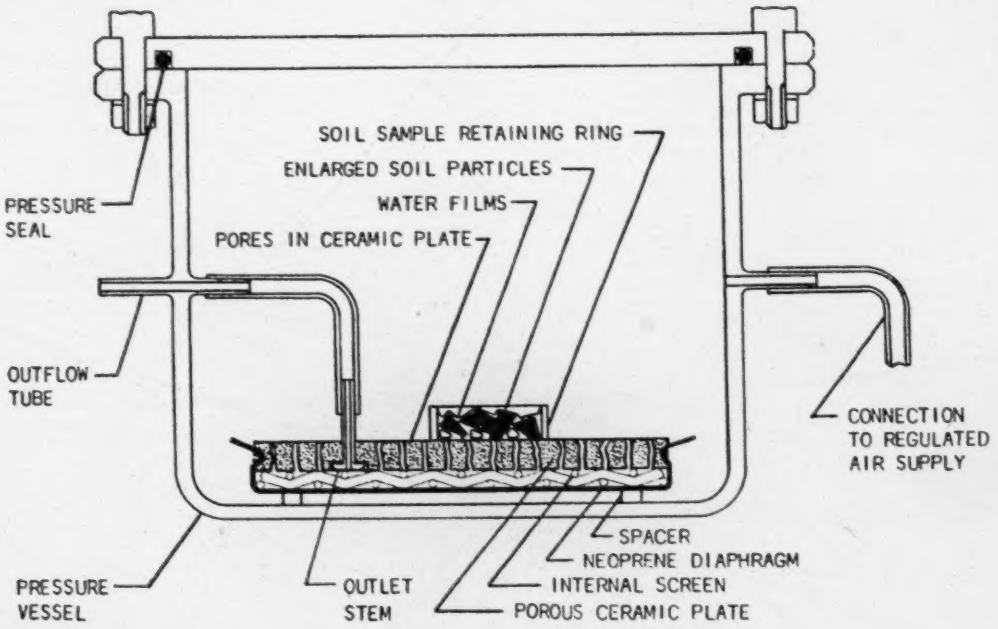

Figure 3-3 The components of a pressure plate extractor to measure soil-moisture characteristic curves (modified from Soilmoisture Equipment Corporation).

The main components (Figure 3-3) and generalized procedure for obtaining soil-moisture characteristics are (Fredlund and Rahardjo 1993):

- A high air-entry porous ceramic plate was saturated and maintained in contact with a reservoir of distilled water at zero water pressure;
- 10 cm^3 soil samples were placed on the pressure plate in retaining rings and the chamber was pressurized by an externally regulated air supply. The air pressure applied was equal to the matric suction because the pore-water was maintained at zero pressure. Applied pressures were 0.1 bar, 0.33 bar, 1 bar and 15 bar to determine how soil moisture varied over a large range of suction;

- Pore-water drained out the outflow tube until the reduced, equilibrium water content was reached. This water content was measured gravimetrically following the method of Gardner (1986) and related to the applied matric suction to construct capillary pressure-saturation curves.

The difference in mass between the moist and dry samples is the mass of water in the soil sample at equilibrium with a given matric suction. The ratio of the mass of water (M_{water}) to the mass of dry soil (M_{soil}) is the gravimetric moisture content of the sample (θ_g):

$$\theta_g = \frac{M_{water}}{M_{soil}} \tag{3-1}$$

To enable comparison to neutron probe measured values, the gravimetric moisture contents were converted to volumetric moisture contents (θ_v). The relation between gravimetric and volumetric moisture content is (Hillel 1982):

$$\theta_v = \left(\frac{\rho_{dry}}{\rho_{water}} \right) \theta_g \tag{3-2}$$

where ρ_{dry} is the dry bulk density of the soil and ρ_{water} is the density of water. Dry bulk density was assumed from literature values for specific soil textures. The density of distilled water is normally assumed to be 1000 kg/m^3.

3.4.3 Guelph Permeameter

A Guelph permeameter (Figure 3-4) was used to measure the field saturated hydraulic conductivity (K), which can be related to the unsaturated hydraulic conductivity, $K(\psi)$. The measurement method, briefly described here, is described in detail by Reynolds and Elrick (1986):

Figure 3-4 A field setup of the Guelph permeameter.

- An uncased, cylindrical well of known radius is completed in the unsaturated zone;
- A constant head is established in the well. The rate of steady-state recharge from a reservoir, the Mariotte bottle (Figure 3-4), required to maintain the constant head is measured;
- The procedure is repeated several times with different constant heads in the well to obtain an average value for the steady-state recharge required to maintain a constant head in the well;

- The steady-state recharge value is used to calculate, by tested theoretical relationships, parameters related to K_{fs} in the vadose zone.

The permeameter was used in the field on October 20, 1999. Wells were established in two locations: one near the horizontal well research zone and one near the pad in the northwest corner of the site (Figure 2-4). The wells were completed to a depth of 20 cm with the auger provided (6 cm cutting diameter) with the permeameter assembly from Soilmoisture Equipment Corporation. The well prep brush provided with the assembly was used to attempt to remove any smeared clay layers that may have been formed during augering of the well.

3.5 Groundwater Monitoring and Testing

3.5.1 1999 Piezometer Installations

Borehole drilling for piezometer installations occurred on July 6 and 7, 1999 (Komex, 2000a). A total of 20 piezometers were installed. On July 6, TerraTest Drilling (Cochrane, Alberta) conducted drilling with a direct push rig. Due to mechanical problems, this rig was unable to penetrate the till to sufficient depth to be useful for a multi-level piezometer installation. Only two shallower single piezometers were installed near the southwest corner of the site (P99-7 and P99-8) (Figure 2-4). These piezometers have 1.5 m screen intervals to ensure that they intercept the shallowest unit that bears water.

On July 7, a truck-mounted B61 continuous-flight auger rig operated by SPT Drilling (Edmonton, Alberta) was used to complete the drilling of boreholes for piezometer installations. Six multi-level piezometer nests (P99-1A/B/C, P99-2A/B/C, P99-3A/B/C, P99-4A/B/C, P99-5A/B/C and P99-6A/B) and one single piezometer (P99-9) were installed around the perimeter of the site (Figure 2-4). This naming of piezometers indicates the year the piezometers were installed (i.e., 1999), the location number and a letter signifying relative depths (i.e., A = shallowest, B = deeper and C = deepest).

The piezometers labelled C, and P99-6B, were constructed using 0.05 m diameter Schedule 40 PVC pipe, while those labelled A and B (except for P99-6B) and the individual piezometers, P99-7 to P99-9, were constructed of 0.025 m diameter Schedule 40 PVC pipe. The screened intervals on the P99-1 to P99-6 piezometer nests were 0.3 m to provide discrete monitoring intervals.

Each piezometer in a nest was completed by threading plain sections of the PVC pipe to the slotted section and then lowering the entire assembled complex to the desired monitoring depth. Frac sand filled the borehole around the screen and to 0.1 m above the screen. A layer of bentonite pellets 0.1 m thick was placed immediately above the sand layer and hydrated to seal the piezometer screen at the desired depth. The borehole space, up to the next screened interval, was filled with bentonite chips and crumble, and then hydrated. A 0.1 m thick layer of frac sand was used to seat the next string of pipe sections. Borehole logs and piezometer construction details are provided in Komex (2000a). The piezometer installations are summarized in Table 3-3.

3.5.2 Other Piezometer Installations

There have been a total of 61 piezometers installed at the GPRS since remediation activities began in 1997 (Komex 2002). Other than the 20 piezometers installed for this project (section 3.5.1), installations by others were as follows (Figure 2-4):

- 27 in the horizontal well research area (97-1 to 97-13; 98-4);
- 6 in the raised pad (former processing) area (HP series; 98-1 and 98-3);
- 8 to assess conditions elsewhere on the site (00-1 and 00-2; 01-1A to 01-3A; both series are not depicted in Figure 2-4)

Piezometer Number	Depth (mbgs)	Ground Elevation (masl)	Location (Figure 2-4)
99-1A/B/C	3.0/6.1/9.0	890.25	N corner of site
99-2A/B/C	2.0/4.0/5.8	887.90	NW of horizontal well, west end
99-3A/B/C	2.0/4.0/5.8	886.72	S of horizontal well, west end
99-4A/B/C	2.0/3.8/5.7	886.74	S of fractured area
99-5A/B/C	1.9/4.0/6.1	888.94	E of raised pad
99-6A/B	2.9/6.1	890.43	NE of raised pad
99-7	3.7	886.70	In N tank berm
99-8	2.7	886.01	In S tank berm
99-9	2.4	889.87	W of storage shed

Table 3-3 Summary of 1999 piezometer installations (Komex 2000a).

As previously described, the 1997 and 1998 series of piezometer nests were installed to evaluate the effectiveness of bioventing in the fractured horizontal well configuration. The 1997 series of piezometers were of 0.05 m diameter Schedule 40 PVC and had screened sections of 1.5 m. The 1998 series of piezometers were of 0.025 m diameter Schedule 40 PVC and had screened intervals of 2.4 m. All of these piezometers were completed in a manner very similar to that described for the 1999 piezometers. Installation details and borehole logs for the 1997 and 1998 series are described in Komex (2000b).

There is very little information regarding the installation or construction details of the HP series of piezometers. The bottoms of these piezometers are at approximately 6 m bgs. The screen interval is unknown, but is thought to be large and straddle the shallow groundwater bearing interval. The 2000 and 2001 series of piezometers were not used in this study.

Two vertically oriented culverts were also installed at the GPRS. A 0.3 m diameter, Schedule 40 PVC culvert was installed concurrently with a geomembrane and weeping tile (Figure 2-4) that were part of an excavation and backfilling project (Komex 2000b). Also, a 0.5 m diameter metal culvert was installed in the raised pad area (Figure 2-4). This culvert is connected to a 10 m long gravel trench, which is oriented approximately northwest-southeast. There are no details available on the construction details of the trench and culvert, or about the extent to which they were used in potential remediation scenarios.

3.5.3 Water Level Measurements

3.5.3.1 Manual Water Level Measurements

There were two purposes for obtaining manual water level measurements with a Solinst Model 101 Water Level Meter:

- To obtain a time series of hydraulic head measurements at each relevant piezometer at the GPRS; and
- To verify the automated hydraulic head measurements recorded by pressure transducers.

A consistent sampling protocol was vital to interpreting time-varying hydraulic heads. The datum from which the water level was measured at each piezometer was the highest point on the well casing. Water levels were measured to the nearest mm by repeatedly lowering and lifting the meter in and out of the water. In the most impacted areas of the site, it was necessary to decrease the sensitivity of the water level meter or it would continuously ring, even when not in the water.

Water levels were generally measured in each monitoring well each time that the site was visited. Exceptions to this included:

- When there was equipment in the piezometer that would not allow insertion of the water level probe. This included piezometers with vacuum lines inserted during dewatering operations and piezometers with transducers. The transducers could not be removed when the ambient air temperature was less than 0°C so that the transducer electronics would not be damaged;
- When the air temperature was below 0°C, some piezometers developed ice accumulations near the ground surface; and,
- When piezometers were inaccessible due to concurrent site activities. Two piezometers (P99-7 and P99-8) were destroyed during site excavation activities in the fall of 2001.

3.5.3.2 Automated Water Level Measurements

Submersible pressure transducers were installed in piezometers and culverts at the GPRS to provide hydraulic head and temperature measurements at selected points at a higher temporal resolution than could be provided by manual measurements. They were also installed to correlate hydraulic head response to meteorological data. In total, eight H_2OFX Model H-310 Submersible Pressure Transducers (Figure 3-5) were installed at the GPRS. Transducer locations are summarized in Table 3-4. Installation locations were limited based on their proximity to the datalogger because of the short cable lengths used to avoid potential degradation of the electrical signal at greater distances.

The transducers have a measurement range of 0 to 10.5 m of water with an accuracy of ±0.02 %. A vented cable (Figure 3-5) provides connection between the transducers and the atmosphere, and thus the transducer measures gauge (water) pressure. The dry air system (Figure 3-5) ensures that the electronics do not corrode. The transducers were lowered to approximately the middle of the screened interval when they were installed, 1-2 m below the water table.

Transducer Identification	Location of Transducer (Figure 2-4)
PT-1	P97-8B: October 14, 1999 to July 12, 2000 P97-13B: from July 12, 2000 onward
PT-2	P97-2A: from October 14, 1999 onward
PT-3	P97-10B: from October 14, 1999 onward
PT-4	Collection tank near metal culvert: October 14, 1999 to January 21, 2000 HP-E: from January 21, 2000 onward
PT-5	HP-S: October 14, 1999 to July 12, 2000 HP-W: from July 12, 2000 onward
PT-6	HP-W: from October 14, 1999 to July 12, 2000 P97-6B: July 12, 2000 onward
PT-7	Metal culvert: from October 14, 1999 onward
PT-8	HP-N: from October 14, 1999 onward

Table 3-4 Pressure transducer installation locations.

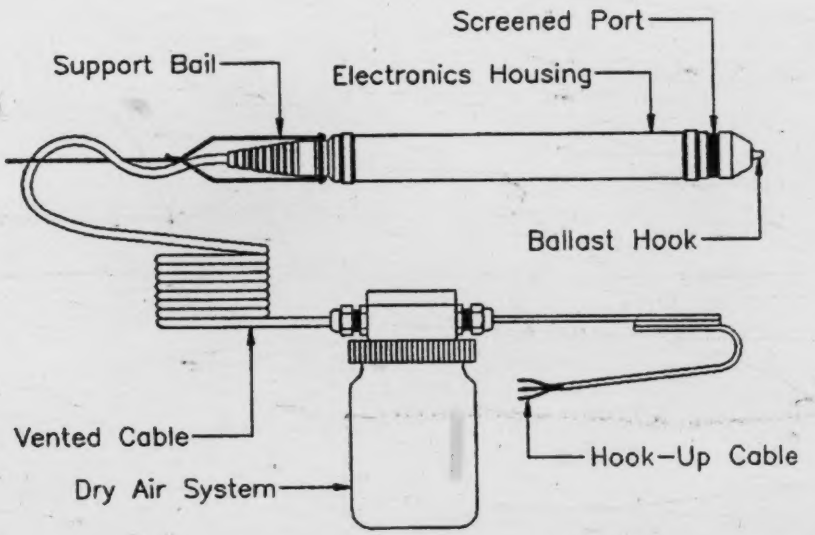

Figure 3-5 A schematic of a H_2OFX Model H-310 Submersible Pressure Transducer (modified from Design Analysis Associates, Inc.)

The transducers were connected in parallel and measurements were taken by the SDI-12 (Serial Digital Interface) command and protocol. The main advantage of having instruments connected in parallel and transmitting and receiving signals through the same signal wire is the space saved on the datalogger circuit board for other digital applications.

3.5.4 Hydraulic Conductivity Determinations

3.5.4.1 2000 Bail (Slug) Testing

To determine in-situ estimates of hydraulic conductivity, single piezometer bail tests were performed on selected piezometers. A bail, or slug, test involves measuring the static water level in a piezometer, instantaneously removing, or adding, a volume of water from/to the piezometer, and then monitoring the recovery of the water level to the static level over time (Freeze and Cherry 1979). Bail tests were performed in conjunction with the purging of piezometers before geochemical sampling.

Bail tests were performed on 11 piezometers at the GPRS (P99-1A, -1B, -1C, -2A, -4A, -4B, -5B, -5C, -6A, -6B, and -7) (Figure 2-4) on June 14, 2000. The piezometers were bailed until they were dry or until the drawdown was as close to dry as could be achieved at that monitoring point. After bailing, the recovery was monitored by taking water level readings while noting the elapsed time of the reading since the disturbance from the static water level. Piezometers were generally monitored until they recovered to approximately the static water level. At monitoring points with very slow recovery rates, the recovery was monitored as long as was practical (the length of a field visit).

To analyze the data, a semilogarithmic plot of water level displacement versus time is created, with displacement on the logarithmic axis. The data should fall on a straight line, with potential deviations at later times (Fetter 1994). To facilitate analysis, the data was imported into AQTESOLV for Windows

(HydroSolve Inc. 1996), a curve-fitting program featuring a suite of analytical solutions for slug and pumping test data. The program provided interactive visual and automated curve-fitting capabilities with several analytical solutions.

Due to the relatively small volumes of water removed, the resulting hydraulic conductivity values are interpreted as localized approximations of the field scale K distribution. The non-discrete screen interval of some of the piezometers could potentially cause interpretation difficulties. Given the heterogeneity of surficial till deposits, a field-scale estimate of hydraulic conductivity cannot be achieved by this method. Nevertheless, the results were interpreted as an order of magnitude estimate for in-situ hydraulic conductivity.

3.5.4.2 Bail (Slug) Testing Conducted by Others

Komex International Ltd. staff performed bail tests at three different times on eleven piezometers (Komex 2000b). The measurement protocol and software used were the same as those described in the previous section. The measurement dates and locations (Figure 2-4) included:

- November 21, 1997: 97-1A, -3A, -8A, -8B, -9B
- June 26, 1998: HP-E, -W
- July 14, 1998: 97-1A, -3A, -10B, -11B, HP-S

3.5.5 Dewatering Operations/ Hydraulic Testing

There have been five major periods of groundwater extraction at the GPRS since 1998. The extractions and data monitoring were a co-operative effort amongst staff of Imperial Oil Resources and their contractors, and the hydrogeology group from the University of Alberta (since 1999). There were two main purposes for groundwater extraction:

- Dewatering to enhance bioremediation; and,

- Hydraulic tests to determine porous medium properties.

Given the shift of the remediation program focus (section 2.2.3), dewatering was used to investigate the efficiency of groundwater flushing as a chemical transport mechanism (Komex 2000b). During dewatering, hydraulic head data were also collected. The hydraulic tests were performed specifically to determine the transmission and storage characteristics of various areas of the subsurface.

The periods of groundwater extraction are summarized in Table 3-5. In general, the extraction intervals were for the time period indicated in Table 3-5. However, there were intermediate periods when the pumps were stopped, for operation troubleshooting, maintenance and intentional shutdowns during groundwater sampling and geophysical measurements.

3.6 Other Installations

Other installations occurred concurrently with those described in the previous sections, although the data collected was used by other researchers.

3.6.1 Multi-Level Vapour Monitoring

To monitor subsurface concentrations of gases relevant to biodegradation (O_2, CO_2, CH_4), three nests of soil vapour samplers were installed, labelled U99-1 to U99-3 (Figure 2-4). The boreholes for the samplers were drilled at the same time as those for the 1999 groundwater monitoring piezometers on July 7, 1999 (section 3.5.1).

Type of Operation and Dates	Pump Type [Supplier]	Piezometers Tested	Data Monitored (see note)
• dewatering • 4/22/98 to 6/25/98	liquid ring vacuum pump [IWR Ltd. in Calgary, AB]	P97-8B, P97-6B, HP-W	1, 2a, 4
• hydraulic test • 10/15/98 to 10/26/98	pneumatic pump [PCT Ltd. Calgary, AB]	P97-8B	1, 2a, 2b
• hydraulic test • 10/19/99 to 1/21/00	float activated electric pump [Imperial Oil Resources]	Metal culvert, gravel trench	2a, 2b, 3a, 3b
• dewatering • 7/13/00 to 11/6/00	liquid ring vacuum pump [Hazco Environmental Services Ltd., Vancouver, B.C.]	P97-8B, metal culvert, gravel trench	1, 2a, 2b, 3a, 3b, 4
• dewatering • 6/7/01 to 10/4/01	multi-phase extraction pump with rotary lobe blower [Sequoia Environmental, Calgary, AB]	P97-4B, P97-8B, P97-10B, P97-12B	1, 2a, 2b, 3a, 3b, 4

Note: 1 = cumulative pumped volume, 2a = manual water levels, pumping, 2b = manual water levels, recovery, 3a = automated water levels, pumping, 3b = automated water levels, recovery, 4 = groundwater samples

Table 3-5 Summary of groundwater extraction at the GPRS since 1998.

Each borehole was drilled to 4 m bgs, with monitoring ports every 0.5 m, for a total of 8 monitoring ports per profile. The sampling ports comprised a Walbro 125-527 chainsaw fuel filter, with the foam removed, wrapped in nylon mesh to act as a screen. The ports had 6.35 mm O.D. polyethylene tubing running to the surface to enable withdrawal of samples via syringe. At the surface, each line

was fit with a three-way Luer lock stopcock via a short length of Tygon tubing. All ports and tubing were secured to a 19.1 mm I.D. Schedule 80 PVC pipe with cable ties. The soil vapour samplers were constructed on the surface and lowered as a unit into the borehole and then completed with sand around the sampling ports and bentonite in the intervals between ports. Installation details and borehole logs can be found in Komex (2000a).

3.6.2 Thermistor Strings

To provide profiles of subsurface temperature, two thermistor strings were installed at the site on October 10, 2001 in conjunction with a soil sampling and piezometer installation program. The temperature measurements are relevant to geophysical projects, vapour and groundwater transport, and microbiological activity.

Each of the strings was constructed with six thermistors designed to give a temperature profile up to 4 m bgs. The thermistors were standard precision (± 0.2°C) from RST Instruments Ltd. (Coquitlam, B.C.) The thermistor strings were housed in 25.4 mm I.D. Schedule 40 PVC pipe. Campbell Scientific 21-X dataloggers recorded temperature measurements by relating resistance measurements to a manufacturer-provided calibration curve.

CHAPTER 4

FIELD AND LABORATORY RESULTS AND DISCUSSION: METEOROLOGICAL AND VARIABLY-SATURATED ZONE CONDITIONS

Field and laboratory data, as described in the previous Chapter, were collected to develop site-scale conceptual models of groundwater flow. The information was used to:

- Define hydrostratigraphic units;
- Quantitatively define the properties of the porous medium and surrounding environment; and,
- Quantitatively define water fluxes in space and time.

These conceptual models were implemented into numerical groundwater models to enhance the interpretation of site-scale groundwater flow derived from the analysis of field and laboratory data. Conceptual model development is described in this Chapter and Chapter 5, while numerical groundwater modelling is described in Chapter 6. All of the field data collected and analyzed, along with base case modelling scenarios, can be found in Appendix A.

4.1 Meteorological Conditions

The meteorological data were analyzed in three ways. Firstly, data from the GPRS and the other locations (Breton Plots and Edmonton International Airport) were compared to ensure that the instruments at the GPRS were collecting representative data. If not, data from one of the other locations was used as a surrogate in the quantification of water fluxes. Secondly, meteorological data provided a means of comparing short-term site data to historical, regional data to determine whether the meteorological conditions deviated from statistical

normals during the study period. Thirdly, the data were used to estimate evapotranspiration at the site for both vegetated and bare soil conditions.

4.1.1 Data Analysis and Selection

Site-specific data were collected from late 1999 until the end of 2001 (Table 3-1). There were three potential outcomes for data use:

- The data were deemed inadequate for the entire time period;
- The data were deemed inadequate for periods during the study, but were valid during other times; or,
- The data were deemed valid for the entire time period.

Ambient air temperature data were deemed inadequate for the entire study period because the temperature probe never recorded realistic numbers. This was attributed to equipment malfunction, incorrect calibration or incorrect connection to the datalogger. Representative air temperature data were obtained from the Breton Plots Research Station for the duration of the study.

The barometric pressure data from the site were also found to be unsatisfactory. Compared to data acquired from the Edmonton International Airport, the site barometer appeared to record anomalous increases in pressure when the barometric pressure increased (Figure 4-1). However, barometric pressure patterns from the site and the airport were nearly coincident if the apparently anomalous rises recorded by the site barometer were discounted (Figure 4-1). Therefore, the barometric pressure data recorded at the airport were deemed representative for the site.

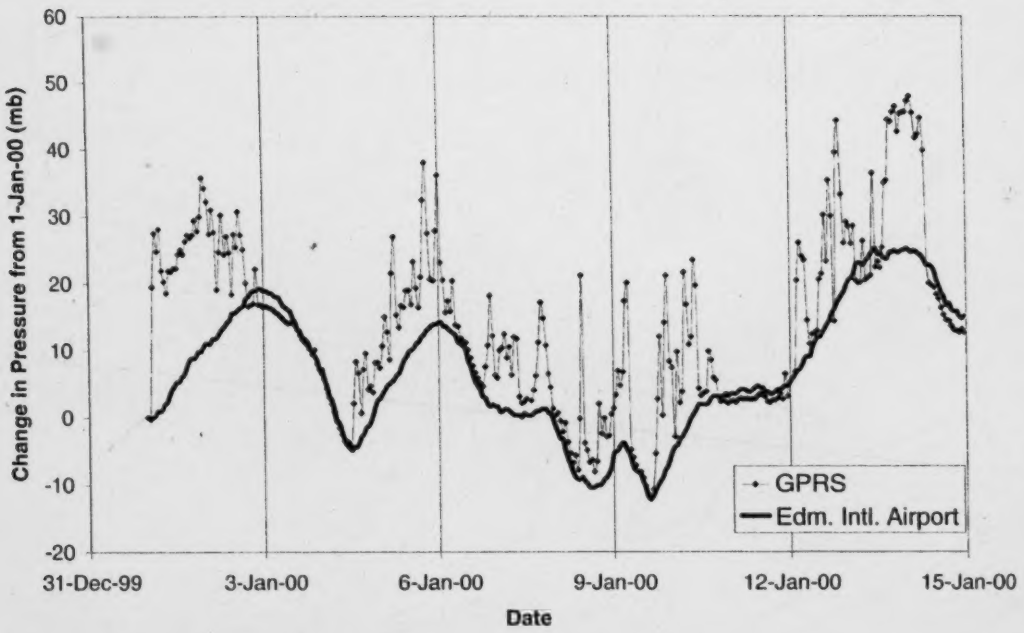

Figure 4-1 Hourly barometric pressure from the GPRS and the Edmonton International Airport, January 1 to 14, 2000.

The instruments that provided valid data for a portion, but not the entire period, of the study include the pyranometer, net radiometer, and relative humidity sensor. Like the barometer, the pyranometer seemed to record anomalously large rises in incoming solar radiation, from December 2000 to April 2001 and a small part of September 2001 (Figure 4-2). Solar radiation data were augmented by pyranometer data from the Breton Plots during those periods. The other radiation instrument, the net radiometer, also periodically displayed large fluctuations in its recorded data. Evapotranspiration calculations required either net radiation or total incoming solar radiation, and therefore, pyranometer data was used in the evapotranspiration estimates. The relative humidity sensor was functioning properly for the entire study period, except for a period of repair and recalibration from April to August 2001.

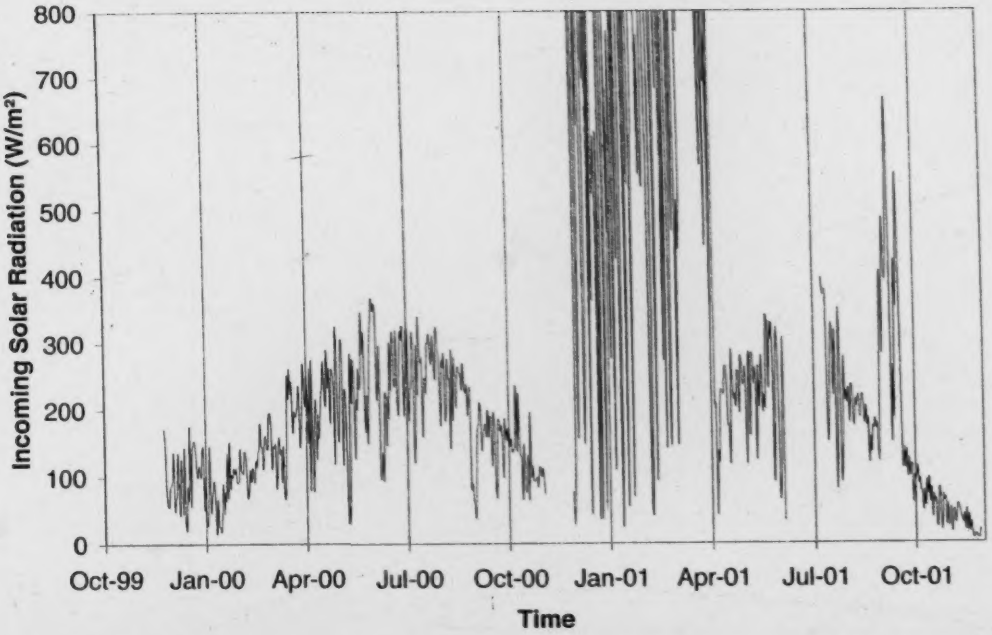

Figure 4-2 Average daily incoming solar radiation at the GPRS, November 1999 to November 2001.

Parameter	2000	2001
Air temperature (°C)	3.0[2]	4.3[4]
Relative humidity (%)	59	46*
Precipitation (rain) (mm)	494	404
Barometric pressure[3] (kPa)	93	93*
Incoming solar radiation[1] (W/m^2)	159	143
Wind speed (m/s)	2.4	3.1
Wind direction (°)	209	198

1= GPRS supplemented by Breton, 2= Breton supplemented by Airport, 3= Airport (pressure data not corrected to sea level), 4= Breton, *= incomplete dataset

Table 4-1 Mean annual meteorological parameters for representative data collected at the GPRS in 2000 and 2001.

The instruments that provided valid data for the duration of their installation at the GPRS included the tipping bucket rain gauge and the anemometer (wind speed and direction). Annually averaged results for representative data for 2000 and 2001, the most complete years of data acquisition, are summarized in Table 4-1.

4.1.2 Historical and Spatial Comparison

The two parameters, among those measured at the GPRS, that are the most often reported as indicators of regional climate are temperature and precipitation (Briggs et al. 1993). The mean annual temperature recorded in the Western Alberta High Plains (at Rocky Mountain House) is 1.6°C (Tokarsky 1971) and the mean annual precipitation is 400 to 500 mm (Dzikowski 1990). Table 4-1 shows that these regional values are representative of the mean annual temperature and precipitation recorded at the GPRS.

A more complete description of regional climate can be obtained by analyzing all of the parameters measured in Table 4-1 (Briggs et al. 1993). It is also important to consider the elements of climate on different timescales and at the appropriate spatial scale. Monthly mean temperatures for 2000 for the Breton Plots and the Edmonton International Airport are displayed in Figure 4-3, while the monthly precipitation from the Breton Plots and the GPRS are displayed in Figure 4-4.

Monthly observations reveal the seasonal nature of temperature and precipitation, which is of vital importance to water budget calculations. Also, although the monthly patterns at different locations in the region are similar, there are some noticeable variations, even though the stations are less than 100 km apart. For example, airport data can be negatively influenced by the local aridity (Allen 2000a). Therefore, it seemed important to use site-specific meteorological data whenever possible to develop the most accurate description of climate for the GPRS.

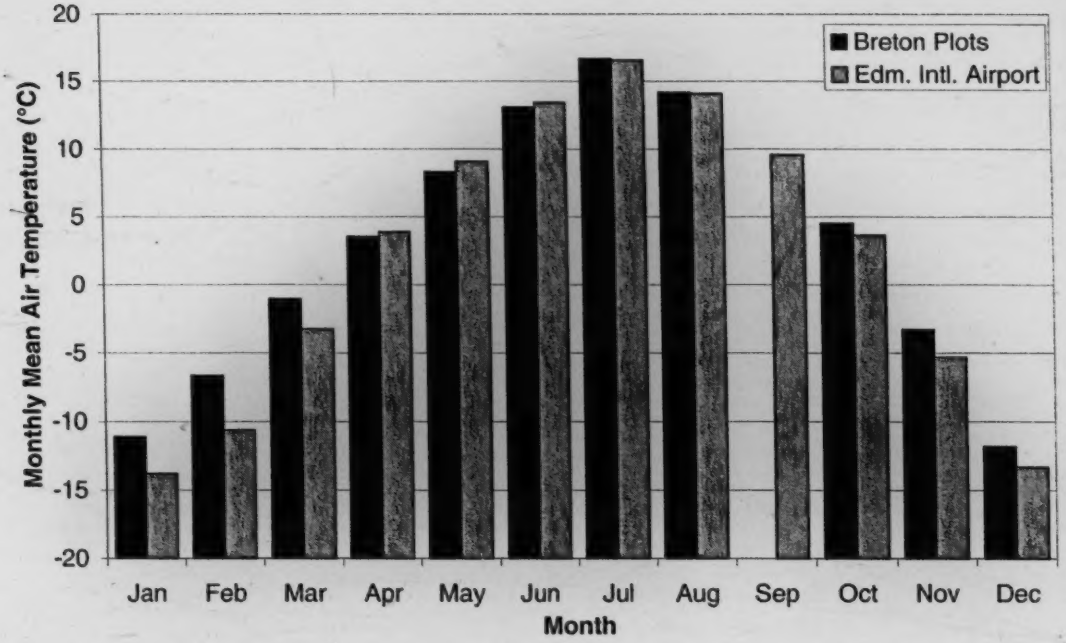

Figure 4-3 Monthly mean air temperatures recorded in 2000 at the Breton Plots and the Edmonton International Airport.

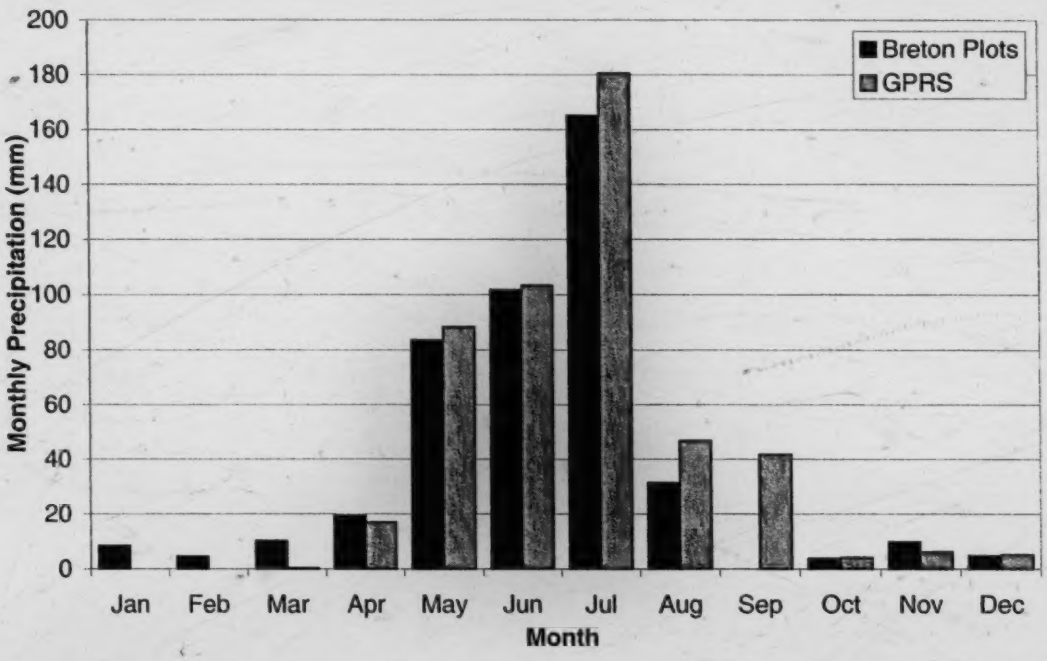

Figure 4-4 Monthly precipitation (rainfall) recorded in 2000 at the Breton Plots and the GPRS.

4.2 Water Budget Components

4.2.1 Precipitation and Groundwater Recharge

Although groundwater recharge can refer to water reaching the saturated zone from any direction (down, up or laterally) (Scanlon et al. 2002), the main focus of the investigations at the GPRS was "the volume of water that crosse[d] the water table and [became] part of the groundwater flow system" (Anderson and Woessner 1992). Groundwater recharge is often defined as a boundary condition in numerical models and thus its determination is a key component of field-based studies.

There are no universally applicable methods for estimating groundwater recharge. Although a variety of methods have been tested and reported (e.g., Lerner et al. 1990; Scanlon et al. 2002), the results are often problem dependent (de Vries and Simmers 2002) and cannot be applied even to other apparently similar sites. This is not surprising given that practitioners have found recharge to be dependent on many factors, including climate, geology, morphology, soil condition and vegetation (de Vries and Simmers 2002). Recharge estimates are also dependent on both the spatial and temporal scales at which they are measured (Scanlon et al. 2002), which ultimately depend on the purpose of the study, including numerical modelling goals.

The determination of recharge (i.e., a surface boundary flux) requires the analysis of how much precipitation enters the saturated zone. Many modelling practitioners define a spatially uniform recharge value as some percentage of the mean annual rainfall (Anderson and Woessner 1992). There is usually not enough hydrogeologic information to justify the zonation of recharge. This is especially true in heterogeneous prairie tills, as the response to precipitation is highly spatially variable (Keller et al. 1988). Groundwater models can be used to constrain the distribution and rate of recharge if other modelling parameters have been determined in sufficient detail (Sanford 2002).

Given the abundance of acquired precipitation and groundwater level data, the field-based method to be employed to estimate recharge is the water table fluctuation (WTF) method (Healy and Cook 2002). Estimation techniques based on groundwater level data are among the most widely used, dating back to the early part of the 20th century, because of the wide availability of data and the ease of implementation. The WTF method will be described when groundwater level data are analyzed in Chapter 5.

4.2.2 Evapotranspiration

Evapotranspiration refers to the processes, at or near the surface of the earth, that transform liquid water to gaseous atmospheric water (Dingman 1994). Evapotranspiration is the major output of water from groundwater systems in all but extremely humid and cool climates (Fetter 1994), exceeding even runoff in most major river basins (Dingman 1994). For the most accurate model implementation, evapotranspiration is usually incorporated as a mixed-type boundary condition, representing some type of interaction with recharge and/or surface water boundaries (Sanford 2002).

Generally, two types of evapotranspiration are calculated: potential evapotranspiration and actual evapotranspiration. Potential evapotranspiration is the maximum evaporation rate from a surface that is not limited by water supply (Dingman 1994). This concept was originally developed as part of a climate classification scheme that assumed evapotranspiration depended only on climate. The concept may be suitable for open water or fully saturated surfaces; however, actual evapotranspiration from soil surfaces is known to depend on several surface characteristics (Dingman 1994) and occurs at rates that are much less than the potential rate (Wilson et al. 1994).

4.3 Calculation of Evapotranspiration at the GPRS

To quantitatively estimate evapotranspiration at the site, the dual crop coefficient method was applied (Hatfield and Allen 1996; Allen et al. 1998). The dual crop coefficient method is represented by:

$$ET_c = K_c ET_o \quad (4\text{-}1)$$

and

$$K_c = K_{cb} + K_e \quad (4\text{-}2)$$

where ET_c represents evapotranspiration under standard field conditions, ET_o is the reference, or potential, evapotranspiration from a surface not short of water and K_c is the crop coefficient. K_c can be further refined into a basal crop coefficient (K_{cb}) and a soil evaporation coefficient (K_e). The calculation of ET_o for the 2000 field season is described, followed by the calculation of ET_c, which is the basis of evapotranspiration estimates used in numerical groundwater modelling.

4.3.1 Reference Evapotranspiration (ET_o) Calculation Methods

There are several methods to calculate reference evapotranspiration. The methods may be classified on the basis of their data requirements (Dingman 1994):

- Temperature-based methods use only temperature and, sometimes, day length;
- Radiation-based methods use net radiation and air temperature;
- Penman-combination methods use net radiation, air temperature, wind speed and relative humidity; and,
- Pan methods use pan evaporation, sometimes with modifications for wind speed, air temperature and humidity.

For this study, each of a temperature-based (Hargreaves 1985), radiation-based (Priestley and Taylor 1972), and two Penman-combination methods (Wright 1982, 1996; Allen et al. 1998) were chosen to calculate and compare ET_o.

Based on the results of consultations with evapotranspiration researchers in May 1990, the Food and Agriculture Organization of the United Nations recommended that the Penman-Monteith (FAO-56 PM) method be the sole method for calculating ET_o (Allen et al. 1998). The Kimberly-Penman method (Wright 1982, 1996) was chosen to show how Penman-combination ET_o might vary with a different wind function. Details on the calculation of ET_o can be found in Appendix B.

4.3.2 Reference Evapotranspiration (ET_o) Results

The daily average ET_o for each month, together with the 6-month sum of ET_o, is presented in Figure 4-5, while the daily ET_o for a selected month (June) is presented in Figure 4-6.

Although no independent estimates of evapotranspiration were available, White (1997) concluded for a similar study, approximately 100 km to the south of the GPRS, that ET_o calculated with the Penman (1948) method agreed with measured pan evaporation data from the region for the months of April to September 1996. The monthly averaged FAO-56 PM ET_o values presented in Figure 4-5 compare well with the monthly averages calculated by White (1997) (3-5 mm/d). Therefore, it is assumed that ET_o calculated by the FAO-56 PM is representative of local reference evapotranspiration.

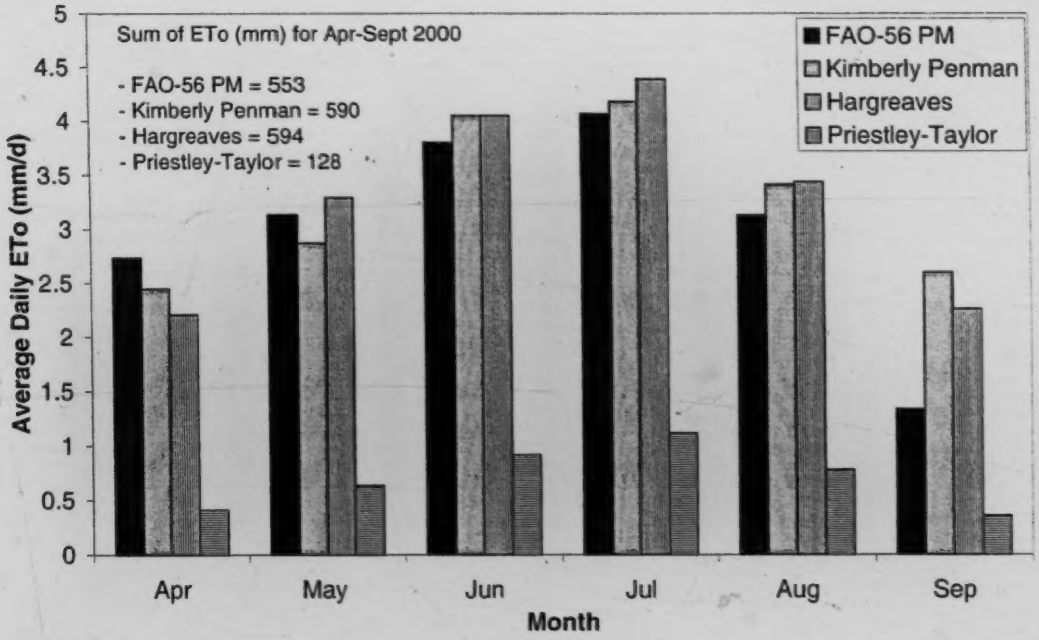

Figure 4-5 Average daily ET_o estimates in monthly increments and 6 month sum of ET_o during the 2000 growing season.

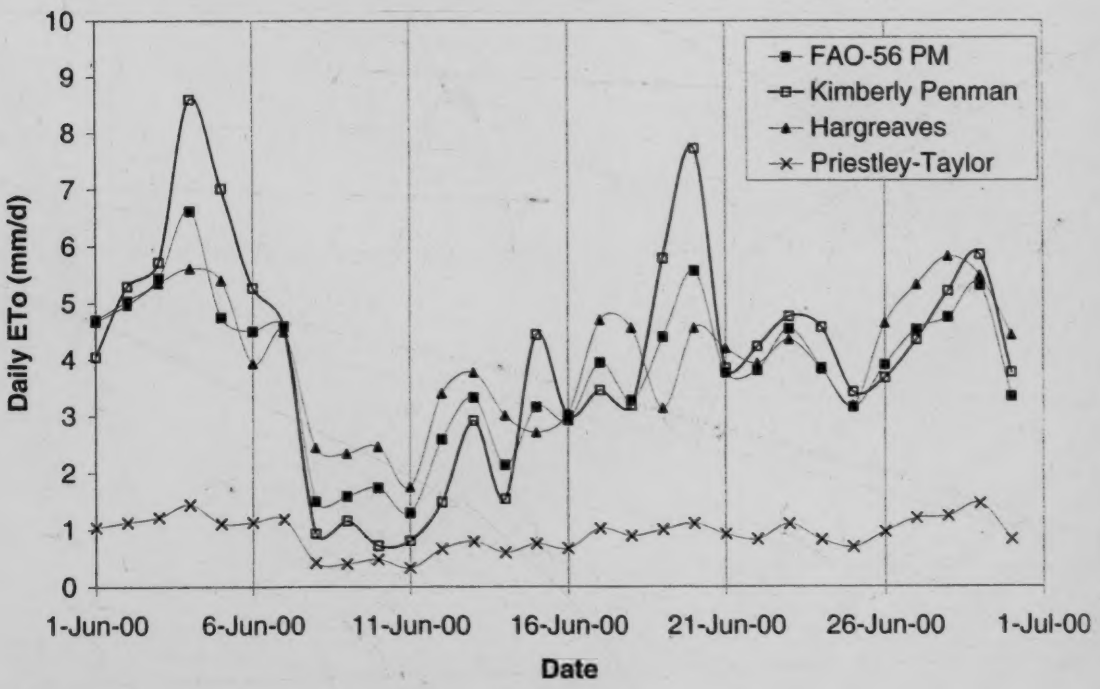

Figure 4-6 Daily ET_o estimates for June 2000.

Even if Penman combination methods could not be validated locally, Jensen et al. (1990) found that they compared favourably to lysimetric measurements in 10 of 11 different climate regimes around the world. These combination methods consistently showed the least error, as compared to lysimetric ET measurements, among 19 methods investigated (Jensen et al. 1990). For a large-scale study in Turkey, the FAO-56 PM method consistently predicted within 10% of precision weighing lysimetric ET values for a calendar year of monitoring (Allen 2000b).

The Kimberly-Penman (Wright 1982, 1996) results overestimated the FAO-56 PM results by 7% for the 6 months studied (Figure 4-5), but generally followed the same daily patterns (Figure 4-6). Jensen et al. (1990) found that the Kimberly-Penman method was within 5% of the FAO-56 PM method for arid sites, which are defined to have a mean annual relative humidity of less than 60%. This is the case for the GPRS (Table 4-1). Steiner et al. (1991) found that in a windy environment, Penman-combination equations with a locally calibrated wind function tend to overestimate ET_o. Analyses of data from the GPRS reveal that for the 10 days in which the mean daily wind speed exceeded 5 m/s, the Kimberly-Penman method overpredicted the FAO-56 PM method by an average of 65%.

The temperature-based Hargreaves (1985) method similarly overestimated the FAO-56 PM method by 7% (Figure 4-5). Most studies find that the Hargreaves (1985) method underestimates the FAO-56 PM method, but only by 10-16% (Jensen et al. 1990, Amatya et al. 1995, Allen 2000b). For its simplicity and the small amount of data required, the Hargreaves (1985) method could be considered an excellent first estimate of ET_o for this region.

The largest deviation from the FAO-56 PM method was the radiation-based Priestley-Taylor (1972) method, underestimating the FAO-56 PM method by 77% (Figure 4-5). This is not unusual for arid sites, as Jensen et al. (1990) found that

the Priestley-Taylor (1972) method underestimated the FAO-56 PM method by an average of 30% at the 11 sites under consideration. The Priestley-Taylor (1972) method only works under conditions of minimal advection (Parlange and Katul 1992). At arid sites, the vapour pressure deficit increases and the sensible heat flux to the ground increases relative to more humid sites. Thus, to better estimate ET_o, an increase in the Priestley-Taylor constant from 1.26 (Appendix B) is likely justifiable for arid sites (Jensen et al. 1990). Given the uncertainties in estimating net radiation (20%) and soil heat flux (100%) (Kite and Droogers 2000) and their significance in radiation-based methods, the poor performance of the Priestley-Taylor (1972) method is not surprising.

4.3.3 Actual Evapotranspiration (ET_c) Calculation Methods

Values of actual evapotranspiration can be calculated by several methods, which fit into three general categories (Hillel 1982, Dingman 1994):

- The water balance approach, where liquid and/or atmospheric water inputs, outputs and changes in storage are measured and the unknown component of the water budget, evapotranspiration, is determined. This method is limited by the precision with which the components of the water budget can be measured;
- The turbulent transfer or energy balance approach, which modifies the Fickian (diffusive) mass balance evaporation equation to relate it to measurable meteorological parameters. This method requires measurements at two levels to obtain the gradient of vapor pressure from the surface to the atmosphere, and thus it is only used in elaborately instrumented studies; and,
- The potential evapotranspiration or combination approach, which calculates actual evapotranspiration as a fraction of potential evapotranspiration based on relevant surface characteristics such as soil moisture and vegetative cover. The crop coefficient method is in this

category. Difficulty in obtaining accurate field measurements or having extensive instrumentation, as for the first two categories, often results in evapotranspiration being determined from weather data with the combination approach (Allen et al. 1998).

4.3.3.1 Crop Coefficient Method

The crop coefficient method's utility for the calculation of ET_c at the GPRS lies in its explicit treatment of evapotranspiration under deficient water supply (Hatfield and Allen 1996), which could be the case for field scenarios where there are extended periods without precipitation. The method is also useful because the GPRS has a variety of vegetation as well as bare soil conditions. Thus, evapotranspiration rates may be variable across the site. A description of the procedure for calculating ET_c by the dual crop coefficient method is provided in Appendix B.

4.3.4 Actual Evapotranspiration (ET_c) Results

Daily ET_c calculated for both bare soil and foxtail barley, the chosen, representative vegetation (Appendix B), conditions are displayed in Figure 4-7. The patterns of ET_c for both conditions are nearly coincident at most times, except for deviations in April, late May and early June, and late August. It is not surprising, then, that the sums of ET_c for each condition from April to September are nearly equal: 545 mm for bare soil and 575 mm for foxtail barley.

The similarities, or differences, in the daily ET_c patterns correlate to the stage of drying that the soil was defined to be in, either stage I or stage II. Stage I drying occurred when the soil surface was at or near saturation and evaporation was determined by climatic conditions. Stage II drying occurred when the soil moisture content was reduced and evaporation was determined by both the conductive properties of the soil and climatic conditions.

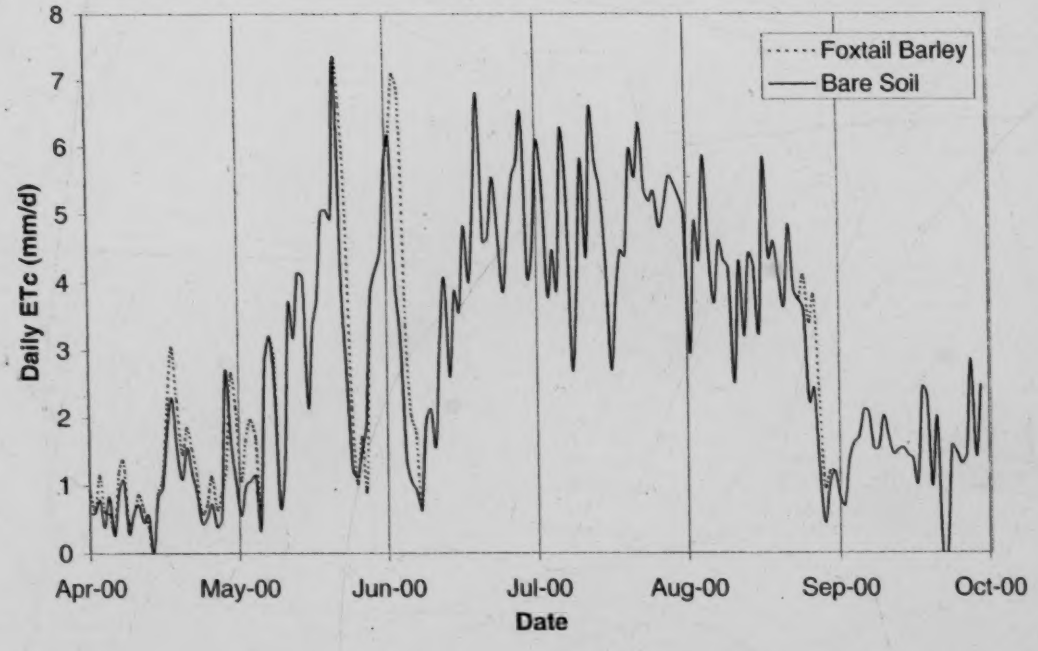

Figure 4-7 Daily ET_c estimates for vegetated and bare soil conditions during the 2000 growing season.

For example, Figure 4-8 shows a plot of daily ET_c for the month of April, when stage II drying was defined to be in effect for the entire month. In April, the daily ET_c for foxtail barley was usually elevated compared to that of bare soil (Figure 4-8). In contrast, the entire month of July remained in stage I, or energy-limited, evaporation and there is no difference in ET_c between the two methods (Figure 4-7).

For stage I drying, there is no distinction between vegetated and non-vegetated surfaces because the energy at the surface can satisfy both transpiration and evaporation components, which occur at the energy-limiting rate regardless of whether the ground is vegetated or not. In stage II drying, there is an energy deficit for evaporation from bare soil after the transpiration component is taken

into account (Allen 2000b), meaning that vegetated surfaces evapotranspire more water than bare soil surfaces under deficient energy and water regimes.

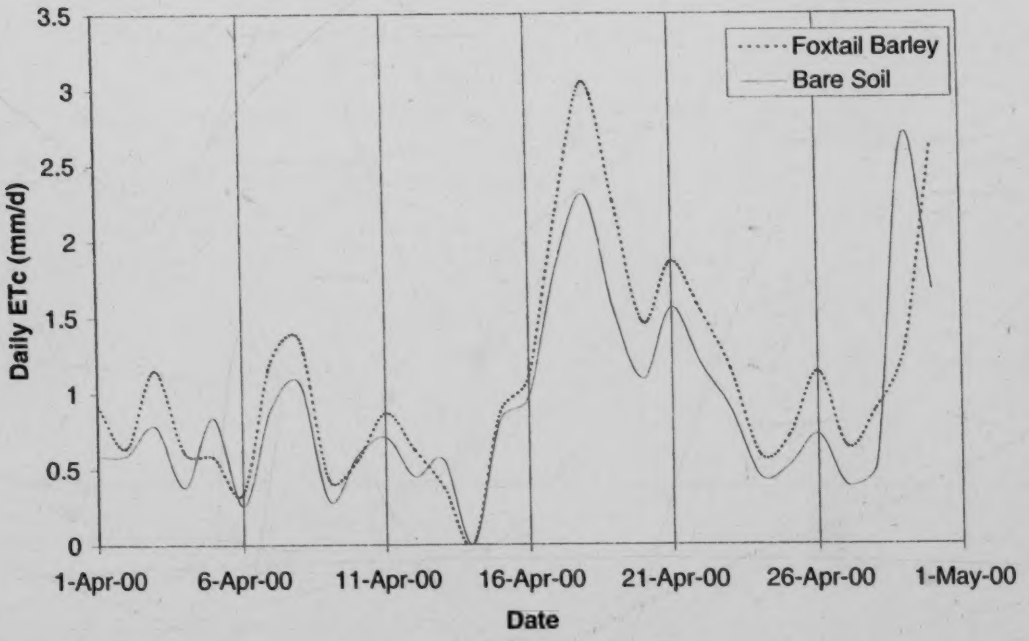

Figure 4-8 Daily ET_c estimates for vegetated and bare soil conditions during April 2000.

There is a large amount of uncertainty in the ET_c results given the many assumptions required for the calculations. For example, soil evaporation properties were estimated from tables. However, the results seemed justifiable since water was available at nearly all times (i.e., stage I drying) due to the large amounts of sustained precipitation received over the study period and also because the porous medium remained saturated for long periods (evident from soil moisture data, to be discussed). The capillary rise of water in clay-rich soils is also found to be significant in making available water remain near the surface (Kite and Droogers 2000, Beyazgul et al. 2000).

There is also uncertainty in the transpiration calculations because many assumptions were made regarding the crop type and its properties. Given the uncertainty already inherent in estimating climatic and soil parameters, the crop coefficient method is most readily used for agricultural crops (Kite and Droogers 2000) where there is published information on plant density, leaf area, rooting depth, ground coverage and crop coefficients. This information helps to avoid additional uncertainty in calculating ET_c.

4.4 Variably-Saturated Zone Conditions

4.4.1 Soil Moisture

Time series of volumetric soil moisture profiles were produced for each of N99-1, N99-2 and N99-3 (Figure 2-4) from July 1999 to November 2000 (Figure 4-9). Patterns remained similar for measurements performed in 2001. Soil moisture contents were based on the calibration equations developed for the various neutron probes used at the site. The equation for the "DSC" probe was:

$$\theta_v = 28.04546 * CR - 13.70096 \qquad (4\text{-}3)$$

where CR is the ratio of neutron counts measured to a standard neutron count performed on a standard wax shield during each field visit. All soil moisture contents presented in Figure 4-9 are from the "DSC" probe. Soil moisture results from the "DSC" probe were verified with a similar neutron probe ("Range") on July 21, 1999.

Moisture contents vary by 15-20% along each depth profile, which reveals the textural heterogeneity of the subsurface. For intervals of relatively uniform volumetric moisture contents, values are generally 20-25%, reflecting the effective porosity of the till (Figure 4-9). Soil moisture content is known to depend on texture (Van Pelt and Wierenga 2001) and has been used to locate textural boundaries in field applications (Hendrickx et al. 1986).

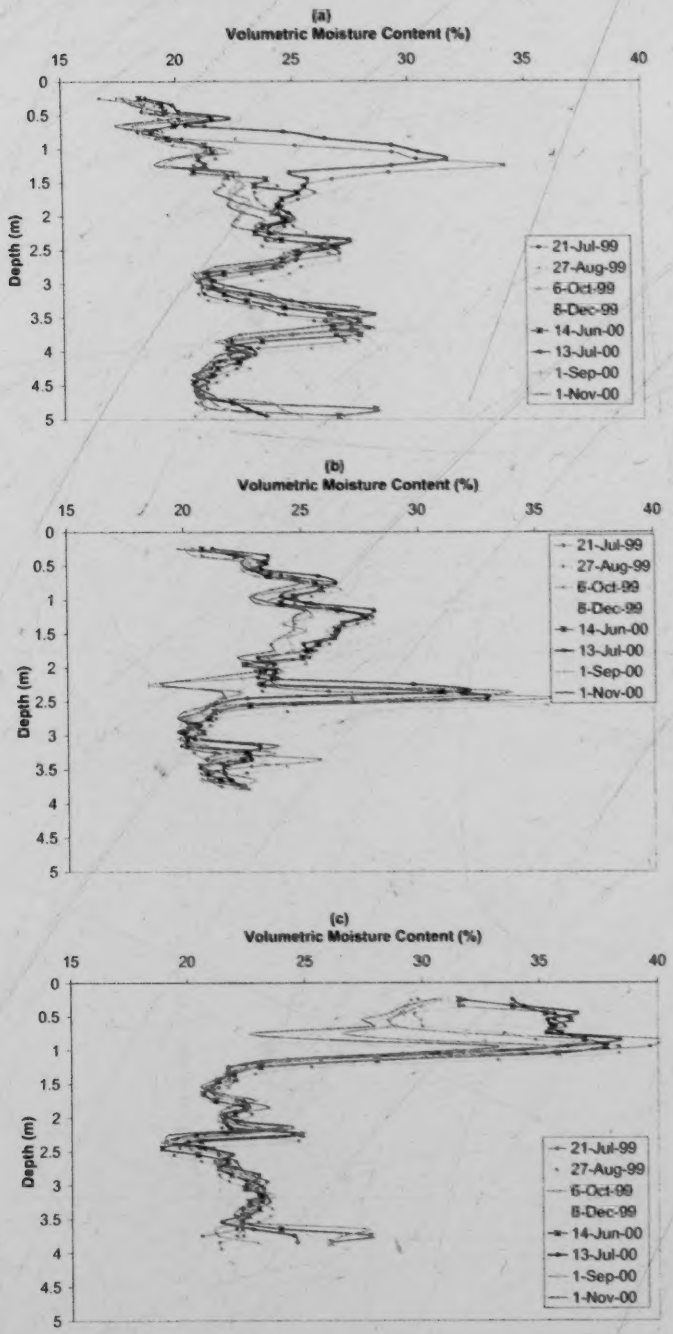

Figure 4-9 Soil moisture profiles at (a) N99-1, (b) N99-2, and (c) N99-3 from July 1999 to November 2000.

Features of the flow system at the GPRS explain some peculiarities on the soil moisture profiles. For N99-3, the profile shows great soil moisture variation in the upper 1 m of the subsurface (Figure 4-9). There are higher moisture contents for measurements taken during the spring and early summer (July 21, 1999, June 14, 2000 and July 13, 2000) while measurements taken during the fall (October 6, 1999, December 8, 1999, September 1, 2000 and November 1, 2000) have lower moisture contents.

Borehole logs for N99-3 and piezometers in the southwest corner of the site show coarse gravels and wood fragments to approximately 2 m bgs (Komex 2000a, 2000c). The wood fragments are extensive and appear to be from site clearing and burial before operations began. The gravel and wood fragments likely increased the permeability of the shallow subsurface in the area near the access tube. Therefore, water is more readily transmitted in the area. Thus, this area of the site is more susceptible to seasonal moisture content fluctuations (i.e., input of precipitation during the summer, seasonal decline during the fall) than a less permeable soil would be.

For N99-2, the moisture profile shows alternating sharp increases and decreases in soil moisture content at approximately 2.5 m bgs. The sharp decreases occur for the last two measurement times, September 1 and November 1, 2000, while the increases in moisture content are seen for all previous measurement times (Figure 4-9). The borehole log for this access tube reveals that grey sand was encountered at 2.5 m bgs during drilling (Komex 2000a).

Because of the area in which N99-2 is completed, the sand is likely frac sand from a hydraulically induced fracture. The sand-filled fracture creates a path of pores larger than the surrounding matrix, thus becoming a conduit for more rapid flow (Tindall and Kunkel 1999). Under saturated field conditions, such as those where the increases in moisture content are seen, the fracture can transmit more water than the soil matrix. Under dewatering conditions, such as those that

occurred in the summer of 2000 (Table 3-5), the fracture is preferentially dewatered because of less resistance to flow, and thus the sharp decreases in moisture content seen in the fall of 2000. This implies that the hydraulically induced fractures in the area of the horizontal well contribute to the development of dual porosity flow.

Other than these variations, the spatial patterns of soil moisture generally remain consistent throughout the observation period (Figure 4-9). This can be attributed to the high fraction of fine-grained material at the site. Clay minerals incorporate water directly into their structure (swell) and retain it for long periods (Hillel 1982). Slight variations in the patterns at different times can be explained by the non-repeatability of measurements at exact depths due to user error. Even if soil moisture values are consistent throughout time, some measurement error is introduced due to the random nature of radioactivity. If a normal distribution is assumed for the thermal neutron counts taken in any reading, then the precision of the reading is proportional to the ratio of the square root of the counts to the counts (CPN Company 1985). Because the count readings for the DSC probe exceeded 10 000, the precision of the counts is within 1%.

The temporal stability of soil moisture has been demonstrated by many researchers (e.g., Kachanoski and de Jong 1988, Goovaerts and Chiang 1993, Van Pelt and Wierenga 2001). They found that although the magnitude of soil moisture (absolute or relative to the field mean) changes throughout time, the pattern of spatial variability does not. The significant covariants in these studies were soil texture and topography (Van Pelt and Wierenga 2001). The results were applicable to the different soil textures at each site and to the cases where topography was either flat (Goovaerts and Chiang 1993, Van Pelt and Wierenga 2001) or gently undulating (Kachanoski and de Jong 1988).

4.4.2 Soil-Water Characteristic Curve Fitting

The soil-water characteristic curve describes the relationship between the degree of saturation and the matric potential of soil. The curve is central to linking theory, soil material properties and soil-water behaviour (Barbour 1998). Analytical models were fit to laboratory measured pressure-saturation data, not only to be able to predict matric potential from easily measured field soil moisture data, but also to develop moisture-conductivity relationships as input for potential variably-saturated numerical models.

One of the most common analytical models used is that of van Genuchten (1980), which uses a closed-form analytical expression to fit parameters to the shape of the soil-moisture characteristic curve. These fit parameters are then used in expressions developed to produce a curve of unsaturated hydraulic conductivity as a function of the matric suction of the medium. Many models work well on the soils upon which the experiment is conducted, but do not work well on other soils. The analytical model used to fit laboratory-measured retention data for this study was that of Fredlund and Xing (1994), which closely matches the van Genuchten (1980) model with some modifications. The Fredlund and Xing (1994) model is expressed as:

$$\theta = C(\psi)\frac{\theta_s}{\left\{\ln[e + (\psi/a)^n]\right\}^m} \tag{4-4}$$

where θ is the moisture content, θ_s is the saturation moisture content, e is the base of the natural logarithm, ψ is the matric suction (kPa), and a, n and m are least-squares curve fitting parameters:

$$a = \psi_i \tag{4-5}$$

$$m = 3.67 \ln\left(\frac{\theta_s}{\theta_i}\right) \tag{4-6}$$

$$n = \frac{1.31^{m+1}}{m\theta_s} 3.72 s \psi_i \quad (4\text{-}7)$$

$$s = \frac{\theta_i}{\psi_p - \psi_i} \quad (4\text{-}8)$$

where θ_i is the moisture content at the inflection point, ψ_i is the matric suction at the inflection point (kPa), s is the slope of the tangent line at the inflection point and ψ_p is the matric suction at the intercept of the tangent line and the matric suction axis (kPa).

$C(\psi)$ is a correction factor to ensure that θ goes to 0 at very high suction so that there is no discontinuity between zero saturation and the true residual saturation. The model of Fredlund and Xing (1994) also removes restrictions from the fitting parameters that van Genuchten (1980) places on his analogous fitting parameters, thereby allowing more flexibility in the curve fit.

Laboratory data were fit with the Fredlund and Xing (1994) method using SoilCover 4.0 (SoilCover Manual 1997). Once curve fits were generated for the eight samples studied, relative permeability-saturation relationships could be estimated using a method developed by Fredlund et al. (1994) that is embedded in the SoilCover program. Table 4-2 lists the fitting parameters for each of the eight samples from the GPRS, while Figure 4-10 displays an example of the curve fit to experimental data for a sample depth of 0-0.5 m.

Depth of Homogenized Sample (m)	a fitting parameter (kPa)	m fitting parameter	n fitting parameter
0.0-0.5	33.98	2.24	0.43
0.5-1.0	31.92	2.11	0.40
1.0-1.5	50.12	1.57	0.46
1.5-2.0	33.37	2.13	0.38
2.0-2.5	40.85	1.70	0.46
2.5-3.0	41.35	1.71	0.41
3.0-3.5	31.12	2.13	0.37
3.5-4.0	34.04	2.11	0.39

Table 4-2 Fitting parameters to laboratory measured data for the Fredlund and Xing (1994) method.

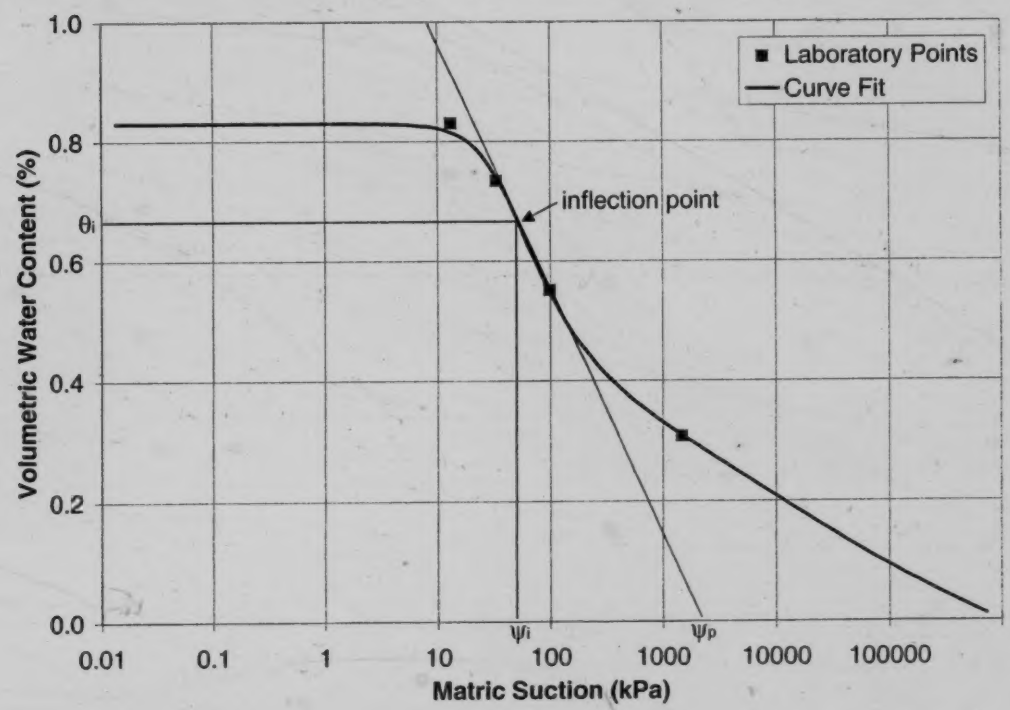

Figure 4-10 Pressure-saturation data and curve fit by the Fredlund and Xing (1994) method for a sample depth of 0-0.5 m.

4.4.3 Variably-Saturated Zone Material Properties

4.4.3.1 Dry Bulk Density

Wet bulk density depth profiles were determined for each access tube. Wet bulk density was interpreted from the "Department 501" probe counts based on the calibration equation provided:

$$\rho_{wet} = \left[\frac{-\ln\left(\frac{CR_{den} - 6.5713}{-1.63} \right)}{-0.4274} \right] \tag{4-9}$$

where ρ_{wet} is the wet bulk density of the medium surrounding the probe (g/cm^3) and CR_{den} is the ratio of field gamma counts to the standard number of gamma counts performed on a wax shield during the field visit. To convert from wet bulk density to dry bulk density (Fetter 1994):

$$\rho_{wet} = \frac{M_{water} + M_{solid} + M_{casing}}{V_{sample}} \tag{4-10}$$

$$\rho_{dry} = \frac{M_{solid}}{V_{sample}} \tag{4-11}$$

$$\rho_{dry} = \rho_{wet} - \left(\frac{M_{water} + M_{casing}}{V_{sample}} \right) = \rho_{wet} - \rho_{water}\theta_v - \frac{M_{casing}}{V_{sample}} \tag{4-12}$$

where ρ_{dry} is the dry bulk density of the medium (g/cm^3), ρ_{water} is the density of water (taken as 1.00 g/cm^3), M is the mass of the given component of the bulk density (g), and V_{sample} is the volume of the subsurface sampled during the wet bulk density determination (cm^3). This assumes that the steel casing of the access tube was a component of the wet bulk density determined by the probe.

Results for dry bulk density with depth for each of the neutron probe access tubes are presented in Table 4-3. The results for each tube were averaged over 0.5 m intervals from the ground surface to the bottom of the tube. The approximate volume of the subsurface sampled by the probe is a sphere with a radius of 10 cm to 25 cm (Hillel 1982).

The results show that dry bulk density remains relatively uniform with depth, averaging approximately 2.40 g/cm^3. The calculated dry bulk density is much lower for the upper 1 to 1.5 m of N99-3 (Table 4-3), where the backfilled woody material was uncovered.

Depth of Averaged Reading (m)	N99-1 Dry Bulk Density (g/cm^3)	N99-2 Dry Bulk Density (g/cm^3)	N99-3 Dry Bulk Density (g/cm^3)
0.0-0.5	2.48	2.38	1.76
0.5-1.0	2.36	2.33	1.70
1.0-1.5	2.29	2.31	2.28
1.5-2.0	2.42	2.33	2.42
2.0-2.5	2.42	2.34	2.43
2.5-3.0	2.45	2.42	2.41
3.0-3.5	2.46	2.41	2.41
3.5-4.0	2.41	2.42	2.42
4.0-4.5	2.49	-	-

Table 4-3 Dry bulk density determinations for each neutron probe access tube location.

The values obtained for dry bulk density were considerably higher than what should be expected. The dry bulk densities of unconsolidated materials range from 1.22 g/cm^3 for clays to 1.92 g/cm^3 for gravel and sand (Tindall and Kunkel 1999). The field-measured dry bulk density values are of a magnitude that only consolidated materials such as sandstone (2.13 g/cm^3) and limestone/shale

(2.78 g/cm^3) can attain (Tindall and Kunkel 1999). Therefore, either there is considerable measurement error or components contributing to the dry bulk density other than soil and water are significant.

The measurement error of the probe is unknown, although if it was functioning similarly to the "DSC" probe, then the precision should similarly be within 1% for the large amounts of counts recorded. Two features likely elevated the dry bulk density: the amount of erratics in the till and the steel casing used for the neutron probe access tubes.

High amounts of erratics have been noted in the till, both during site installations and in regional studies (Boydell et al. 1974). These are parts of bedrock formations that have remained consolidated during their transport and deposition and therefore, raise the average bulk density measured at the site. Also, given that the approximate density of the steel access tubes is 7.9 g/cm^3 (Lide 1999), and that gamma radiation strongly interacts (and is often shielded) with steel (CPN Company 1993), it is likely that the steel in the access tubes also raised the measured wet bulk density readings. The effect of the steel tubes was not removed from the calculated dry bulk densities. In most applications, aluminum access tubes are used (Hillel 1982), which have a density of 2.7 g/cm^3 (Lide 1999) and are less likely to interact with the gamma radiation.

4.4.3.2 Unsaturated Hydraulic Conductivity from Guelph Permeameter

The intention of the Guelph permeameter measurement was to obtain values for unsaturated hydraulic conductivity, which is directly proportional to the field-saturated hydraulic conductivity measured by the permeameter (Reynolds and Elrick 1986):

$$K(\psi) = Ke^{(\alpha\psi)} \qquad (4\text{-}13)$$

where $K(\psi)$ is the unsaturated hydraulic conductivity (m/s), K is the field saturated hydraulic conductivity measured by the permeameter (m/s), α is the slope of ln K versus ψ (m^{-1}), and ψ is the soil water pressure head (m).

The experimental design was unsuccessful and therefore $K(\psi)$ was not determined. There was no measurable change in the level of the reservoir in the Mariotte bottle over significant periods of time and, therefore, the required calculation of the steady-state rate required to maintain the head in the well could not be performed. This suggests that K was locally below 10^{-8} m/s where the trials were conducted (Reynolds and Elrick 1986). A larger radius well and a greater head difference between the reservoir and the well may have facilitated the measurement, although were not investigated.

4.4.3.3 Grain Size Distribution and Other Soil Properties

Wong and Alfaro (2001) determined several soil properties at the GPRS, including the specific gravity (particle density), liquid and plastic limits, and the grain size distribution. Soils were then classified based on the Unified Soil Classification System (Day 2001). The results of their work are presented in Table 4-4.

Depth (m)	Unified Soil Classification	Specific Gravity	Liquid Limit (%)	Plastic Limit (%)	Sand (%)	Silt (%)	Clay (%)
1.30	CL	2.66	42	15	23	42	34
2.50	CL	2.63	38	17	31	27	41
3.00	SC	2.66	43	21	54	20	24
4.00	CL	2.66	46	23	27	35	35
4.50	CL	2.64	45	23	30	31	36

Table 4-4 GPRS soil properties as determined by Wong and Alfaro (2001).

In the Unified Soil Classification System, CL is an inorganic clay of low plasticity, while SC is defined as a clayey sand (Day 2001). The values of specific gravity are very close to that described for a silicate-dominated medium (Tindall and Kunkel 1999, Day 2001).

There is no indication of the exact location where these properties were determined, although it was "near a vertical well" in the area of the horizontal well (Wong and Alfaro 2001). The high sand fraction in the sample from 3 m depth may be natural or may be from sand introduced during hydraulic fracturing operations. It was noted that it was difficult to obtain representative, undisturbed samples due to the presence of cobbles and the heterogeneity of the subsurface (Wong and Alfaro 2001).

4.5 Summary of Key Points for Conceptual Model Development

- Measured temperature and precipitation data were representative of historical measurements in the region (Tokarsky 1971, Dzikowski 1990). The low annual relative humidity classifies the site as arid (Jensen et al. 1990), which enhances the importance of determining the effect of evapotranspiration timing on groundwater levels.
- Precipitation is the main water input to the system and was determined to be 494 mm in 2000 and 404 mm in 2001. The data could be resolved to hourly inputs for implementation in a numerical model, if necessary.
- Evapotranspiration is the main water output from the system and was calculated to be between 545 mm and 575 mm for bare soil and vegetated regimes respectively for the 2000 growing season (April to September 2000). Calculated evapotranspiration exceeded precipitation during this period, as was found for historical data, and was assumed to be negligible at other times based on historical data in

the region (Tokarsky 1971). The data can be resolved to daily inputs for implementation in a numerical model, if necessary.

- Soil moisture monitoring revealed the temporal consistency of measurements along each of the depth profiles in the low permeability environment. In areas of stable moisture content values, soil moisture was consistently measured to be 20-25%. Given that the porosity of till is 10-20% or higher for tills with a greater clay fraction (Fetter 1994), some justification is provided to represent the GPRS as a long-term saturated environment. Rapid changes in soil moisture along the depth profiles helped to discern the textural heterogeneity of the subsurface. Heterogeneities occurred vertically on a length scale of much less than 1 m, which would be difficult to represent in a numerical model. Soil moisture monitoring also indicated the potential importance of dual porosity flow in the area of the horizontal well and in the southwest corner of the site where native soil material is disturbed.
- Fitted soil-moisture characteristic curves provided a functional relationship at several depths between θ and ψ, an important relationship if variably-saturated modelling becomes part of the conceptual model. The curves provide the link to the energy status of water in variably-saturated areas such that vertical matric potential gradients may be explored at the GPRS from measured soil moisture data.
- Some material properties were determined for the site. The results for dry bulk density were heavily influenced by the steel access tubes in which they were obtained and are of little use. Unsaturated hydraulic conductivity testing indicated a matrix K of $< 10^{-8}$ m/s. Wong and Alfaro (2001) determined that soils at most depths are generally composed of >70% silt and clay and can be described as inorganic clays of low plasticity in the Unified Soil Classification System (Day 2001).

CHAPTER 5

FIELD RESULTS AND DISCUSSION: GROUNDWATER CONDITIONS

Groundwater flow at the GPRS is assumed to be governed by Darcy's Law, an empirical formula describing fluid flow through porous media (Freeze and Cherry 1979):

$$Q = -KA\frac{dh}{dl} \qquad (5\text{-}1)$$

where Q is volumetric discharge [L^3/T], K is the hydraulic conductivity [L/T], A is the cross-sectional area of flow [L^2], h is hydraulic head [L] and l is the flow length [L]. Darcy's Law is only valid for laminar flow, which is appropriate for the generally slow rates at which groundwater flows (Fetter 1994). It is not known if there is a lower permeability limit for Darcy's Law to be applicable. However, some experiments in very low permeability environments have not shown a linear relation between Q and dh/dl (Ingebritsen and Sanford 1998).

5.1 Site Hydrostratigraphy

Correlation of geologic units between different drilling programs was difficult because several individuals logged core and subjectively interpreted the differences between till units. Difficulty in correlating units, even between relatively closely spaced boreholes, was also expected due to the naturally heterogeneous distribution of tills. Thomas (1999) described similar difficulty in clearly delineating units in an environment with similar stratigraphy approximately 100 km to the south of the GPRS.

The initial site geological characterization (Artemis 1997) was refined during the period of 1997-2001 through fieldwork (testhole drilling, soil sampling, piezometer

installations) by Komex (2000a, 2000b). The surficial geology (material above bedrock) was divided into four different stratigraphic units, described by increasing depth from the ground surface:

- A surficial fill/backfill;
- An olive-brown till;
- A dark brown till; and,
- A grey till/bedrock contact.

The relative distributions of these units across the site are displayed in Figures 5-1 and 5-2. The locations of cross-sections A-A' and B-B' can be seen on Figure 2-4. The cross-sections include data interpreted from testholes and installations up to the summer of 1999. Geologic data acquired after 1999 are not in the area of these cross-sections.

The surficial fill is best described as a sandy clay loam to sandy clay. This unit's depth averages approximately 0.5-1.0 m bgs across the site. The fill unit was presumably created when the site was cleared for operations. It is composed of a mixture of native till materials and materials imported from off site to stabilize the re-worked till. Gravel was noted in this unit, especially in the raised pad area where operations occurred.

Lying below the surface fill is an olive-brown silt till. The approximate thickness of this unit is 2 m, up to a depth of 4 m bgs. This unit appears to be locally continuous only, as some testholes in the southern part of the site did not indicate its presence.

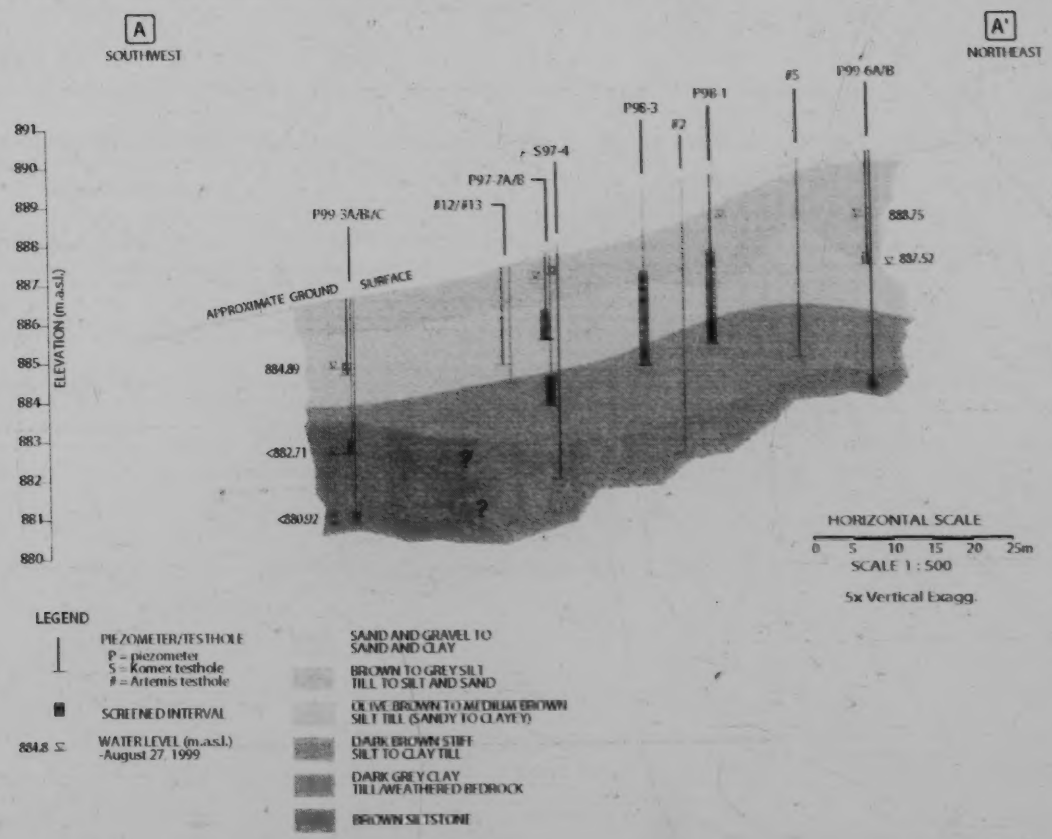

Figure 5-1 Cross-section A-A' describing stratigraphic divisions at the GPRS (modified from Komex 2000a).

Some observed properties of the olive-brown till indicate that there is active groundwater flow within the unit. This unit is commonly associated with a very strong amine odour in the pad area and the horizontal well area, indicating that the soluble processing chemicals were transported to this unit from the ground surface or laterally. Soil mottling was also present in the olive-brown till. Mottling describes a variation in soil colours due to alternating regimes of oxidation and reduction (Briggs et al. 1993). During periods of reduction, usually associated with waterlogging, compounds other than oxygen, typically iron, become reduced, making the soil more dull in colour. Mottling is often associated with a fluctuating water table and/or poor drainage (Buol et al. 1997), which are thought

to be the cause of mottling at the GPRS. Bowles (1998) described mottling in similar tills in a study approximately 100 km to the south of the GPRS.

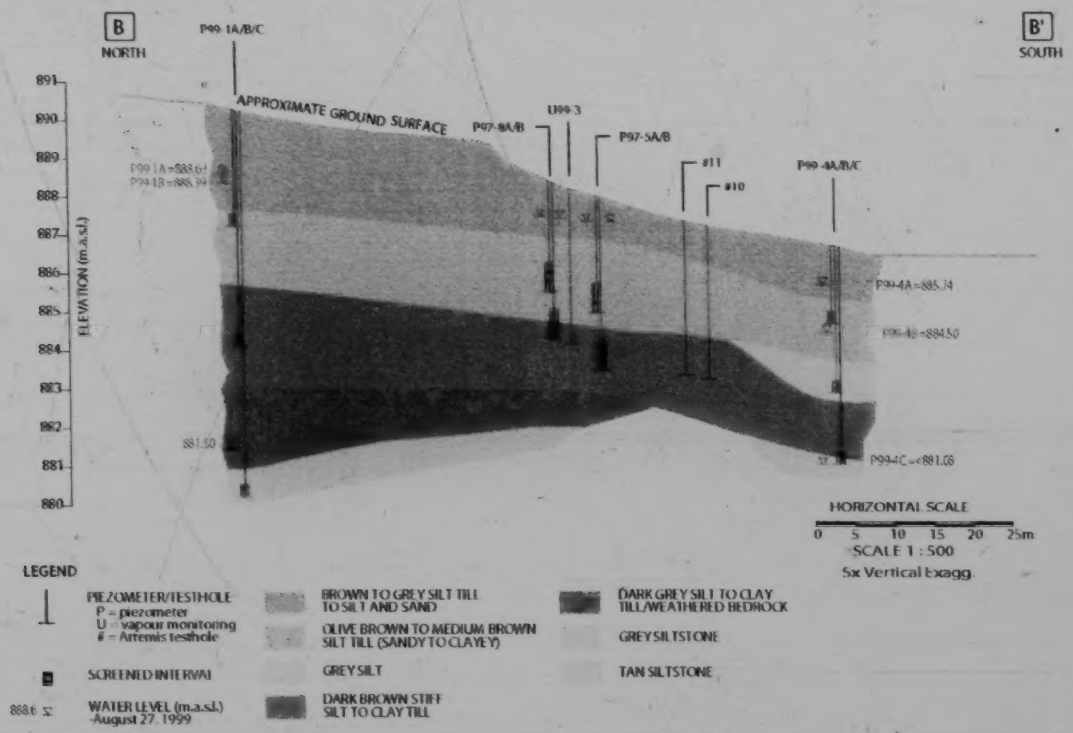

Figure 5-2 Cross-section B-B' describing stratigraphic divisions at the GPRS (modified from Komex 2000a).

The olive-brown till grades into a darker brown, stiff, silt to clay till, which is approximately the same thickness as the overlying till. This unit is locally continuous as well, as testholes in the south part of the site did not indicate its presence. The two brown tills are similar texturally, have discontinuous moist sand and silt lenses within them (verified by moisture content measurements by Komex (2000b)), and are likely part of the same stratigraphic unit. However, they are differentiated hydrostratigraphically because the dark brown till has no indication of processing chemical presence or mottling, used as indicators of groundwater movement in the olive-brown till.

The deepest surficial unit described for the site is a grey silt to clay till/weathered bedrock contact. The extent of this unit is to approximately 6 m bgs across the site. In all areas, fragments of mudstone and siltstone were increasingly found below 4-5 m bgs, indicating that this unit is a weathered contact between surficial tills and the underlying bedrock.

Bedrock was not extensively delineated at the GPRS. The only true confirmation of the depth to bedrock came during piezometer installation at P99-1 (Figure 2-4). At this borehole, grey siltstone was encountered at 9.3 m bgs. The depth to bedrock may decrease in a southerly direction across the site, as it is inferred to be 6 m bgs in the area of the horizontal well and shallower (4 m bgs) in the southwest corner of the site and south of the runoff ponds (Komex 2002). Therefore, the surficial till units tend to pinch out in a southerly direction. It seemed unnecessary to extensively investigate bedrock characteristics, as there was no evidence of groundwater movement or process chemicals below the olive-brown till.

Several other subsurface features, both natural and from site disturbance, have been noted at the GPRS. The till units dip to the south at a shallow angle, following the local 6-8% slope, which is influenced by the lower elevation lake 500 m to the south. Large cobble to boulder-sized materials were noted in the till across the site, which caused some difficulties during installations and soil sampling. Also noted throughout the till were occasional sand and gravel lenses, and woody materials in the southwest corner of the site. These textural heterogeneities were confirmed in the field by soil moisture monitoring (section 4.4.1).

Both natural and hydraulically induced fractures are present in the subsurface. Relatively intense natural fracturing was noted in the upper 2 m of the till, but none below (Komex 2000b). If there are fractures below 2 m bgs, they need to

be confirmed by hydraulic evidence. The locations of the induced fractures have been mapped by electrical resistivity tomography (ERT) and tiltmeter analysis (Wong and Alfaro 2001). Fractures from a vertical well propagated 5 m away, while the fractures mapped from the horizontal well propagated more than 5 m from the well. Fracture apertures ranged from 1 mm to 20 mm. The preferred fracturing orientation from both well types was horizontal, indicating subsurface overconsolidation (Wong and Alfaro 2001). Overconsolidation can occur after ice sheet unloading and the permanent rise of the water table (Craig 1992).

Several results of the description of stratigraphy agree with previous studies, both proximal to the site and across the Western Glaciated Plains (Figure 1-1):

- There are two distinct till types overlying bedrock (Grisak et al. 1976; Hendry 1982, 1989; Keller et al. 1986, 1988, 1989; Cravens and Ruedisili 1987; D'Astous et al. 1989; Ruland et al. 1991; Shaw and Hendry 1998; others);
- The uppermost till is highly weathered and fractured and has a distinct brown colour indicating oxidation (Rodvang and Simpkins 2001);
- The lowermost till is not weathered, only sometimes fractured and has a grey colour indicating reducing conditions (Rodvang and Simpkins 2001);
- Bedrock fragments increase with depth;
- The tills can generally be described as clayey loams with a significant fraction of fine-grained material (Pawluk and Bayrock 1969);
- The tills contain a significant number of erratics (Boydell et al. 1974);
- Bedrock encountered was siltstone and mudstone (Glass 1997); and,
- The till and bedrock units are sub-horizontal (Tokarsky 1971), but this is more a reflection of the local lake valley geomorphology.

5.2 Hydraulic Conductivity Results

5.2.1 2000 Bail Test Results

Although there are several analytical models available to calculate K from bail test data, the method of Bouwer and Rice (1976) (updated by Bouwer (1989)) was used. The method is simple to implement, is applicable to fully or partially penetrating wells in both unconfined and confined aquifers and was used by previous researchers at the GPRS (Komex 2000b). The solution to the mathematical model on which the Bouwer and Rice (1976) method is based is:

$$K = \frac{r_c^2 \ln(R_e/r_w)}{2l} \frac{1}{t} \ln \frac{h_0}{h_t} \qquad (5\text{-}2)$$

where r_c is the well casing radius [L], r_w is the horizontal distance from the centre of the well to the aquifer [L], l is the length of the well screen [L], h_0 is the initial water level displacement in the well [L], h_t is the water level displacement at time t [L] and R_e is the effective radial distance over which head loss is dissipated in the system [L].

Plots of the logarithmic response of displacement versus time reveal three different types of responses for the eleven piezometers tested. The first type of response was observed in one piezometer, P99-1A, and is shown in Figure 5-3. In this piezometer, one linear response developed at the beginning and then another linear response representing a greater rate of recovery developed at later times. The second type of response was observed in five piezometers: P99-1B, -2A, -4B, -6A and -7. The response of P99-7 is shown in Figure 5-4. These piezometers also displayed two (sometimes three) different linear responses, but the rate of recovery decreased at later times. The third response (not presented) was observed in piezometers P99-1C, -4A, -5B, -5C and –6B. These piezometers showed little recovery over the time interval (8 hr) for which displacement was measured. Therefore, the logarithmic response of

displacement versus time was essentially a horizontal line. Some piezometers completed in low permeability till have response times to perturbation of over 1 year (Keller et al. 1989).

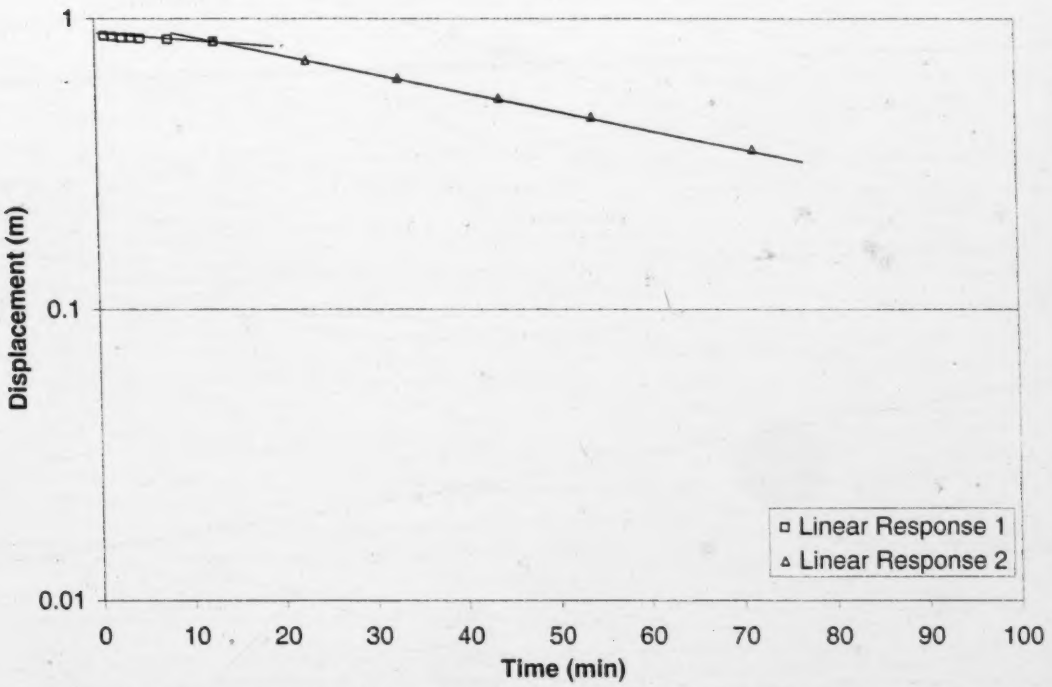

Figure 5-3 Semi-logarithmic plot of water level displacement versus time for the bail test performed on P99-1A.

Multiple straight lines, as could be fit for P99-7 (Figure 5-4), have been noted by some users of the Bouwer and Rice (1976) method (Bouwer 1989). The first straight line portion is due to an immediate response after initial drawdown, which is usually attributed to a high permeability sand pack or developed zone adjacent to the well screen. In the case of P99-7, the fact that the screened interval is 1.5 m, sand and gravel intervals are all along the screen and the backfilled woody material is in the vicinity (Komex 2000a) contribute to this quick initial response. The second straight line portion is more of a reflection of the flow from the formation into the well (Bouwer 1989), and this is what was used to determine the K for this piezometer.

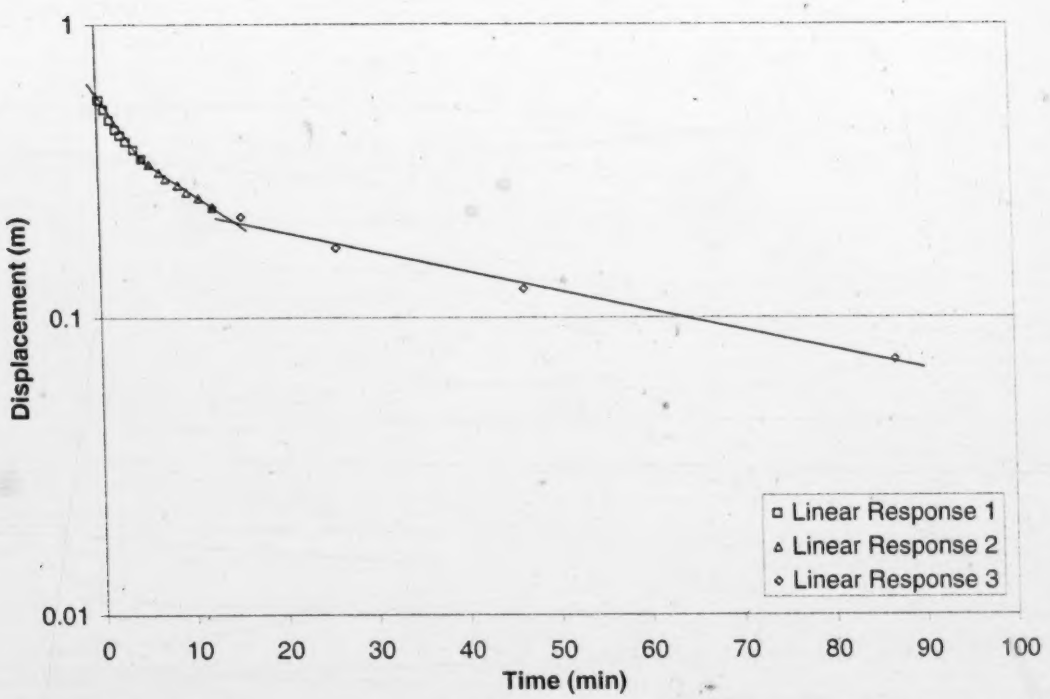

Figure 5-4 Semi-logarithmic plot of water level displacement versus time for the bail test performed on P99-7.

At large t and small h, it is not unusual for the rate of recovery to decrease to produce a concave upward-shaped curve, when storage mechanisms influence the response of the data (Butler 1998). As time increases, drawdown of the water table near the well becomes more significant as the piezometer recovers. Therefore, the second straight-line portion of the data, rather than any subsequent portions of the data, should be used to evaluate the relation between the logarithm of drawdown and time to calculate K (Bouwer 1989).

The case of the rate of recovery increasing over time (Figure 5-3) is not readily explained. If different rates may be attributed to heterogeneity along the well screen, it is almost certain that higher K materials would respond more quickly and at a higher rate than lower K materials, and thus the rate of recovery should decrease over time.

The uncertainty about anisotropy and which portion of the curve to fit are of practical importance for the method, as the assumption of isotropy has been found to misestimate K by a factor of 2 or more for this method (Butler 1998). For a heterogeneous domain, Keller et al. (1986) found that the results provided by standard analyses were expected to be higher than the actual K value.

The results for single well recovery tests are presented in Table 5-1. The uncertainty arising due to visual curve matching is estimated to be less than a factor of 5, which is the same uncertainty described by Bowles (1998), who used a similar methodology.

Piezometer	Hydraulic Conductivity (m/s)	Arithmetic Mean K for Completion Depth (m/s)	Geometric Mean K for Completion Depth (m/s)
P99-1A	1.2×10^{-7}	1.5×10^{-7}	7.0×10^{-8}
P99-2A	2.3×10^{-7}		
P99-4A	6.2×10^{-9}		
P99-6A	2.7×10^{-8}		
P99-7	3.6×10^{-7}		
P99-1B	3.7×10^{-7}	1.1×10^{-7}	2.5×10^{-8}
P99-4B	4.3×10^{-8}		
P99-5B	1.4×10^{-9}		
P99-6B	1.8×10^{-8}		
P99-1C	2.8×10^{-8}	5.5×10^{-8}	4.8×10^{-8}
P99-5C	8.2×10^{-8}		

Table 5-1 Hydraulic conductivity results for single well bail tests performed in the 2000 field season.

As expected due to heterogeneity, a wide range of K was determined by the tests, ranging over about 2 orders of magnitude (Table 5-1). The expected range

of K for till is 6 orders of magnitude, from 10^{-6} m/s to 10^{-12} m/s (Freeze and Cherry 1979). The range of K determined in this study reflects values for clayey/silty till.

Although based on a small number of samples, arithmetic mean values indicate that K decreases with the depth of the installation. Given that the distribution of K is log-normal in most materials (de Marsily 1986), the geometric mean K values may be more representative of average K values at each completion depth. The geometric mean K value at the C completion depth is higher than at the B completion depth, demonstrating the high natural variance of K in till, although the mean at the B completion depth is strongly influenced by the K measured at P99-5B.

Several researchers (Keller et al. 1986, 1988, 1989; Hendry 1988; Simpkins and Bradbury 1992; Shaw and Hendry 1998) have found that K decreases with depth in glaciated till plains. The results of K determinations for some of these researchers in shallower and deeper tills are presented in Table 5-2.

The differences in shallow and deeper K have been attributed to the completion of piezometers in weathered and unweathered zones, respectively. The enhanced permeability of the weathered zone is attributed to extensive fracturing, generally causing the zone to be hydraulically active and have a bulk K 1 to 3 orders of magnitude greater than the matrix (lab) K (van der Kamp 2001).

Researchers	Location	Shallow, Weathered Till K (m/s)	Deeper, Unweathered Till K (m/s)	Laboratory (Matrix) K (m/s)
Keller et al. (1986)	Dalmeny, Saskatchewan	2.1×10^{-7} to 2.3×10^{-8}	3.0×10^{-8} to 9.8×10^{-10}	7.7×10^{-11} to 1.1×10^{-11}
Keller et al. (1988)	Warman, Saskatchewan	7.9×10^{-9} to 1.0×10^{-9}	5.5×10^{-11} to 1.4×10^{-11}	1.9×10^{-11} (mean)
Simpkins and Bradbury (1992)	Southeastern Wisconsin	7.0×10^{-8} to 1.3×10^{-10}	4.7×10^{-9} to 1.4×10^{-10}	Not measured
Shaw and Hendry (1998)	Birsay Plain, Saskatchewan	1.3×10^{-8} to 6.5×10^{-9}	4.5×10^{-11} to 2.4×10^{-11}	3.2×10^{-11} to 1.3×10^{-11}

Table 5-2 Hydraulic conductivity results of various researchers in glaciated till plain settings.

Generally, the bulk K in the unweathered zone is similar to that of the matrix (Table 5-2), suggesting that secondary permeability features are not significant at depth for these investigations. There are notable exceptions to this, such as the Dalmeny site in Saskatchewan, where both weathered and unweathered K are similar and are higher than the matrix K. The Dalmeny and Warman sites are only 15 km apart, but have stratigraphy-dependent hydraulics, suggesting that the origins of deep fracturing are dependent on something other than post-depositional surface weathering (Cherry 1989).

K results for the deeper (C) piezometers at the GPRS are similar to the K results for the upper (A and B) piezometers, which are completed in a till unit where fractures have been noted. The K for the deeper piezometers is nearly 3 orders of magnitude higher than any matrix K noted in Table 5-2. Although only based on the results from two piezometers, this may suggest that secondary

permeability structures exist in some parts of the deeper GPRS subsurface, or that the till has a naturally high variance in its K distribution.

5.2.2 Other Bail Test Results and Other Hydraulic Conductivity Results

Bail tests performed by Komex International Inc. staff showed that hydraulic fracturing in the area of the horizontal well was successful in increasing the local K near a few piezometers, but did not greatly affect K on a large scale (Komex 2000b). The salient results from these tests are:

- Piezometers near the horizontal well, but outside the fractured area (P97-1A and P97-3A) have K values of 4.9×10^{-7} m/s and 8.6×10^{-7} m/s;
- Three piezometers within the fractured area (P97-8B, -10B and –11B) have slightly higher K values, ranging from 2.6×10^{-6} m/s to 1.1×10^{-6} m/s. The borehole log of P97-8B shows extensive frac sand, while the others may have intercepted minor fractures, although the borehole logs do not reveal this;
- Other piezometers in the fractured area (P97-4B, -8A and -9B) have lower values of K, ranging from 4.6×10^{-7} m/s to 2.2×10^{-7} m/s; and,
- K values for piezometers completed in the pad area (HP-E, -S and -W) range from 1.2×10^{-7} m/s to 7.4×10^{-9} m/s.

More K estimates were obtained by Komex International Inc. staff while monitoring the recovery of piezometers after dewatering in spring 1998 and during an aquifer test in October 1998 (Komex 2000b). The methods of analysis were the Theis recovery method and the Cooper-Jacob method, respectively. For more details on these operations and methods, refer to Komex (2000b), Kruseman and de Ridder (1990) and Dawson and Istok (1991). The results of these bulk tests were:

- From the dewatering recovery, the mean value of K determined was 1.5 x 10^{-8} m/s;
- From the aquifer test, the mean value of K determined was 4.6 x 10^{-8} m/s.

Thus, in the area of the horizontal well, there appear to be two populations of K values: a higher K localized near induced fractures and a lower bulk K in other areas. The larger scale analyses (dewatering and aquifer test) tend to smooth the effects of the fractures on K. There does not appear to be any significant correlation of K with depth, unlike what was found for the outer wells.

5.3 Water Level Measurements: Results and Analysis

Some typical hydrographs, as determined from manual water level measurements, are presented in Figures 5-5 through 5-8. They are grouped by area on the site:

- Near the horizontal well, outside the influence of hydraulic fracturing (Figure 5-5);
- Near the horizontal well, inside the influence of hydraulic fracturing (Figure 5-6);
- In the raised pad area (Figure 5-7); and
- Outer areas (i.e., the 1999 series of piezometers) (Figure 5-8).

An obvious feature of all hydrographs is their seasonal nature. Water levels increase after spring snowmelt and continue to increase during the period of significant seasonal precipitation until approximately the end of July. Then, throughout the remainder of the year, the water levels recede. The magnitude of increase and decrease is similar each year, with differences attributed to inter-annual variability in climate (snow and rain input, evapotranspiration output).

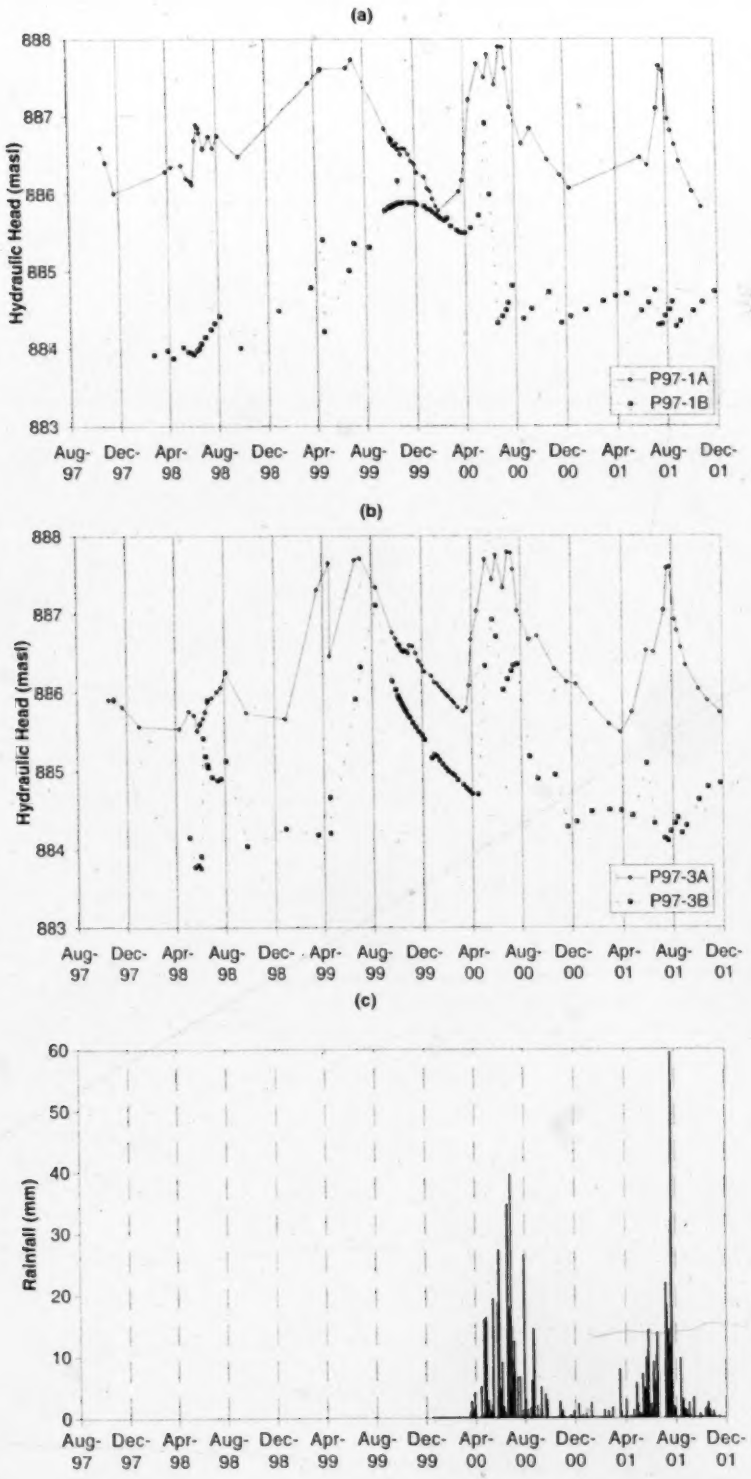

Figure 5-5 Hydrographs for (a) P97-1, (b) P97-3 and (c) rainfall.

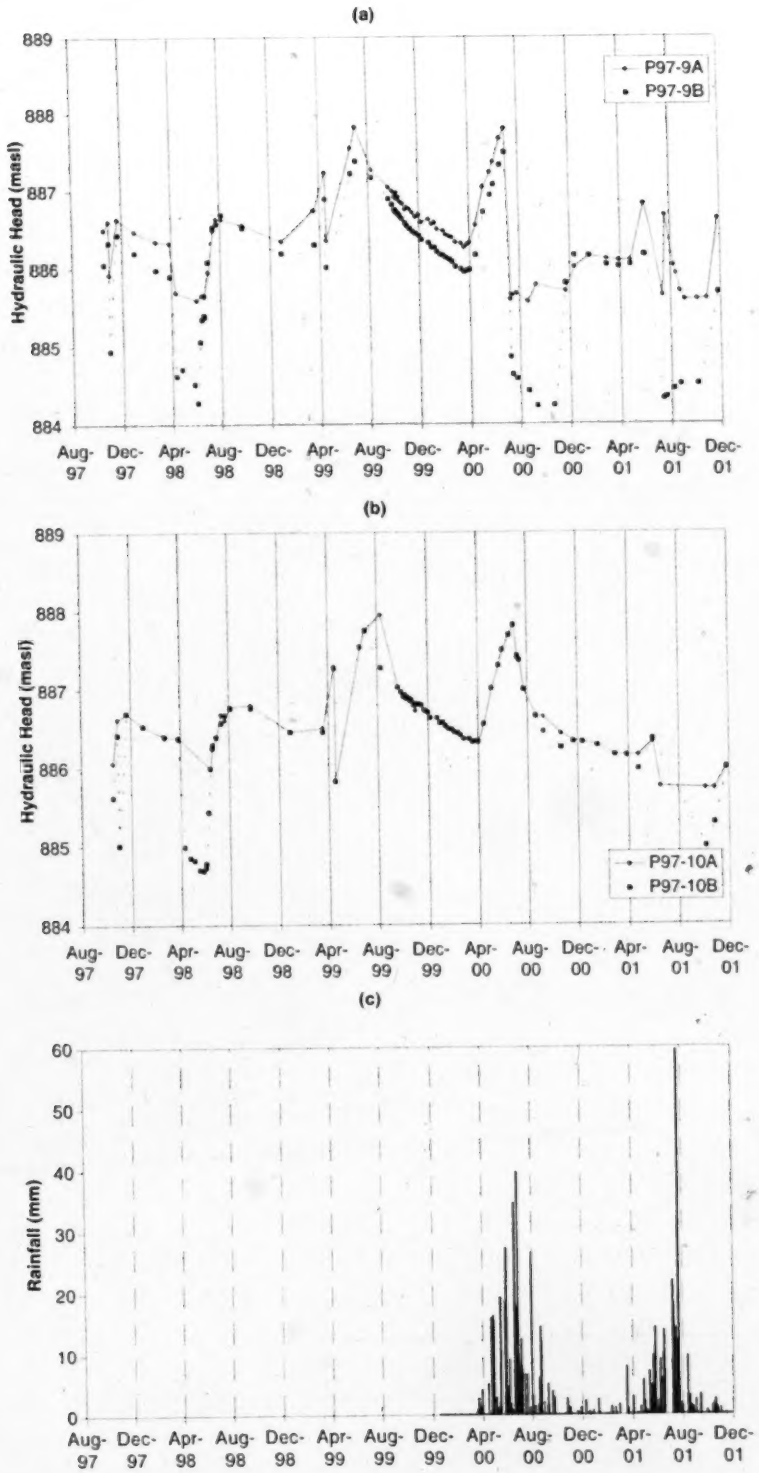

Figure 5-6 Hydrographs for (a) P97-9, (b) P97-10 and (c) rainfall.

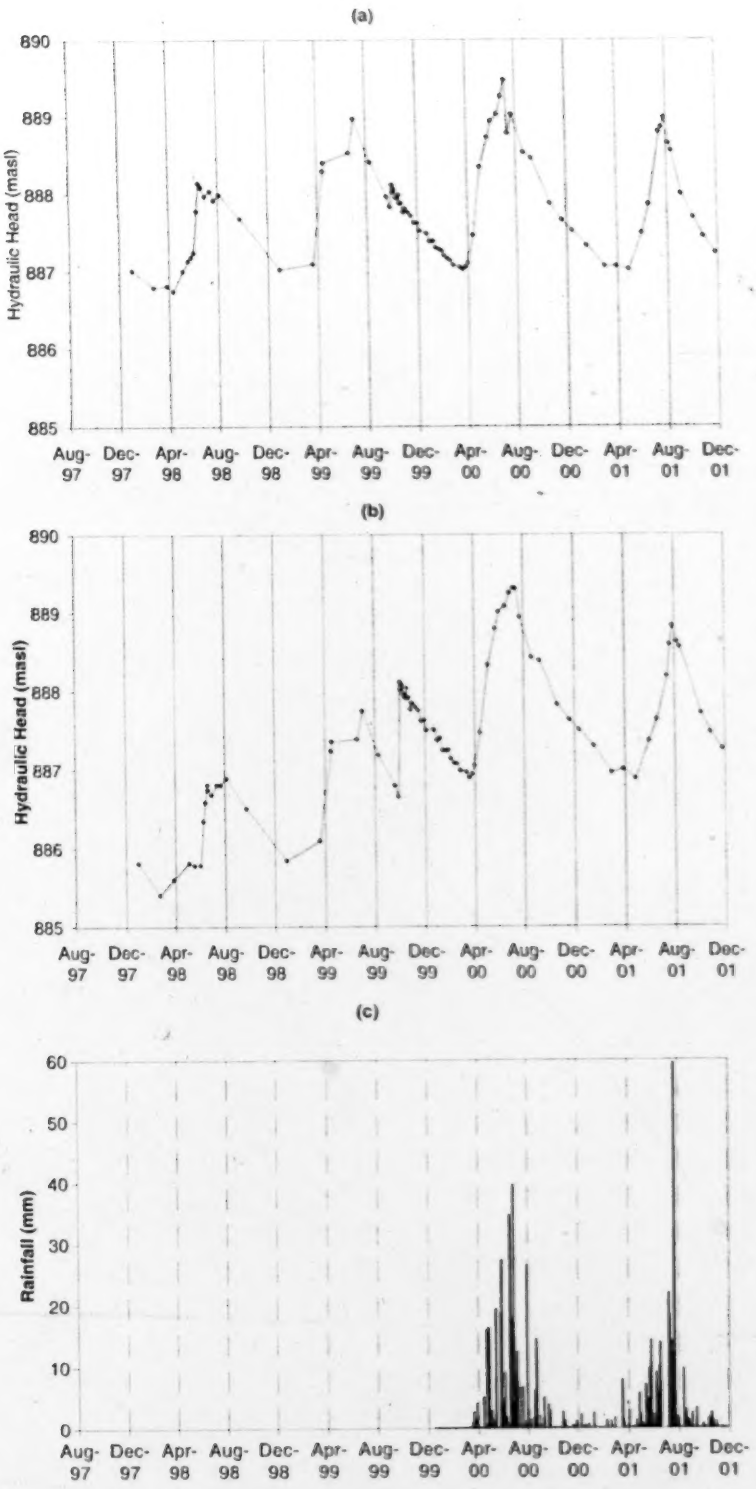

Figure 5-7 Hydrographs for (a) HP-N, (b) HP-W and (c) rainfall.

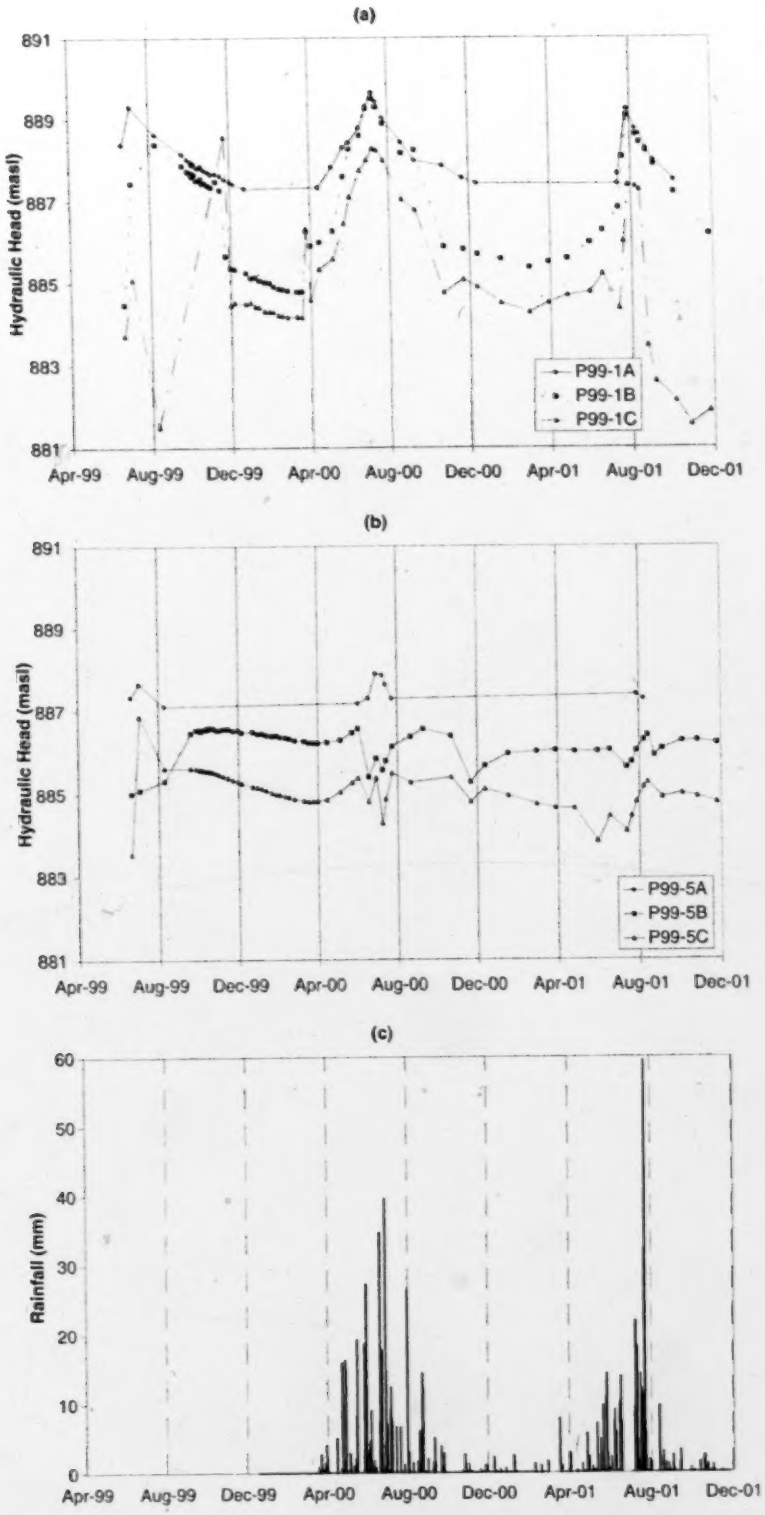

Figure 5-8 Hydrographs for (a) P99-1, (b) P99-5 and (c) rainfall.

The temporal variability of inputs and outputs is fundamental for evaluating the importance of climate to the hydrographs. Given that annual evapotranspiration exceeds annual precipitation at the site (historically and from ET_c calculations (section 4.3.4)), it may be erroneously assumed that water levels should decline annually. The hydrographs do not display such behaviour. It is apparent that most recharge occurs from infrequent, large precipitation events and sustained precipitation events over longer periods, when the rate of input exceeds the rate at which water is output by evapotranspiration or drainage. Depending on the temporal scale investigated in numerical modelling, it may be misleading to consider a long-term average value of recharge or evapotranspiration (de Vries and Simmers 2002).

Several researchers have documented such seasonal fluctuations in till deposits in Canada and the northern United States (Williams and Farvolden 1967; Hendry 1982, 1988; Keller et al. 1986, 1989; D'Astous et al. 1989; Ruland et al. 1991; Simpkins and Bradbury 1992; Husain et al. 1998; Shaw and Hendry 1998; others). In conjunction with climatic fluctuations, these researchers suggest a strong geological control on seasonal water level fluctuations in tills, namely the degree and depth to which the till is fractured. If the till is highly fractured, fluctuations will penetrate deeper, while fluctuations are dampened to low amplitude over small distances in unfractured till (van der Kamp 2001). Fractures provide sufficient permeability to enable active groundwater flow (D'Astous et al. 1989; Ruland et al. 1991), while till matrices are not permeable enough for measurable groundwater flow.

The main diagnostic tool of these researchers is the analysis of hydrographs in vertical profile. As an example, hydrographs from a multi-level piezometer installation from the research of Keller et al. (1989) are presented in Figure 5-9. The till is oxidized and fractured to a depth of 5 m, while tills below are unoxidized. The only piezometer showing any response to seasonal fluctuations is completed at 4.9 m. The very slow initial recovery of the deeper piezometers

also helps to distinguish completions that are not influenced by fracture flow, along with the slow response to falling head tests in 1986. The attenuation of amplitude with depth and phase lag can be seen in the water level hydrographs presented in Figures 5-5 and 5-6.

Hydraulic evidence is often used in conjunction with other independent lines of evidence to distinguish weathered zones from unweathered zones. Usually, this involves visual evidence of fractures in cores, large diameter boreholes or excavations (e.g., Grisak 1975; Hendry 1982, 1988; D'Astous et al. 1989; Keller et al. 1989; Ruland et al. 1991; McKay et al. 1993) or from isotopic and geochemical groundwater investigations (e.g., Grisak 1975; Hendry 1982, 1988; Keller et al. 1986, 1988; Ruland et al. 1991; Simpkins and Bradbury 1992; Gerber et al. 2001). However, it is not usually practical for investigators to use multiple methods in their investigations (Keller et al. 1986).

At the GPRS, natural fracturing was noted to 2 m bgs (Komex 2000b). The seasonal fluctuations in the hydrographs presented in Figures 5-5 to 5-8 would seem to indicate that there are some fracture effects at all depths investigated. This is an obvious conclusion for the piezometers in the area of the horizontal well, which are influenced by natural and hydraulic fractures. It is somewhat more inconclusive for outer piezometer nests (Figure 5-8). B level piezometers (approximately 4 m bgs) tend to mimic the patterns of the shallower A level piezometers. The C level piezometer at P99-1 (9 m bgs) does as well, but the C level piezometer at P99-5 (6 m bgs) does not show large seasonal fluctuations after an initial recovery period. The C level piezometer at P99-1 was partially completed in bedrock and thus may reflect the properties of a bedrock flow regime and not the till. All other C level piezometers have been dry for the duration of the project, signifying perched water table conditions and an impermeable boundary at the base of the weathered till.

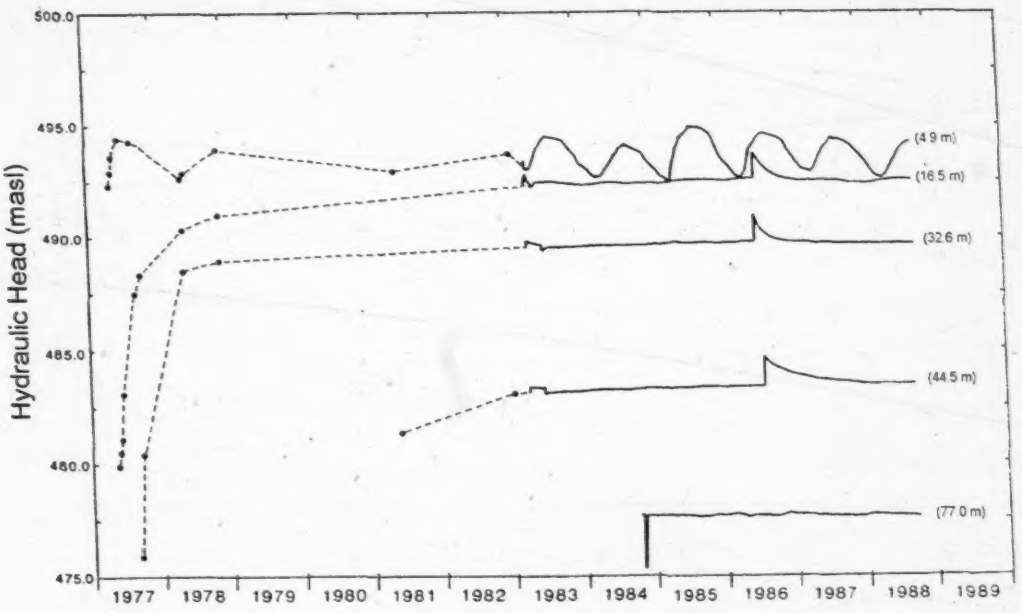

Figure 5-9 Hydrographs from a multi-level piezometer installation in clay till in Saskatchewan (adapted from Keller et al. 1989).

The analysis of seasonal fluctuations is complicated by numerous factors. Direct hydraulic connection between completion depths in a piezometer nest can occur if the bentonite seal is breached or the casing is cracked (van der Kamp and Keller 1993). This effect is apparent in piezometer nest P97-10 (Figure 5-6), where both piezometers have had nearly coincident heads since their installation. If insufficient volumes of water were used to hydrate the bentonite (since the till matrix does not provide appreciable hydration), then all of the piezometers at the GPRS could demonstrate some degree of hydraulic connection to other piezometers completed in the same borehole.

Water levels, as determined from pressure transducers, for the spring 2000 snowmelt period for a shallower (P97-2A) and a deeper (P97-8B) piezometer are shown in Figure 5-10. There were two major inputs of water to the system during the period: snowmelt and 12.4 mm of rain from March 25 to April 15 and 50.4

mm of rain from May 4 to May 11. The water level in the shallow piezometer responds more to the input of water and sooner than the deeper piezometer, even though the deeper piezometer is connected to an induced fracture at depth.

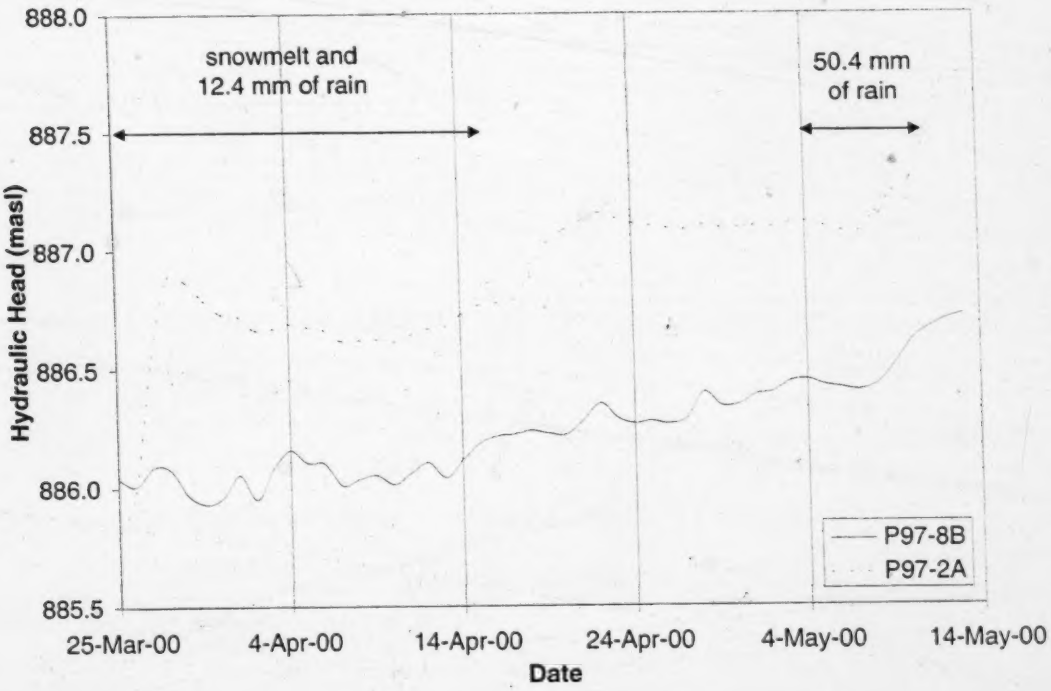

Figure 5-10 Hydraulic heads determined by pressure transducers at a shallow (P97-2A) and a deeper (P97-8B) piezometer during the spring 2000 snowmelt period.

The interannual patterns of recession throughout the winter are relatively constant at each monitoring point (Figures 5-5 to 5-8). For each year, the rate of decline was highest when the water table was at its highest point and then gradually decreased throughout the winter (Figures 5-5 to 5-8). During the separation of hydrographs into components, most hydrologists represent baseflow recession as an exponential decline (Dingman 1994). In this study, successively decreasing linear rates of water level decline are used as an approximation of exponential decline.

Linear rates of water level decline were calculated during two periods for the piezometers instrumented with transducers. These rate calculations were necessary to provide antecedent recession rates for the water table fluctuation method (section 5.4). The first period was from July 1999 to October 1999, after the peak of the water table in July. The second period was from January 2000 to March 2000 in the latter stages of decline before spring snowmelt and precipitation. Least squares lines of best fit were applied to the hydrographs over each period and the slope of the line was determined to be the linear decline rate of the piezometer (in mm/d) for that period. The results are presented in Table 5-3 and consistently show that the rate of water level decline decreased during the recession period (approximately July to March).

Piezometer Location	Linear Decline, Jul-99 to Oct-99 (mm/d)	Linear Decline, Jan-00 to Mar-00 (mm/d)
P97-8B	-10.1	-4.6
P97-10B	-9.3	-3.4
P97-2A	-12.1	-5.6
HP-E	-8.8	-2.4
HP-S	-17.9	-15.9
HP-W	-12.8	-5.8
HP-N	-13.4	-5.2

Table 5-3 Linear decline rates for instrumented piezometers from July 1999 to October 1999 and January 2000 to March 2000.

The controls on the decline rates are presumed to be climatic and geological. Evapotranspiration peaked in June and July (Figure 4-7) and its magnitude decreased into October, whereafter it became negligible. It is expected that the decline rates would be strongly tied to the seasonally transient rates of

evapotranspiration because evapotranspiration is the major groundwater output from the system.

The decline rates described in Table 5-3 cannot be explained by evapotranspiration alone, as peak daily ET_c values only attained approximately 7 mm/d (Figure 4-7). Thomas (1999) described a similar decrease in decline rates for a site approximately 100 km to the south of the GPRS. At Thomas' (1999) site, conductive glaciofluvial sediments overlie tills. He conceptualized that when recharge occurred and the water table rose into the glaciofluvial sediments, horizontal fluxes increased as the permeable sediments drained away water, thus yielding a higher rate of decline when the water table was high. This could be similar to the GPRS, where the upper 2 m is fractured, increasing its permeability, and hydraulic conductivity decreases with depth.

There may be other controls on the linear decline rate as well. In situations where horizontal fractures are not continuous, vertical drainage may dominate (Ruland et al. 1991). Hendry (1988) hypothesized that much of the water entering weathered tills as recharge may be lost not only to evapotranspiration, but also to capillary rise. Some very shallow water may be immobilized due to freezing during the winter as well (Keller et al. 1986).

The hydrographs in profile (Figures 5-5 to 5-8) show that hydraulic heads decline with depth throughout the till. This is common throughout fractured tills in glaciated plains (Williams and Farvolden 1967; Schwartz et al. 1987; Hendry 1988). Therefore, the vertical hydraulic gradient in these tills is generally upward, indicating the potential for downward flow. This was especially true for the P99 series of piezometers (Figure 5-8 and other data not presented). Upward gradients for these piezometers generally varied between 0 and 1, with a maximum of approximately 2.5, with higher values in the spring and summer months.

Analysis of vertical hydraulic gradients in the area of the horizontal well reinforced the complexity of groundwater flow near the well. Due to the variable responses to input and output at various depths, the vertical hydraulic gradient sometimes reversed and became negative (Figure 5-6). Each piezometer in the fractured area of the horizontal well displayed both upward and downward vertical hydraulic gradients over time. An exception was P97-10, which consistently had a gradient near zero due to hydraulic connection between the monitoring points.

Most P97 piezometer nests displayed the same seasonality in vertical gradients as the P99 piezometers (i.e., a higher upward gradient in the summer, approaching 0 in the winter). However, variability was prevalent to the extent that no pattern was discernible at all in some nests. P97-8 consistently had a downward gradient, suggesting that the screen of the B piezometer intercepts a hydraulically conductive fracture. The magnitudes of the upward vertical gradients for the P97 series were similar to those of the P99 series. Downward vertical gradients did not exceed approximately -0.5 and averaged approximately -0.2.

5.4 Groundwater Recharge From Precipitation

The water table fluctuation (WTF) method is among the most widely used methods for quantifying groundwater recharge, and can be described by (Healy and Cook 2002):

$$R = S_y \frac{dh}{dt} \tag{5-3}$$

where R is the rate of recharge [L/T], S_y is the specific yield of the sediment [-], h is the watertable elevation [L] and t is the time [T]. The value of the method lies in the simplicity of its application to readily obtained water level data and its

insensitivity to the mechanisms with which water flows through the variably saturated zone to the water table.

There are several assumptions in the mathematical model and recommended conditions of use for the WTF method (Healy and Cook 2002, Scanlon et al. 2002). The key assumptions are that water reaching the saturated zone goes instantaneously to storage and that infiltrating water is partitioned only to storage and not to groundwater flow, baseflow or evapotranspiration. The latter assumption may be valid if the method is applied over a short interval following precipitation due to the time lag required for the redistribution of water in the subsurface.

The method is best used with shallow piezometers that display sharp rises following precipitation events, as infiltration events are normally attenuated with depth (section 5.3). Uncertainty may arise if the causes of fluctuations other than precipitation are significant and not quantified. Examples of these include barometric pressure effects, pumping effects and the effects of entrapped air between the water table and the infiltrating water (Healy and Cook 2002).

Although gross values of recharge are calculated by analyzing responses to individual precipitation events, it is also possible to calculate seasonal net recharge values (Healy and Cook 2002). This is accomplished by modifying Δh to be the difference between the seasonal peak in hydraulic head and the low point to which a calculated antecedent recession curve would fall at the time of the seasonal peak. Recession curves may be extrapolated with the recession constants calculated in the previous section (Table 5-3).

Also required for the calculation is an estimate of S_y for the porous medium. Values of S_y for till are found to range over an order of magnitude, from 0.005 to 0.06 (Zaltsberg 1985, Domenico and Schwartz 1990). Lower values are for tills with high clay contents while higher values are described for fractured tills. S_y is

probably not constant across the site due to heterogeneity. It probably also changes with depth due to the compressibility of till (Shaver 1998). Given the range and the direct proportionality of S_y to the recharge estimate, the S_y value selected might be a considerable source of uncertainty.

Net recharge was calculated for the 2000 field season for the same monitoring points that recession rates were calculated for (Table 5-3). S_y was chosen to vary from 0.02 to 0.05 to represent clayey to fractured till. The recession constants for the period of January 2000 to March 2000 were used to correct the initial head levels, as required to calculate net recharge. Results for recharge estimates for the 2000 field season using the WTF method are presented in Table 5-4.

Piezometer Location	Head At Initial Rise (m)	Head at Peak (m)	Δh (m)	Δt (d)	R (mm/d)
P97-8B	885.45	887.87	2.42	104	0.5-1.2
P97-10B	885.96	887.76	1.80	99	0.4-0.9
P97-2A	885.15	887.87	2.72	118	0.5-1.2
HP-E	886.39	888.48	2.09	108	0.4-1.0
HP-S	882.37	888.93	6.56	114	1.2-2.9
HP-W	886.58	889.54	2.96	103	0.6-1.4
HP-N	886.44	889.59	3.15	112	0.6-1.4

Table 5-4 Recharge estimates for instrumented piezometers for the 2000 field season using the WTF method and estimating S_y to be between 0.02 and 0.05.

All monitoring points, with the exception of HP-S, show similar ranges in the calculated rate of recharge (Table 5-4). HP-S displayed anomalous behaviour throughout the field program and is thought to be connected to hydraulic fractures and disturbed soil from site activities. Piezometric variables

(completion depth, location on site, screen length) do not appear to have an influence on the calculated rate of recharge. Therefore, the values in Table 5-4 are expected to be representative of the site as a whole to the depth of these completions (~ 2-4 m).

Other than uncertainty about the representativeness of the S_y estimates, uncertainty arises from the violation of assumptions made when using the WTF method. The use of S_y implies that recharge is through an unconfined zone to the water table and changes the volume of water stored in the pore space (Freeze and Cherry 1979). There is some evidence to the contrary. Transient measurements of soil moisture indicated that soil moisture contents at the GPRS are stable over time (section 4.4.1), except in zones with high permeability (sand lenses and disturbed soils).

There is also frequently discrepancy between precipitation values and the observed water table rise. For example, 50.4 mm of precipitation fell from May 4 to 11, 2000. The observed water table rise in P97-2A (Figure 5-10) was 0.68 m, or 680 mm. Assuming a S_y of 0.05, only 34 mm of infiltration from precipitation would be required for this water table rise, meaning that 16.4 mm of precipitation was not accounted for. This could suggest several things:

- S_y was underestimated. This could suggest that the influence of recharge through saturated fractures increased the overall S_y of the till, even if the S_y of the till matrix was likely 0.05 or less;
- If S_y was estimated correctly, then infiltrating water was quickly partitioned elsewhere, violating the assumption that all precipitation goes to groundwater storage.

The latter suggestion could readily be explained by two mechanisms: capillary rise and evapotranspiration. Gillham (1984) reasoned that fine-grained materials such as clay may display considerable capillary rise and may be tension

saturated for several metres above the water table. Thus, infiltrating water is held close to the ground surface for energy-limited evapotranspiration.

Evapotranspiration estimates from bare soil were 13.1 mm for May 4 to 11 (the period of precipitation) and 17.4 mm for May 7 to 13 (the period of the water table rise in P97-2A). Therefore, evapotranspiration could readily account for the missing 16.4 mm of precipitation. This also better constrains the estimated value of S_y to 0.05. Capillary rise coupled with evapotranspiration is the same mechanism that Hendry (1988) described for loss of recharge in a shallow weathered-unweathered till system in southern Alberta.

5.5 Barometric Efficiency of Till Deposits

5.5.1 Barometric Pressure Effects

The effect of barometric pressure on water levels is an inverse one i.e., an increase in barometric pressure causes a decrease in water levels and vice-versa (Rasmussen and Crawford 1997). An example of barometric and water level fluctuations (HP-W) over the period of a week in February 2000 is shown in Figure 5-11. The ratio of the water level change to the barometric pressure change, the barometric efficiency, is typically 20% to 75% in confined aquifers (Freeze and Cherry 1979). The effect is also recognized in unconfined aquifers (e.g., Weeks 1979) although it is often ignored (Hare and Morse 1997).

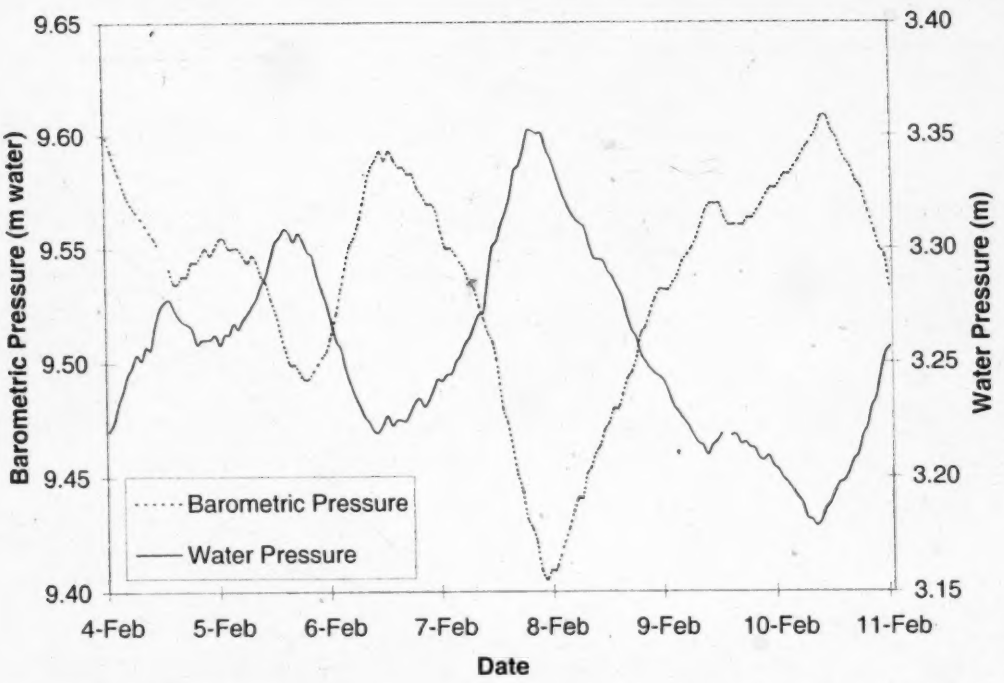

Figure 5-11 Barometric pressure and pressure head fluctuations at HP-W during a week in early February 2000.

The water level record of a piezometer is a composite of the various transient effects acting on water in both the piezometer and the aquifer (Furbish 1991). Barometric pressure fluctuations can mask the effects of other stress components acting on the aquifer, especially when the response of the aquifer to the other components is of lower magnitude than the response to barometric pressure. For example, the seasonal decline of water levels, or the response of lower permeability materials to pumping stresses at distant piezometers may be of lower magnitude than the response to barometric pressure. To resolve these lower magnitude components, it may be necessary to remove barometric pressure fluctuations from water level records.

Even though barometric influences on water level records are widely recognized, a standardized procedure on how to quantify and remove them is lacking (Rasmussen and Crawford 1997). Least squares regression is sometimes

applied, but the forms of other transient effects must be known to determine the barometric efficiency. When the response of the hydraulic head to barometric fluctuations is rapid and assumed to be constant over time, a constant barometric efficiency is applied to quantify the fluctuations (Davis and Rasmussen 1993).

5.5.2 Clark's Method

Clark (1967) developed a method to estimate the barometric efficiency of an aquifer based on incremental changes in barometric pressure and water levels. Using Clark's (1967) notation, the barometric efficiency of a formation is defined as:

$$\alpha = -\frac{\Delta W}{\Delta B} \tag{5-4}$$

where α is the barometric efficiency, ΔW is the change in the piezometer's water level during an arbitrary period of time, and ΔB is the change in barometric pressure during that same period of time.

Using Clark's (1967) method does not require specification of the form of underlying trends (Davis and Rasmussen 1993). The method is applied by following a set of rules for observed barometric pressure and water level changes (Clark 1967). The procedure assigns water level changes (ΔW) a positive sign when the water level is increasing, and assigns barometric pressure changes (ΔB) a positive sign when the barometric pressure is decreasing. Summations of ΔW and ΔB are made over constant time intervals, giving $\Sigma\Delta W$ and $\Sigma\Delta B$, by the following guidelines:

(1) When ΔB is 0, neglect any corresponding value of ΔW in obtaining $\Sigma\Delta W$;
(2) When ΔW and ΔB have similar signs, add $|\Delta W|$ when obtaining $\Sigma\Delta W$;
(3) When ΔW and ΔB have dissimilar signs, subtract $|\Delta W|$ when obtaining $\Sigma\Delta W$;

(4) To obtain $\Sigma\Delta B$, sum $|\Delta B|$ over all time increments.

The estimated barometric efficiency, α^*, is thus:

$$\alpha^* = \frac{\Sigma \Delta W}{\Sigma \Delta B} \qquad (5\text{-}5)$$

There is some uncertainty in the use of the "constant time interval" in the calculation. Clark (1967) does not specify a time interval. Davis and Rasmussen (1993) report efficiency values for every 20 days of their data record, but it is not clear what time interval they used in the calculation of efficiency. Spectral analysis of the barometric pressure data revealed peaks in the frequency spectrum at 24 hour intervals (data not presented). Thus, an interval of 24 hours was used to ensure that water level records were equally influenced by periodic barometric trends.

Selected graphs displaying the calculation of barometric efficiency by Clark's (1967) method are shown in Figure 5-12. The sinusoidal behaviour of the graphs can be attributed to periods when barometric fluctuations are alternately reinforced and dampened by other stresses (Clark 1967). Over a long enough period, the reinforcement and dampening should balance. Results for barometric efficiencies and correlation coefficients (R^2), which measure the tendency of water levels and barometric pressure to co-vary, at monitoring points with pressure transducers are presented in Table 5-5.

Most of the calculated correlation coefficients are high, indicating that water level fluctuations are explained quite well by barometric pressure fluctuations. An exception is HP-S, which may be hydraulically connected to a sand-filled fracture and disturbed soil, and behaved relatively erratically throughout the project.

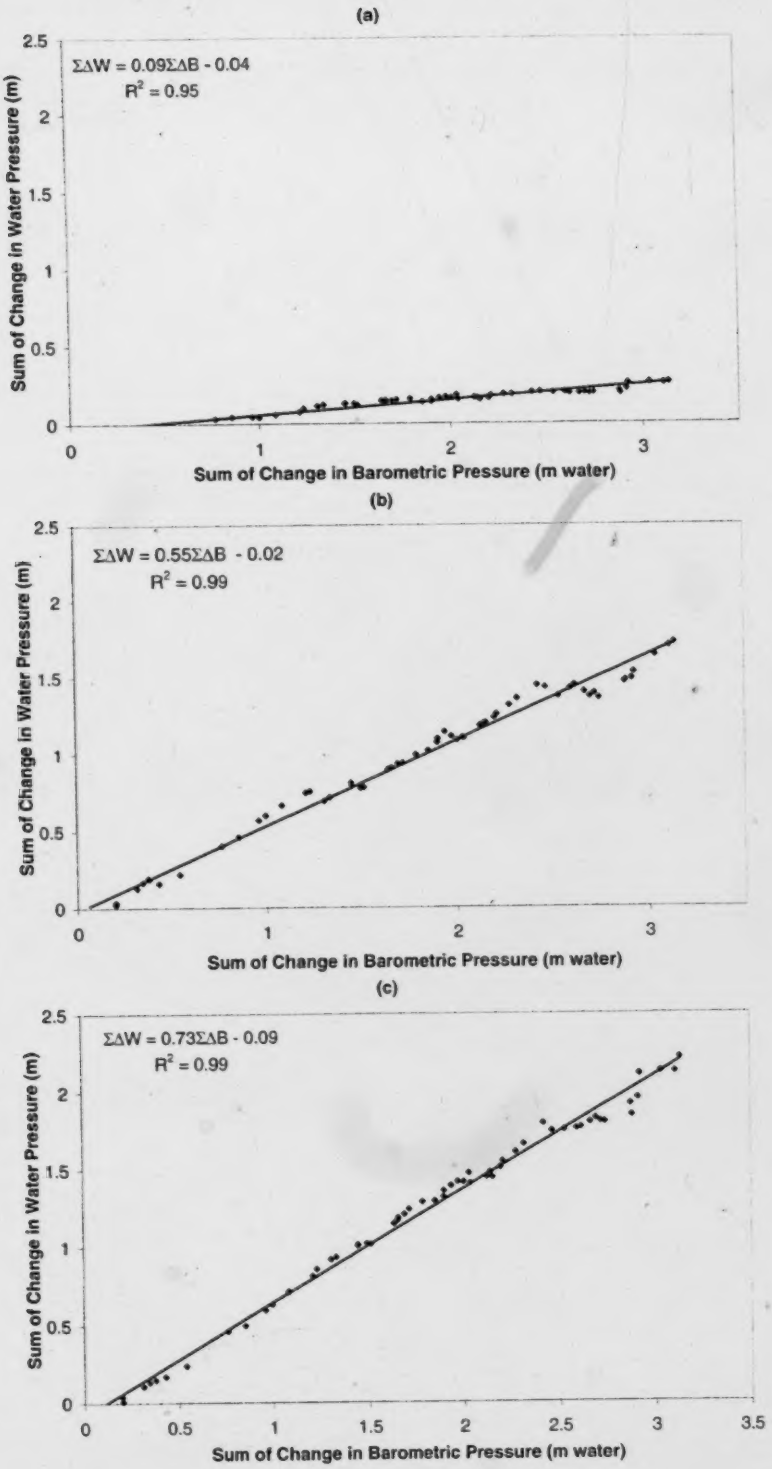
(a)
ΣΔW = 0.09ΣΔB - 0.04
R² = 0.95
Sum of Change in Water Pressure (m)
Sum of Change in Barometric Pressure (m water)
(b)
ΣΔW = 0.55ΣΔB - 0.02
R² = 0.99
Sum of Change in Water Pressure (m)
Sum of Change in Barometric Pressure (m water)
(c)
ΣΔW = 0.73ΣΔB - 0.09
R² = 0.99
Sum of Change in Water Pressure (m)
Sum of Change in Barometric Pressure (m water)

Figure 5-12 Calculation of barometric efficiency for (a) P97-2A, (b) P97-8B and (c) HP-W with Clark's (1967) method.

Piezometer	Barometric Efficiency (%)	Correlation Coefficient (R^2)
P97-2A	10	0.95
P97-8B	55	0.99
P97-10B	21	0.99
HP-N	24	0.98
HP-W	73	0.99
HP-S	10	0.89
HP-E	21	0.99
Metal Culvert	7	0.97

Table 5-5 Calculated barometric efficiencies and correlation coefficients for instrumented piezometers using Clark's (1967) method.

There is high variability in the calculated efficiencies and there does not appear to be any similarity in the efficiencies of neighbouring installations. For example, P97-8B and P97-10B are approximately 7.5 m apart, but their calculated efficiencies vary by a factor of 2 (Table 5-5). Similarly, the range of calculated efficiencies for the HP piezometers is over 60% (Table 5-5). Some of this variability may be attributed to the heterogeneous nature of till. The invalidity of the assumptions that the aquifer is confined, elastic, of uniform thickness and infinite horizontal extent (Davis and Rasmussen 1993) also contributes to variable responses. Due to a lack of information on HP piezometers, the influence of piezometric variables (location on site, screen length) was indeterminate.

It appears that efficiencies increase with the depth of the screen interval. Heads in the shallow till take less time to equilibrate to barometric pressure changes than at deeper points. The highly disturbed nature of the surface fill increases it's gas diffusivity, which depends on porosity, permeability and soil moisture (Tindall and Kunkel 1999). High diffusivities and shallow water tables typically result in smaller barometric effects (Weeks 1979; Rasmussen and Crawford 1997).

Perfectly unconfined aquifers often have efficiencies near zero. Therefore, a shallower piezometer, such as P97-2A, should have greater hydraulic connection to barometric pressure changes. The resulting water level head response to these changes is of lower magnitude due to a lower pressure gradient between the formation and the piezometer, meaning a lower efficiency.

The response of the deeper piezometers to barometric fluctuations reveals the confining nature of the silt and clay till. Jacob's (1940) model for barometric effects on confined aquifers assumed that barometric pressure changes are transmitted to the aquifer and the pressure change is shared by the aquifer skeleton and pore water. The pressure change is borne entirely by the water in an open well, thereby setting up a pressure imbalance between the well and the aquifer, which has not equilibrated to the pressure change, causing the instantaneous fluctuations. Therefore, although the shallow groundwater system at the GPRS is not truly confined, the instantaneous response to barometric pressure effects is similar to that of a confined system due to the presence of low-permeability materials (Hare and Morse 1997).

The lowest calculated value of efficiency (7%) was that of the trench and culvert system (Table 5-5). This was due to the time delay required for water to flow from the trench to the culvert, or a borehole storage effect (Rasmussen and Crawford 1997). The efficiency was also low in P97-2A, likely due to connection with loose soil surrounding a pipeline near the piezometer. One of the conditions implicit in the use of a constant barometric efficiency is minimal borehole storage effects so that the water level change reflects changes in the geologic formation (Davis and Rasmussen 1993). Therefore, as expected, the calculated value of efficiency for the trench and culvert system was lower than for the other points, which are small diameter piezometers.

5.5.3 Correction of Measured Water Levels

With barometric efficiency estimates, corrections were made to the time-series of water level data using:

$$W(t) = W_0 + \alpha(B_t - B_0) \qquad (5\text{-}6)$$

where W(t) is the corrected water level at the end of a 24 hour time interval t, W_0 is the water level at the beginning of the interval, B_t is the barometric pressure at the end of the interval and B_0 is the barometric pressure at the beginning of the interval.

Results for the maximum changes between measured and corrected values, along with the average correction for 24-hour intervals, are presented in Table 5-6. The maximum positive corrections at each monitoring point occurred in the period between February 1 and February 3 when there was a large, persistent decrease in the barometric pressure. Otherwise, the average corrections for a 24-hour interval were all less than 5 cm.

The correction of a hydrograph with constant barometric efficiency is shown in Figure 5-13. It seems that correcting heads with a constant barometric efficiency is effective at dampening the water level fluctuations. However, the average correction for a 24-hour interval is small and it remains difficult to interpret the response of the system to influences other than barometric pressure. It appears that notable barometric effects remain even after the corrections are made.

Piezometer	Maximum Positive Difference (cm)	Maximum Negative Difference (cm)	Average Absolute Difference (cm)
P97-2A	2.1	-1.3	0.5
P97-8B	12.3	-8.6	2.9
P97-10B	4.6	-2.8	1.1
HP-N	5.4	-3.2	1.2
HP-W	16.1	-9.6	3.7
HP-S	2.2	-1.3	0.5
HP-E	4.7	-2.8	1.1
Metal Culvert	1.6	-0.9	0.4

Table 5-6 Differences between measured and corrected hydraulic heads during the barometric efficiency study.

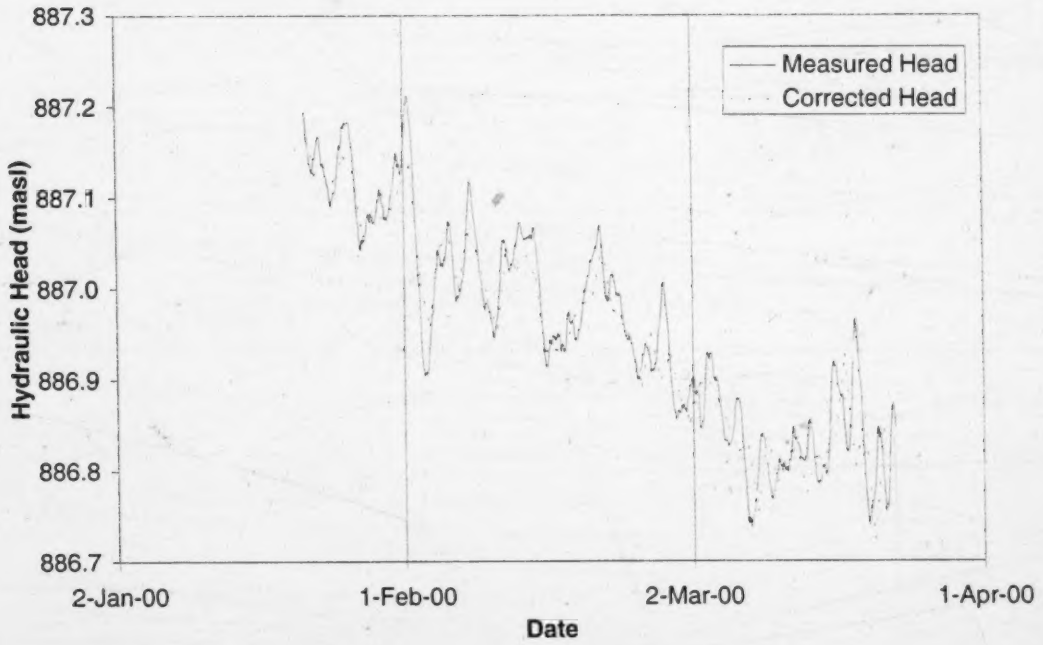

Figure 5-13 Water level corrections for HP-W from January to March 2000 using a constant barometric efficiency.

Given that barometric fluctuations have been shown to have a significant influence on water level records in tills, it seems that a more rigourous method is required to effectively remove these fluctuations. It is difficult to distinguish other stresses on the system, even when the spatially variable barometric pressure effects are taken into account. Methods other than applying a constant barometric efficiency are recommended to more effectively remove noise from the time series of water level measurements, although no other methods are investigated for this project. Therefore, the uncertainty in measured heads due to barometric fluctuations is deemed acceptable.

5.6 Horizontal Groundwater Fluxes

5.6.1 Relation of Water Table to Topography

Given that the site is located on the slope of a lake valley, topography was expected to influence the hydraulic head distribution. Figures 5-1 and 5-2 show that the water table elevation (as determined by shallow piezometers) is essentially a replica of the ground surface, with some variations. This is generally found to be true under all but the most extreme hydrogeologic conditions (great topographic relief or extreme climates) (Ingebritsen and Sanford 1998).

The hydrologic effects of small-scale variations in topography at the GPRS were likely lessened when the site was cleared and graded. For example, local ponding of precipitation occurred, but local topographic gradients were not large enough to cause overland flow to be a significant part of the flow regime. In contrast, Buttle (1989) found overland flow to dominate the runoff response of a till hillslope (drumlin) with slope gradients ranging from 2° to 6°. Otherwise, the hydrologic responses of the GPRS and the drumlin setting of Buttle (1989) showed many similar characteristics, such as seasonal fluctuations in response to snowmelt and precipitation, significant capillary rise and the development of perched conditions.

The influence of topography on the position of the water table can also reveal the control of subsurface features on hydrologic response. When the water table is a subtle reflection of the topography, such as at the GPRS and at the Dalmeny, Saskatchewan, site studied by Keller et al. (1988), variations in the shallow flow regime are controlled by the variability in water inputs, which can in turn be controlled by small-scale topographic variations (on the order of 10's of cm). These properties are able to influence the variability of the flow regime because of the high bulk K due to fracturing (Keller et al. 1988). In contrast, the water table position in unweathered, low K units at the Warman, Saskatchewan, site was not found to depend on topographic features (Keller et al. 1988).

5.6.2 Contour Maps of Hydraulic Head

Water table maps were created to visualize the spatial distribution of hydraulic head measured at different times. Maps were created by projecting the water table surface on the location map (Figure 2-4) utilizing manually measured water level data. All maps were created with Surfer 7, a contouring and surface mapping program (Golden Software Inc. 1999).

To create the maps, point hydraulic head observations were extended across the area under investigation. This was accomplished through kriging, a linear interpolation scheme that minimizes the expected value of the squared error of the estimated variable between observation points (Gelhar 1993). Kriging was performed with *kt3d*, a program in the Geostatistical Software Library (GSLIB) (Deutsch and Journel 1992). Kriging is well established as an estimation method in geoscience and a full statistical description and analysis lies outside the scope of this work. For further details, the reader is referred to de Marsily (1986), Deutsch and Journel (1992), Gelhar (1993) and Kitanidis (1997).

Kriging relies on the weighting of observations based on their proximity to the estimated location and the spatial correlation of the variable between the known

and estimated locations. The length of correlation is expected to be small for the heterogeneous subsurface: water levels in neighbouring piezometer nests were observed to be quite different over small scales in the area of the horizontal well. Spatial variation was modelled as a linear variation based on the surface slope, representing that the water table is a subdued replica of the ground surface elevation.

Contour maps were constructed for different times using shallow piezometer heads (completion intervals near 2 m bgs) to investigate water table conditions under different stress regimes. Of these maps, three are presented in Figures 5-14 through 5-16 for December 1999, May 2000 and September 2000, respectively. These maps enable the analysis of the effects of climate, as well as pumping induced stresses. The maps are overly smooth, which is an artifact of kriging in locations with sparse data and does not imply that the water table surface is actually that uniform.

In general, potential horizontal flow directions across the site are to the south or southwest. This is consistent regardless of time of year or induced stresses. This was also documented by previous studies in 1997 and 1998 (Komex 2000b) and continued throughout 2001 as well. Local complexities abound, especially near the horizontal well, but a consistent pattern of radially outward flow from the raised pad area is also apparent.

The highest groundwater elevations are consistently in the raised pad area near the culvert and trench system. Another artifact of the trench and culvert system is a series of open wells in the raised pad area that were used to re-circulate water in the trench prior to the GPRP. These wells, plus the high amount of gravel in the pad area, enhanced recharge in the pad area. Data from May 2000 (Figure 5-15) suggest that a seasonally transient, northward component of flow may develop in the raised pad area. This was also noted in previous years (Komex 2000b).

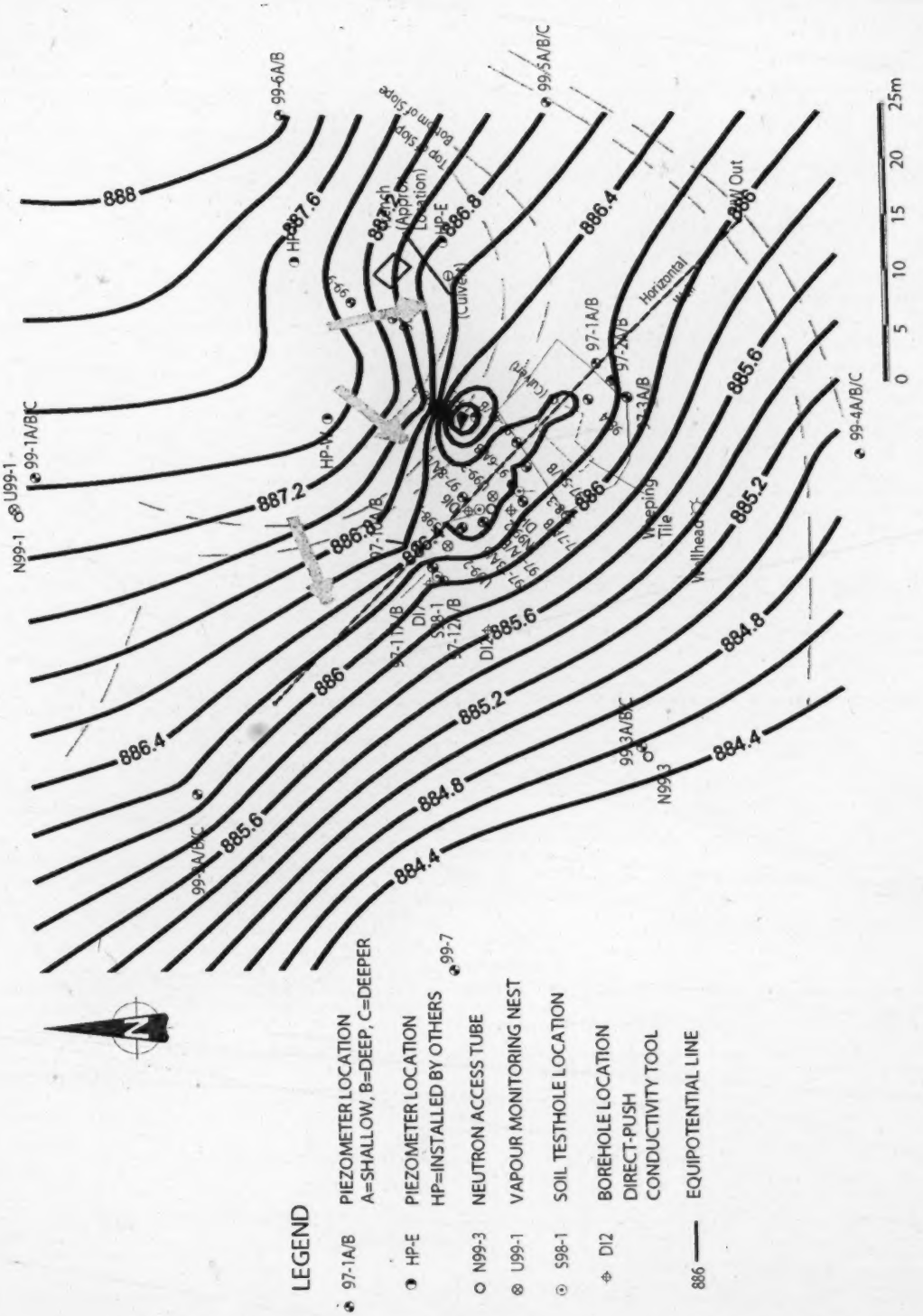

Figure 5-14 Water table map from December 21, 1999 superimposed on the site location map.

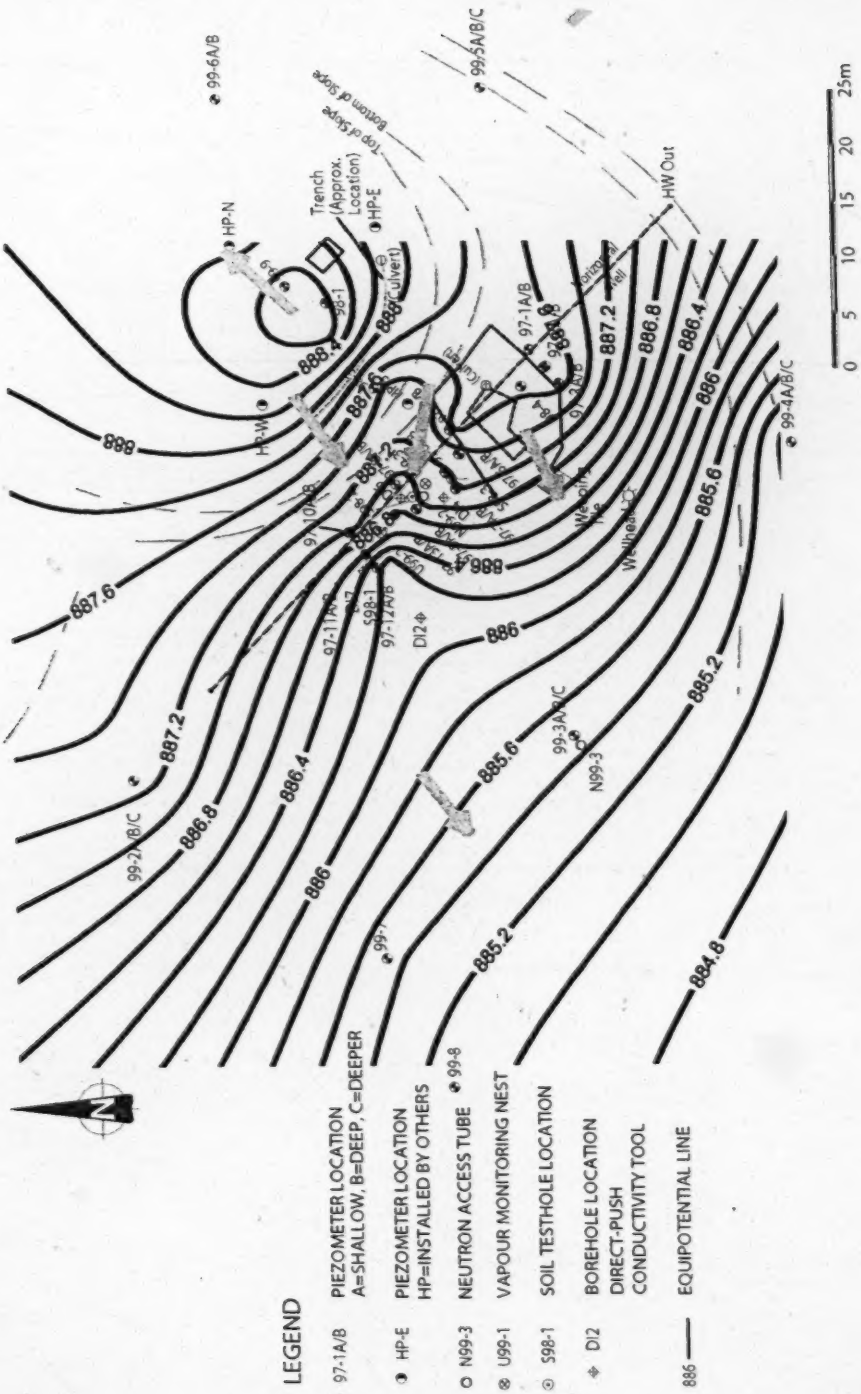

Figure 5-15 Water table map from May 18, 2000 superimposed on the site location map.

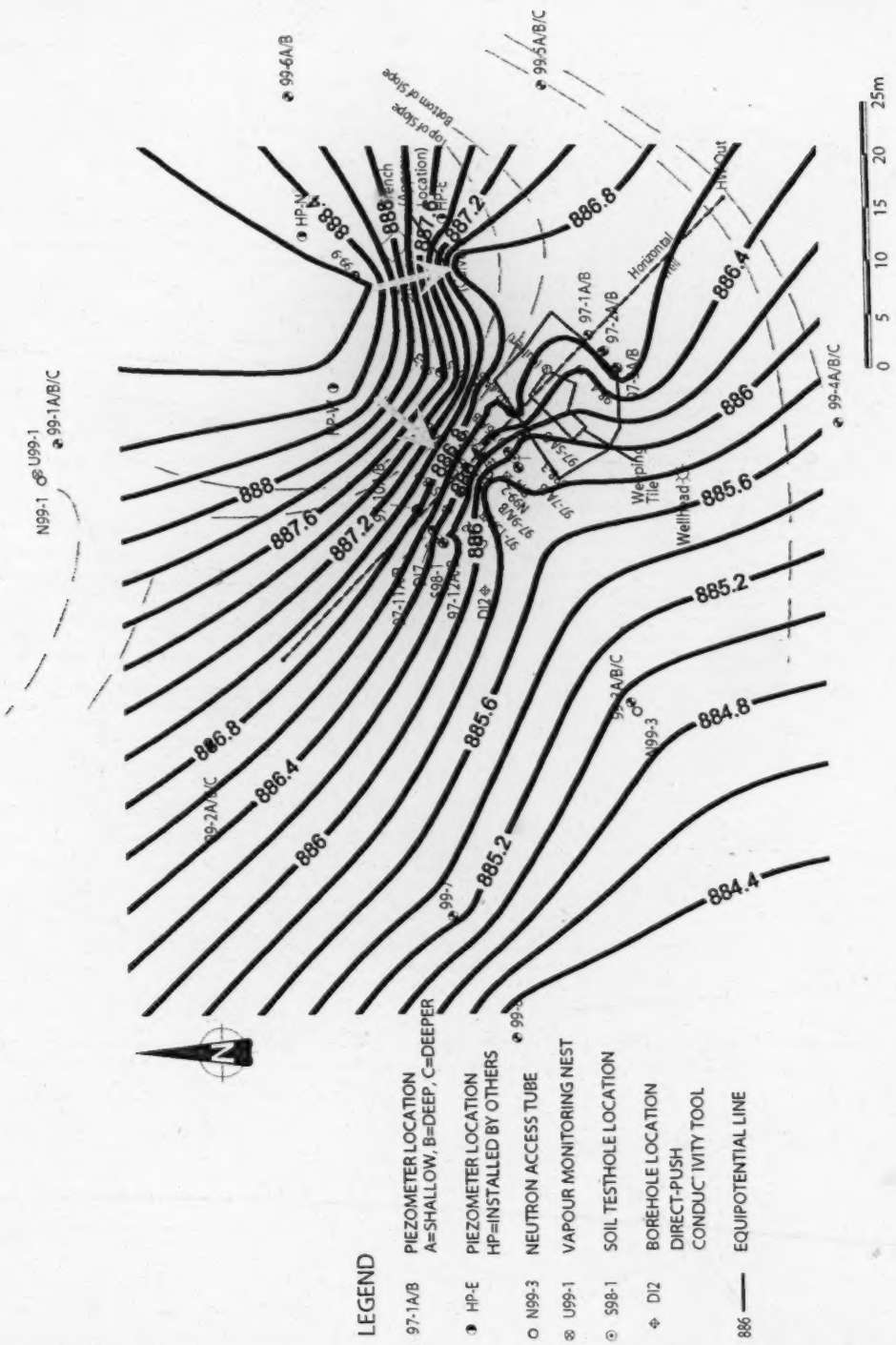

Figure 5-16 Water table map from September 1, 2000 superimposed on the site location map.

It is also apparent from Figure 5-15 that flow is focused towards the hydraulically fractured area during periods of recharge. Along with the previously described effects of dewatering on soil moisture in these induced fractures (section 4.4.1), this is consistent with a dual porosity system, where the majority of horizontal flow is through continuous, conductive fractures in the till. Thus, the fractures preferentially fill with water during periods of recharge.

The impact of the hydraulic test and dewatering events can be seen in Figures 5-14 and 5-16. The hydraulic test in the trench and culvert in the fall of 1999 (Table 3-5, Figure 5-14) had minimal impact on the local flow system. In contrast, dewatering in the summer of 2000 (Table 3-5, Figure 5-16) had a significant impact, inducing increased gradients and localized depressions in the area of the horizontal well and the metal culvert, the areas from which water was extracted.

There are many more complexities in the flow system than can be resolved by the distribution of the shallow piezometers. For example, some shallow piezometers (e.g., at P99-3) were consistently dry. This may suggest a thinning of the shallowest water bearing material towards the south end of the site, although more data would be required to conclude this. Previous site activities have disturbed groundwater flow. This is readily apparent in the area of the horizontal well, which was heavily instrumented, but is probably also true in areas with sparse data. For example, the wood waste burial area in the southwest corner of the site has likely enhanced horizontal flow, although not enough is known about its extent to estimate its possible impact on the site. Also, the numerous subsurface pipelines and their associated soil disturbance have likely impacted groundwater flow, but it is not possible to determine the scale of their impact.

5.6.3 Horizontal Groundwater Gradients and Velocities

An important question at most remediation sites is the potential rate of solute migration. The advective flux of chemicals depends directly on the average linear groundwater velocity (Bedient et al. 1994):

$$F = v n_e C \tag{5-7}$$

$$v = \frac{K}{n_e}\frac{dh}{dl} \tag{5-8}$$

where F is the one-dimensional advective flux [$M/L^2/T$], v is the average linear groundwater velocity [L/T], n_e is the effective porosity [-] and C is the chemical concentration [M/L^3]. The overall solute flux also depends on diffusion, dispersion and degradation, which depend on particular chemical and subsurface properties. In the clay till matrix, diffusion may be the dominant process (Cherry 1989), but the overall solute flux should be controlled by advective flux through fractures in the till (McKay et al. 1993).

Horizontal hydraulic gradients calculated over the period of approximately 1 year (October 1999 to September 2000) are presented in Table 5-7. Gradients were similar for 2001. On the dates for which maps (Figures 5-14 to 5-16) were produced, gradients were estimated from both maps and field data as a means to validate the maps. The gradients were calculated in three areas on the site based on where geochemical, geophysical and hydrogeological data indicated that chemical migration might be most likely to occur:

- South of the fractured area of the horizontal well. It was conceptualized that the fractured area may act as a source zone for the soluble chemicals present on-site;

- Between the raised pad area and the horizontal well. There is some indication that the processing chemicals moved from the pad area to the area of the horizontal well; and,
- Between the raised pad area and areas to the north. This gradient was only determined at one time (May 18, 2000) when contour maps indicated the potential for a northward component of flow from the raised pad area.

Gradients were not directly calculated in the area of the horizontal well due to the complexity of flow patterns and potential connections among piezometers.

The gradients calculated from maps and from field data are similar, increasing confidence in the gradients calculated solely from maps south of the horizontal well. Gradients from HP-W to P97-10 gradually decrease over the fall and winter and then increase again during recharge, indicating some seasonal dependence. The highest gradients calculated between HP-W and P97-10 occurred during dewatering, indicating that dewatering stress has the potential to induce greater flow than natural conditions. This calculation assumes a linear gradient, which is likely untrue. Much of the head loss during dewatering probably occurs in conductive fractures.

Average linear groundwater velocities were also estimated for the same times and locations for which the hydraulic gradients were calculated (Table 5-8). The effective porosity used for all calculations was 0.2, based on soil moisture results (section 4.4.1). Hydraulic conductivities were chosen as the maximum and minimum of field measured data relevant to each area of the site:

- South of the horizontal well, the maximum and minimum of the 2000 bail tests in shallow piezometers were chosen (Table 5-1);
- Between the raised pad area and the horizontal well, the maximum and minimum of Komex bail tests in shallow horizontal well piezometers were chosen (section 5.2.2);

- Between P99-9 and HP-N in the raised pad area, the maximum and minimum of Komex bail tests in raised pad area piezometers were chosen (section 5.2.2).

Date	Location and Method	Hydraulic Gradient
6-Oct-99	S of horizontal well – map	0.08
	HP-W to P97-10 – map	0.09
	HP-W to P97-10 - actual	0.09
21-Dec-99	S of horizontal well – map	0.08
	HP-W to P97-10 – map	0.07
	HP-W to P97-10 - actual	0.06
2-Mar-00	S of horizontal well – map	0.05
	HP-W to P97-10 – map	0.07
	HP-W to P97-10 - actual	0.05
18-May-00	S of horizontal well – map	0.04
	HP-W to P97-10 – map	0.10
	HP-W to P97-10 – actual	0.10
	P99-9 to HP-N – map	0.05
	P99-9 to HP-N - actual	0.05
1-Sep-00	S of horizontal well – map	0.04
	HP-W to P97-10 – map	0.14
	HP-W to P97-10 - actual	0.13

Table 5-7 Horizontal hydraulic gradient estimates for October 1999 to September 2000.

Date	Location	v (m/s)	v (m/y)
6-Oct-99	S of horizontal well	2.4×10^{-9} to 1.4×10^{-7}	0.076 to 4.4
	HP-W to P97-10	1.0×10^{-7} to 1.2×10^{-6}	3.3 to 39
21-Dec-99	S of horizontal well	2.3×10^{-9} to 1.4×10^{-7}	0.074 to 4.3
	HP-W to P97-10	7.0×10^{-8} to 8.6×10^{-7}	2.2 to 27
2-Mar-00	S of horizontal well	1.6×10^{-9} to 9.5×10^{-8}	0.051 to 3.0
	HP-W to P97-10	5.3×10^{-8} to 8.4×10^{-7}	1.7 to 27
18-May-00	S of horizontal well	1.2×10^{-9} to 6.8×10^{-8}	0.037 to 2.1
	HP-W to P97-10	1.1×10^{-7} to 1.3×10^{-6}	3.3 to 40
	P99-9 to HP-N	2.0×10^{-9} to 3.3×10^{-8}	0.061 to 1.0
1-Sep-00	S of horizontal well	1.2×10^{-9} to 7.0×10^{-8}	0.038 to 2.2
	HP-W to P97-10	1.4×10^{-7} to 1.8×10^{-6}	4.5 to 57

Table 5-8 Average linear groundwater velocity estimates for October 1999 to September 2000.

In general, calculated velocities are quite low. The upper bound estimates between HP-W and P97-10 are probably unrealistic, as the K chosen was that from a piezometer connected to a fracture. The high estimates, if valid at all, would only be valid over very short scales near fractures in the horizontal well. The most probable velocities are less than 5 m/y. All estimates assume that there is continuous hydraulic connection and the gradient is aligned between measurement points. These assumptions are probably not true in the heterogeneous environment.

5.7 Summary of Key Points for Conceptual Model Development

- Site stratigraphy and hydrostratigraphy were shown to be similar to regionally acquired data. Four stratigraphic units were identified above

bedrock (surface fill, olive brown till, dark brown till and grey till/bedrock contact).

- A wide range of local scale K estimates was determined from bail tests and other hydraulic tests, ranging from 10^{-9} m/s to 10^{-6} m/s. In general, K decreases with depth and the transition from weathered to unweathered till. The K results indicated fracture effects and active groundwater flow to approximately 4 m depth, but were indeterminate below this depth. The highest K determined, and region where the most active groundwater flow was expected, was in the area of induced hydraulic fracturing.
- Seasonal fluctuations dominated the local water level response. Piezometers at the B level (4 m bgs) showed delayed and attenuated responses to water input as compared to shallower A level piezometers (2 m bgs). The C level piezometers (≥ 6 m bgs) generally did not respond to seasonal fluctuations and many were dry for the duration of the study, suggesting perched water table conditions and a low permeability boundary at the contact between weathered and unweathered till.
- Hydraulic heads generally decreased with depth, which is common for Alberta till environments. This indicated upward hydraulic gradients and the potential for recharge. Upward vertical gradients greater than 1, and up to 2.5, are also strongly indicative of perched water table conditions. There was a high degree of variability in vertical gradients in the area of the horizontal well due to hydraulic connection with fractures or poor piezometer completions.
- Recharge was quantified by the water table fluctuation method. The range of values calculated across the site varied from 0.4 mm/d to 3 mm/d during the 2000 recharge period. This method also reinforced the importance of vertical fluxes, with infiltrating water accounted for by recharge and evapotranspiration.
- Barometric fluctuations were shown to have a noticeable impact on water levels. Calculated barometric efficiencies ranged from 7% to 73%, with no apparent spatial trends. Water level corrections were quantified, but

barometric effects remained after correcting with a constant barometric efficiency. The uncertainty in measured water levels due to barometric fluctuations was accepted, and no other methods were used to attempt to further correct for the fluctuations.

- Horizontal hydraulic gradients calculated from collected data and contour maps were relatively insignificant compared to vertical gradients. The most probable horizontal velocities calculated did not exceed 5 m/y (Table 5-8). Given the low horizontal gradients, relatively low permeabilities and the lack of evidence for discharging shallow groundwater, it appeared that the vertical fluxes of recharge and evapotranspiration dominated the local flow regime over lateral flow.

CHAPTER 6

NUMERICAL GROUNDWATER MODELS OF THE GPRS

6.1 Objectives and Strategy

The primary objective of numerical modelling was to represent the significant features of the local groundwater flow system described in previous chapters. Numerical model construction and calibration reinforced the conceptual flow model, but also revealed which areas of the conceptual model required further evaluation and development.

It is generally considered good practice to construct several conceptual models at the beginning of a project, and then cull the models that no longer fit as the interpretation proceeds (Poeter and Hill 1996). The modelling strategy included investigating three different timeframes, each building upon the results of the previous scenario to facilitate the interpretation of field-scale flow:

1. The 1999 field season (April 1999 to April 2000) was a simplified model for deriving useful information for the calibration scenario. For example, model response to various initial head conditions was evaluated. The 1999 field season was not included in model calibration due to a lack of field data from the early part of the season and from slowly recovering 1999 piezometer installations.
2. The 2000 field season (April 2000 to April 2001) was used to calibrate the model. After the measurement and input of relevant boundary fluxes, internal stresses and geologic parameters during this time period, manual trial and error adjustment was used to produce simulated heads that approximated field observations.
3. The 2001 field season (April 2001 to November 2001) was used to verify the calibrated model. Parameter values determined during calibration were held constant while simulating a scenario with different boundary

fluxes and internal stresses, as determined from hydrological monitoring in 2001. Verification helped to evaluate uncertainty in the model calibration.

6.2 Conceptual Model

A summary of the physical scenario under consideration is presented in Figure 6-1. The cross-section includes representations of measured hydrological fluxes and stresses, and lithological divisions that were essential to the development of conceptual models.

The subsurface is divided into three layers: a thin, re-worked backfill surface layer, a weathered and certainly fractured silty till, and an unweathered and indeterminately fractured stiff clay till. The hydraulic conductivity of the layered system decreases with depth. Layers below the stiff clay till were not considered to be active parts of the flow system due to persistent dry conditions.

There are two other regions of hydrogeological importance: the gravel trench and the horizontal well with induced hydraulic fractures, both being features with enhanced hydraulic conductivity. It is assumed that the fractured area around the horizontal well can be treated as a continuum and modelled as an equivalent porous medium (EPM).

The major input and output of water from the system were, respectively, precipitation and evapotranspiration. The resulting redistribution of water in the subsurface and seasonal water table fluctuations were monitored with the several multi-level piezometer installations. Groundwater extraction, when occurring from the horizontal well area and from the gravel trench, was an important component of the water budget.

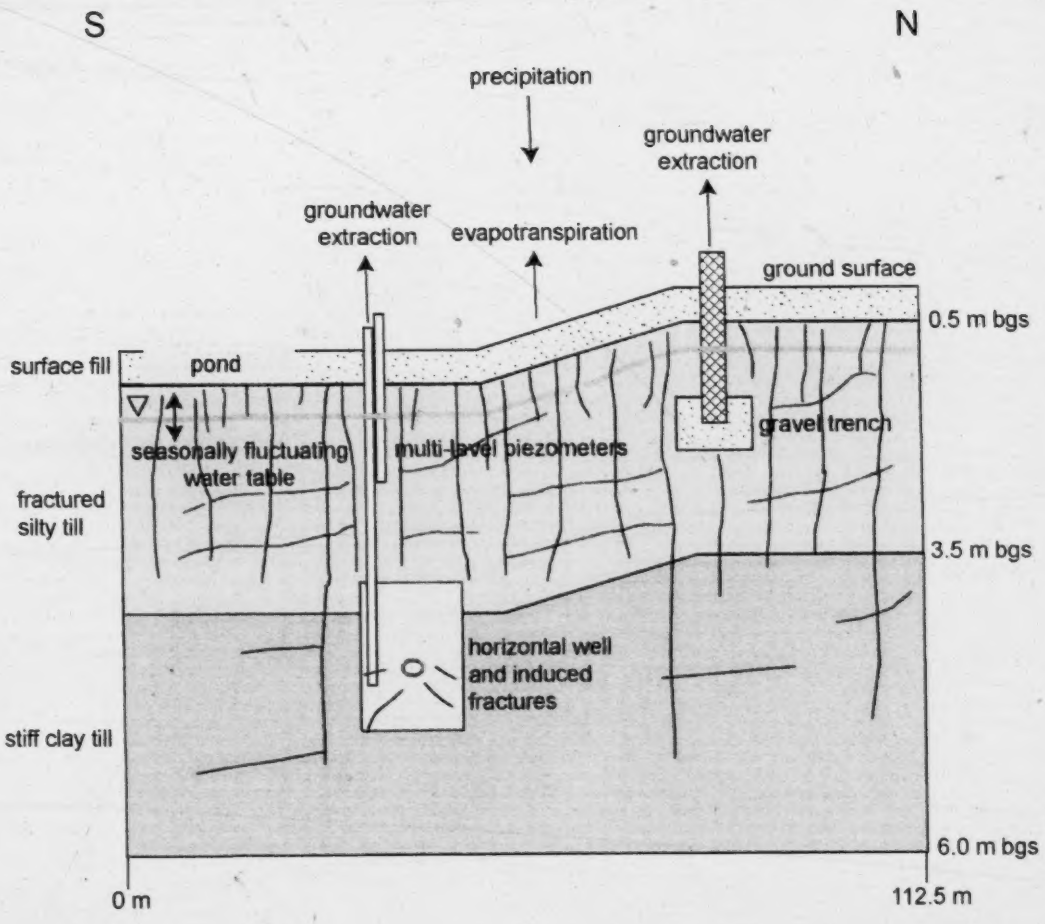

Figure 6-1 Hypothetical N-S cross-section representing the conceptual model under consideration for numerical groundwater modelling of the GPRS.

6.3 Model Design

6.3.1 Code Selection

The numerical simulator chosen to implement the conceptual model was FRAC3DVS (Therrien et al. 2001c), which can simulate three-dimensional variably-saturated groundwater flow and solute transport in both non-fractured and discretely fractured porous media. A pre-processing program called NP (Therrien et al. 2001d) is required to generate the necessary input files for the

model. Details on the use of the pre-processor can be found in the FRAC3DVS Input/Output User's Guide (Therrien et al. 2001a).

To describe three-dimensional transient groundwater flow under variably-saturated conditions, FRAC3DVS uses a modified form of Richards' equation (Therrien and Sudicky 1996), which can be described in a general form as (Huyakorn et al. 1984):

$$\frac{\partial}{\partial x_i}\left(K_{ij} k_{rw} \frac{\partial(\psi + z)}{\partial x_j} \right) \pm Q' = \frac{\partial}{\partial t}(\theta_s S_w), \quad i,j = 1,2,3 \tag{6-1}$$

where K_{ij} is the saturated hydraulic conductivity tensor [L/T], k_{rw} is the relative permeability of the medium [-] (a function of water saturation, S_w [-]), ψ is the pressure head [L], z is the elevation head [L], θ_s is the saturated volumetric water content [-] and Q' is a source/sink term [$L^3/T/L^3$]. To evaluate groundwater flow under saturated conditions, the storage terms on the right-hand side of equation 6-1 are expanded to relate changes in storage to changes in aquifer and water compressibility (Therrien and Sudicky 1996):

$$\frac{\partial}{\partial t}\theta_s S_w \approx S_w S_s \frac{\partial \psi}{\partial t} + \theta_s \frac{\partial S_w}{\partial t} \tag{6-2}$$

where S_s is the specific storage of the porous medium [L^{-1}].

The method of solution implemented in FRAC3DVS is based on the control volume finite-element method (e.g., Forsyth 1991). In general, the steps involved are (Huyakorn and Pinder 1983):

- Discretizing the modelled domain into a series of elements, connected by nodes where dependent variables (heads) are defined;

- Relating variables of each element (K, S_s, n), which are assembled into a global matrix equation representing the entire domain;
- Incorporating boundary conditions and iteratively solving the global matrix with a preconditioned ORTHOMIN solver (Therrien and Sudicky 1996).

Therrien and Sudicky (1996) and Therrien et al. (2001b) provide further details on the implementation of the numerical algorithm.

6.3.2 Model Construction

The description of model construction in this section refers to the calibration scenario (2000 field season). Changes made to the model for sensitivity analyses and verification will be discussed later.

6.3.2.1 Domain and Grid

The modelled domain consisted of a grid of 100 m x 112.5 m x 6 m in the x, y and z directions, respectively. Element size was constant in each direction, with dimensions of $\Delta x = 2$ m, $\Delta y = 1.5$ m and $\Delta z = 0.5$ m for a total of 45 000 elements and 50 388 nodes (Figure 6-2). A plan view of the modelled domain superimposed on a site map is presented in Figure 6-3. The modelled system was rotated on a bearing of 28.5° from N-S such that the model boundaries were closely aligned with the natural site boundaries. Coordinate rotation of surveyed site infrastructure was performed with *rotcoord*, a program in GSLIB (Deutsch and Journel 1992).

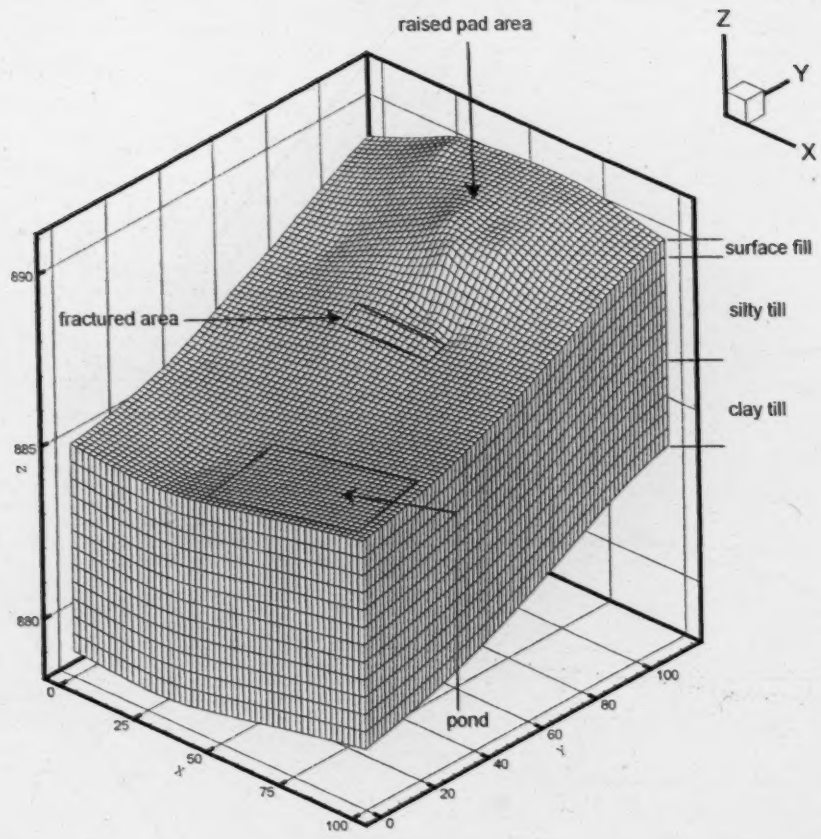

Figure 6-2 Numerical grid representing the modelled domain (10x vertical exaggeration).

Surveyed surface elevations for piezometers were kriged in three dimensions with *kt3d* (Deutsch and Journel 1992). The variogram model for surface elevations was a linear model. Surface elevations ranged from 884.88 m above sea level (masl) to 890.58 masl. Boundaries between model layers mimic the surface topography. The three geologic layers were:

- A disturbed surface backfill layer from the ground surface to 0.5 m bgs (1 element thick);
- A silty till layer from 0.5 m bgs to 3.5 m bgs (6 elements thick); and,

- A stiff clay till layer from 3.5 m bgs to 6 m bgs (5 elements thick).

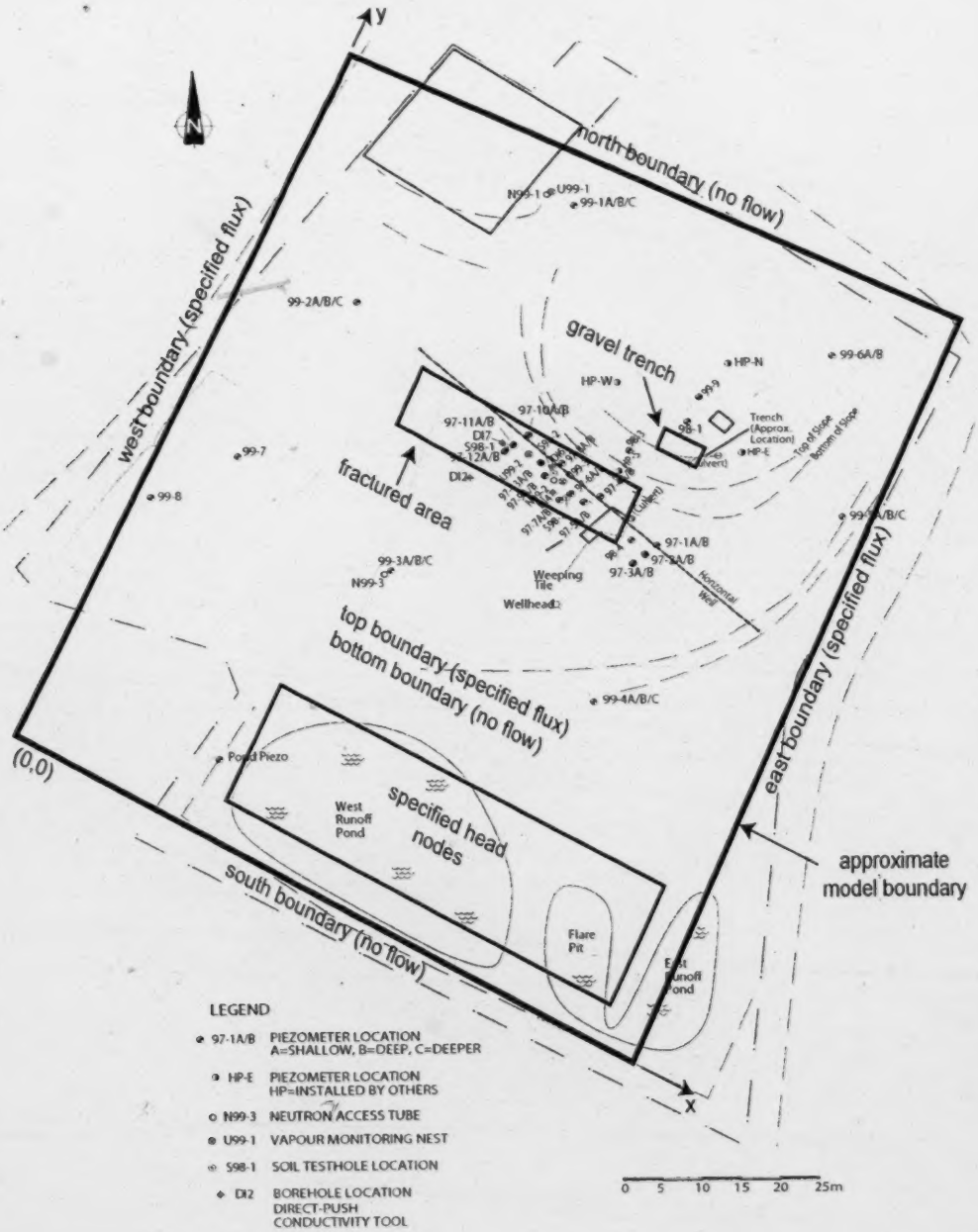

Figure 6-3 Plan view of the modelled domain, with boundary conditions and other important features, superimposed on a site map.

In addition to these three layers, two distinct features were implemented (Figure 6-3):

- A gravel trench (x = 65 to 70 m, y = 76.5 to 81 m, z = 886.4 to 886.9 m);
- A fractured area around the horizontal well (x = 35 to 65, y = 63 to 67.5, z = 885.5 to 887), which it was assumed could be modelled as an equivalent porous medium (EPM).

6.3.2.2 Temporal Discretization

From field observations (Chapters 4 and 5), hydrological stresses could be divided into three broad periods:

- April 1 to July 10, 2000: there is net recharge to the system (precipitation exceeds evapotranspiration);
- July 10 to November 2, 2000: dewatering was occurring and there is net discharge from the system (evapotranspiration exceeds precipitation); and
- November 2, 2000 to April 1, 2001: apart from slightly declining water levels, the system was not dynamic (no precipitation or evapotranspiration).

Timestepping was controlled by an adaptive timestepping procedure based on a method described by Forsyth and Sammon (1986). After obtaining a solution at time level L, the length of the next time step was determined by (Therrien and Sudicky 1996, Therrien et al. 2001b):

$$\Delta t^{L+1} = \frac{\psi^*}{\max\left|\psi_I^{L+1} - \psi_I^{L}\right|}\Delta t^{L} \qquad (6\text{-}3)$$

where ψ^* is the maximum change in pressure head allowed during any given timestep (set to 0.1 m, 20% of Δz), and the subscript I refers to the set of all nodes in the model domain. All simulations had an initial timestep of 60 s at time 0 (April 1, 2000) and adaptively proceeded from there.

6.3.2.3 Material Properties

For the simulation of groundwater flow, estimates of hydraulic conductivity (K), specific storage (S_s) and porosity ($n = \theta_s$ when $S_w = 1$) are required for each geologic layer, the gravel trench and the fractured area. These parameters are included as properties of individual elements. Initial estimates (Table 6-1) were obtained from several sources:

- K estimates were made from arithmetic mean bail test results for two model layers and the fractured area. Since no piezometers were screened in the surface fill, the K of the surface fill was estimated to be slightly higher than the mean result for silty till. The K value of the gravel trench was chosen from literature values;
- Values of S_s and n were estimated from literature values for all layers and zones. Porosity was constrained by soil moisture data (section 4.4.1).

6.3.2.4 Boundary Conditions

Numerical models require mathematical statements at the boundaries of the problem domain to describe how hydraulic heads and hydrological fluxes interact with areas outside of the domain. Boundary condition selection is highly influential to modelled hydraulic head behaviour, especially if flow system transients propagate to the boundaries (Anderson and Woessner 1992). Two types of boundary conditions were used:

- Type I (Dirichlet) conditions, which specify head at the selected boundary nodes; and,
- Type II (Neumann) conditions, which specify the flux across the selected boundary.

Layer	K (m/s)	Source of K estimate	S_s (m^{-1}) †	n (-) ‡
surface fill	6×10^{-7}	slight elevation of silty till result	9.2×10^{-4}	0.2
silty till	4.1×10^{-7}	mean of 97-1A, -3A, 99-1A, -2A	1.3×10^{-3}	0.25
stiff clay till	8.6×10^{-8}	mean of HP-E, -W, -S, P99-1B, -1C, -4B, -5B, -5C, -6B	2.6×10^{-3}	0.3
gravel trench	1×10^{-3}	Fetter 1994	1×10^{-4}	0.3
fractured area	7×10^{-7}	mean of P97-4B, -8A, -8B, -9B, -10B, -11B	1×10^{-4}	0.3

† = Anderson and Woessner 1992, ‡ = Fetter 1994

Table 6-1 Initial porous medium parameter estimates for numerical modelling.

Specified head boundaries were implemented in the area of the runoff ponds (Figure 6-3) for nodes between x = 35 to 95 m, y = 4.5 to 31.5 m and z = 884.5 to 885 m (570 specified head nodes). Surface water bodies are generally considered ideal for type I conditions if they fully penetrate the aquifer (Anderson

and Woessner 1992). Two values were used for the specified head at these nodes, based on transient field observations of runoff pond levels:

- A value of 885.3 m was used from November to July, when heads were generally lower and then slowly began to increase across the site (during spring recharge); and
- A value of 885.6 m was used from July to November, when heads were generally higher and then slowly began to decrease across the site.

Specified flux boundaries were implemented for each of the N, W, S, E, top, and bottom boundaries (Figure 6-3). These can be further subdivided into two categories:

- No-flow boundaries, which were specified for the N, S and bottom boundaries; and
- Non-zero flux boundaries, which were specified for the W, E and top boundaries.

A no-flow boundary was justifiable for the bottom boundary based on the observed dryness of the till/bedrock contact layer below the stiff clay till layer. No-flow boundaries were implemented for the N and S boundaries for two main reasons: vertical fluxes were found to dominate horizontal fluxes (section 5.7), and there are no readily apparent surficial indicators of groundwater flow across the boundaries, such as seepage faces. Also, the proximal location of the first type boundary nodes to the S boundary essentially creates an inexhaustible supply of water to satisfy any boundary flux, which is not likely a realistic response of the system (Anderson and Woessner 1992). There is little field information available to calibrate flux rates across both the N and S boundaries.

The top boundary flux was implemented to represent the difference between infiltrated precipitation and evapotranspiration. Initial recharge estimates were

based on the results of the water table fluctuation method (section 5.4), while discharge estimates were based on evapotranspiration estimates from the dual crop coefficient method (section 4.3.4). The top boundary flux was initially applied as a constant, averaged rate, representing the calculated net difference between recharge and discharge during a defined stress period (section 6.3.2.2).

Side boundary fluxes were created to represent the steep topographic gradients to the W and E of the site, along with enhanced evapotranspiration due to dense, mature vegetation. Evapotranspiration rates for mature poplars (the dominant tree species adjacent to the GPRS) were estimated from 20 year water use records in eastern Washington (Braatne 1999). Initial estimates for the constant, non-zero fluxes implemented into the numerical model are summarized in Table 6-2.

Stress period	Top boundary flux (m/s)	Side boundary fluxes (m/s)
Apr 1-Jul 10	4×10^{-9}	-2.6×10^{-8}
Jul 10-Nov 2	1.9×10^{-10}	-7.7×10^{-9}
Nov 2-Apr 1	0	-7.7×10^{-9}

Table 6-2 Initial Type II boundary constant flux estimates for numerical modelling.

6.3.2.5 Initial Conditions

The main purpose of the 1999 simulation scenario was to obtain reasonable initial conditions for the 2000 calibration scenario. Often, the initial head distribution is taken from the results of a steady-state simulation run prior to the calibration (Anderson and Woessner 1992). Given the strong seasonal and inter-annual dependence of hydraulic heads at the GPRS, it is not likely that a steady-state head distribution would be a reasonable initial head distribution.

Measured hydraulic heads from April 1999 were kriged in 3-D to provide the domain with initial heads representing the end of winter conditions. The spatial variation model was a linear variation based on the surface slope, as was the case for constructed contour maps of hydraulic head (section 5.6.2). The major problem with a kriged distribution is that it does not satisfy the conservation equation (6-1). Therefore, potentially significant flow transients may be created at the start of the simulation that do not exist in the field. These transients may impede model interpretation by causing incorrect responses to imposed stresses.

To alleviate these problems with kriged water levels, dynamic cyclic initial conditions (Anderson and Woessner 1992) were used, where heads were assumed to vary cyclically over the period of 1 year. The 1999 model was run, with trial and error inputs and outputs, for the length of 1 year, until the resulting heads approximated end of winter conditions in spring 2000.

6.3.2.6 Internal Stresses

Very few pumping tests have been performed and described in till settings (Edwards and Jones 1993) because it is difficult to sustain pumping rates over long periods. The hydraulic test and dewatering events at the GPRS are prime candidates for analysis in numerical models because analytical radial flow models are found to be inadequate to describe flow in tills (Edwards and Jones 1993). It would be difficult to select a conceptual flow model suitable for analytical solution in the trench/culvert system.

The trench hydraulic test had little effect on water levels near the trench. This is not surprising given that only 3 m^3 of water were extracted during the test and the volume of voids in the trench exceeds this. The hydraulic influence of dewatering in the area of the horizontal well is limited to that area only. More than 30 m^3 of water were extracted from the area of the horizontal well in both 2000 and 2001 (i.e., >10 times more than during the trench hydraulic test), but the only

piezometers showing significant drawdowns (detectable over barometric fluctuations and natural trends) were in the fractured area of the horizontal well.

A total of 37 m^3 of water was removed from the system during the summer 2000 dewatering (Table 3-5). The culvert and trench contributed 21 m^3, while 16 m^3 was from P97-8B. These volumes were extracted from the model averaged over the 116 d of dewatering, giving extraction rates of:

- Culvert/trench (x = 70 m, y = 81 m, z = 886.4 to 889.4 m): -2.1×10^{-6} m^3/s;
- P97-8B (x = 50 m, y = 72 m, z = 884.7 to 885.5 m): -1.6×10^{-6} m^3/s.

6.3.2.7 Convergence Criteria

Model convergence is attained when the absolute convergence criteria is less than the absolute residual of the previous iteration's flow solution. To enhance the accuracy of the solution, the absolute convergence criteria was decreased from 1×10^{-10} m to 1×10^{-16} m, which resulted in 10 to 20 more iterations at each timestep without a noticeable difference in computational effort.

6.4 Results and Discussion

6.4.1 Calibration Description

Calibration is achieved by specifying a set of boundary conditions, stresses and porous medium parameters such that the model can reproduce field-measured heads within error (Anderson and Woessner 1992). To reduce non-uniqueness in the calibrated model solution, it is also desirable to reproduce field-measured fluxes, although none were directly measured for this project.

Because of the seasonally dynamic, cyclic nature of water levels at the GPRS, a transient calibration was performed. The 2000 field season model was calibrated

to manual water level measurements collected from monitoring wells during April 2000 to April 2001. The trial and error approach to calibration allowed the use of subjectivity in parameter and boundary condition selection, which seemed important given the variable hydrologic responses observed in the highly heterogeneous system.

Calibration targets can be divided into four areas at the site, based on location and the type of field-based responses observed:

- Shallow observation wells near the horizontal well;
- Deeper observation wells near the horizontal well;
- Raised pad area observation wells; and,
- Outer observation wells (the P99 series of piezometers).

Although there are no specific guidelines for setting error criteria for calibrated heads in any given simulation, a value of ± 1 m was selected as an indicator of good proximity between measured and simulated values. This value reflects that the mean absolute difference between measured and simulated (i.e., from the 1999 simulation) heads at the beginning of the calibration simulation was 0.53 m.

6.4.2 Calibration Evaluation

Hydrographs were created for representative monitoring points in the four aforementioned areas to visually compare simulated and field results. The hydrographs are presented as changes in modelled and observed heads during a particular stress period (defined in 6.3.2.2) relative to the respective heads at the beginning of the stress period.

Final parameter estimates are provided in Table 6-3, while final Type II boundary fluxes are provided in Table 6-4. Parameter and flux changes are discussed at relevant points in the text.

Layer	K (m/s)	S_s (m^{-1})	n (-)
surface fill	1×10^{-7}	9.2×10^{-4}	0.2
silty till	6.8×10^{-8}	1.3×10^{-3}	0.25
stiff clay till	1.4×10^{-8}	1×10^{-2}	0.3
gravel trench	1×10^{-3}	1×10^{-4}	0.3
fractured area	7×10^{-7}	1×10^{-4}	0.3

Table 6-3 Final porous medium parameter estimates for numerical modelling.

Stress period	Top boundary flux (m/s)	Side boundary fluxes (m/s)
Apr 1 – Jul 10	6.4×10^{-9} (additional 3.2×10^{-9} in raised pad area)	-1.3×10^{-8}
Jul 10 – Sep 6	From -5×10^{-9} to -1×10^{-9} by increments of 1×10^{-9} every 11.6 d	-7.7×10^{-9}
Sep 6 – Nov 2	From -1×10^{-9} to -5×10^{-10} by increments of 1×10^{-10} every 11.6 d	-7.7×10^{-9}
Nov 2 – Apr 1	0	-7.7×10^{-9}

Table 6-4 Final Type II boundary flux estimates for numerical modelling.

6.4.2.1 Period of Net Recharge

The use of a time-averaged top boundary flux during the period of net recharge reflected the difficulty in simultaneously calibrating to the variable observed responses to precipitation and evapotranspiration. The net top boundary flux was increased to 6.4×10^{-9} m/s during the period of recharge (Table 6-4), which was 3.9 times larger than the field-measured difference between precipitation and evapotranspiration. Given the uncertainty in the recharge generated from precipitation (section 5.4) and evapotranspiration estimates (section 4.3.4), it was

not unexpected that field-measured and modelled results differed by such a factor.

Increasing the magnitude of the top boundary flux (Table 6-4) from initial estimates (Table 6-2) was concurrent with lowering the calibrated hydraulic conductivities of all three layers (Table 6-3) from initial estimates (Table 6-1) during the calibration: surface fill to 1×10^{-7} m/s, silty till to 6.8×10^{-8} m/s and stiff clay till to 1.4×10^{-8} m/s. Since no direct flux observations were made in the field, a unique estimate of recharge could not be made. The ratio of recharge to hydraulic conductivity is all that could be estimated in the calibrated model (Sanford 2002).

During the period of net recharge in the area of the horizontal well (both shallow and deeper observation wells), the increases in modelled heads exceeded the increases in observed heads (the only exception was P97-13B). Figure 6-4 presents the results for shallow (P97-7A, P97-11A) and deeper (P97-4B, P97-13B) observation wells along with measured precipitation and calculated evapotranspiration. The hydrographs are also labelled with bailing events when the piezometers were bailed for hydraulic conductivity testing (section 3.5.4) or prior to geochemical sampling.

The differences between field-observed and modelled data can most likely be explained by the presence of the induced, sub-horizontal fractures in the area of the horizontal well. Given that the average sand-filled fracture aperture in this area varies from 1 to 16 mm (Frac Rite 1997) and that fracture hydraulic conductivity (K_f) is approximately proportional to the square of fracture aperture, it is likely that $K_f >> K$ (de Marsily 1986). As recharge infiltrates the area, water is more rapidly transmitted through the fractures than the matrix, a process that is not explicitly accounted for in the EPM area of the model. Therefore, modelled heads in the area of the horizontal well rise more than what was observed in the field during the period of net recharge.

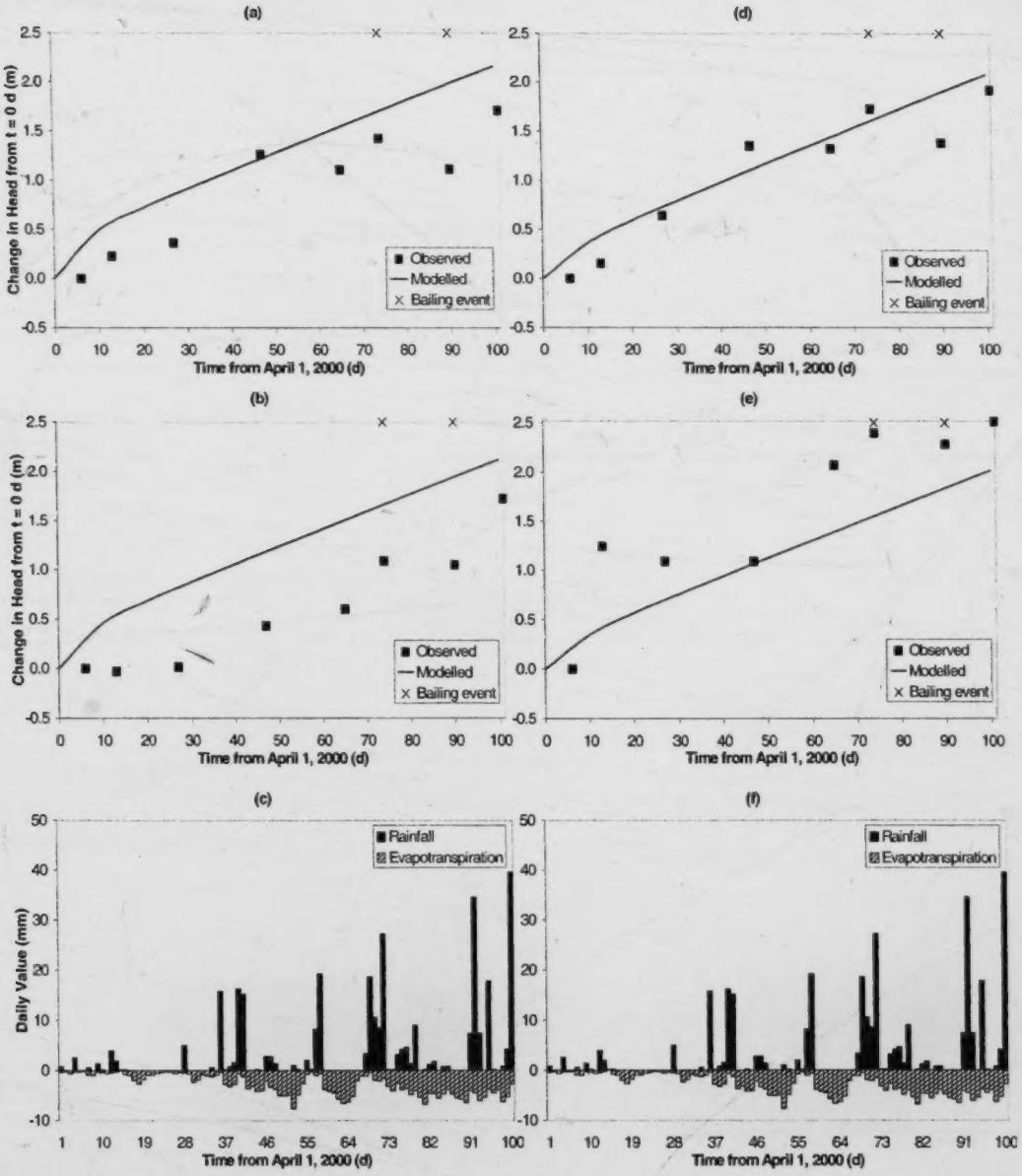

Figure 6-4 Observed and modelled heads during the period of net recharge for shallow piezometers near the horizontal well [(a) P97-7A, and (b) P97-11A], deeper piezometers near the horizontal well [(d) P97-4B, and (e) P97-13B], and (c) and (f), recorded rainfall and calculated evapotranspiration.

During the period of net recharge, the increases in observed heads in the raised pad area generally exceeded the increases in modelled heads. Figure 6-5 presents hydrographs for HP-W and HP-E. The high field measured heads, compared to simulated heads, may be attributed to the increased infiltration allowed by 9 open boreholes (from a previous, undocumented remediation attempt) and sparse vegetation in the raised pad area. High heads might also be attributed to the potentially large screen interval of the pad area piezometers (section 3.5.2).

Observed heads exceeded modelled heads despite an additional recharge flux of 3.2×10^{-9} m/s in the raised pad area (x = 54 to 60 m, y = 85.5 to 93 m) for the calibrated model, making the top boundary flux 1.5 times higher than elsewhere in the domain. Fluxes larger than this in the raised pad area also began to raise simulated heads in the area of the horizontal well, and thus were not justifiable.

Calibration in the outer areas of the model was difficult to evaluate due to variability in field observations. Hydrographs for P99-1A and P99-4A are presented in Figure 6-6. All outer monitoring wells displayed no rise in observed heads until 27 to 65 days after April 1. Observed hydraulic head rises in these monitoring wells ranged from 0.5 m (P99-2A) to 2.0 m (P99-1A), more variable than other areas at the site. The head in P99-2A decreased until the last measurement on July 10. P99-4A was particularly affected by bailing, showing no recovery from the bailing event on day 74. Observations are similar for deeper, outer wells.

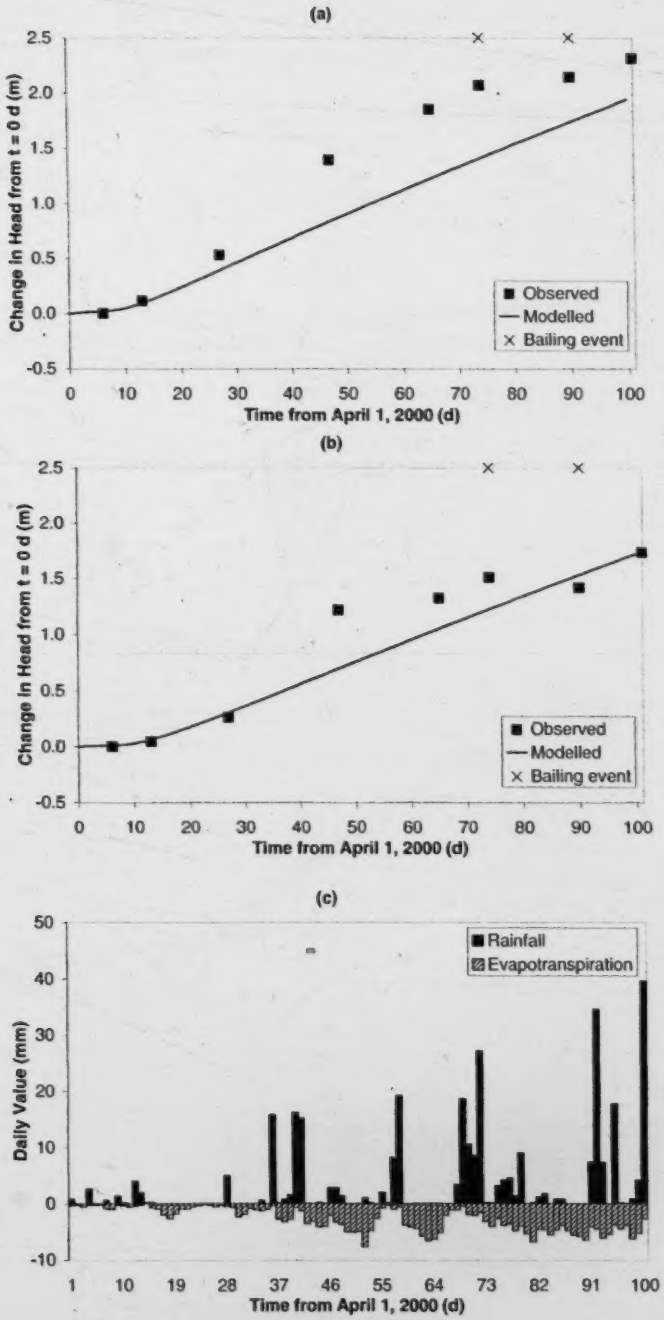

Figure 6-5 Observed and modelled heads during the period of net recharge for raised pad area piezometers [(a) HP-W, and (b) HP-E], and (c) recorded rainfall and calculated evapotranspiration.

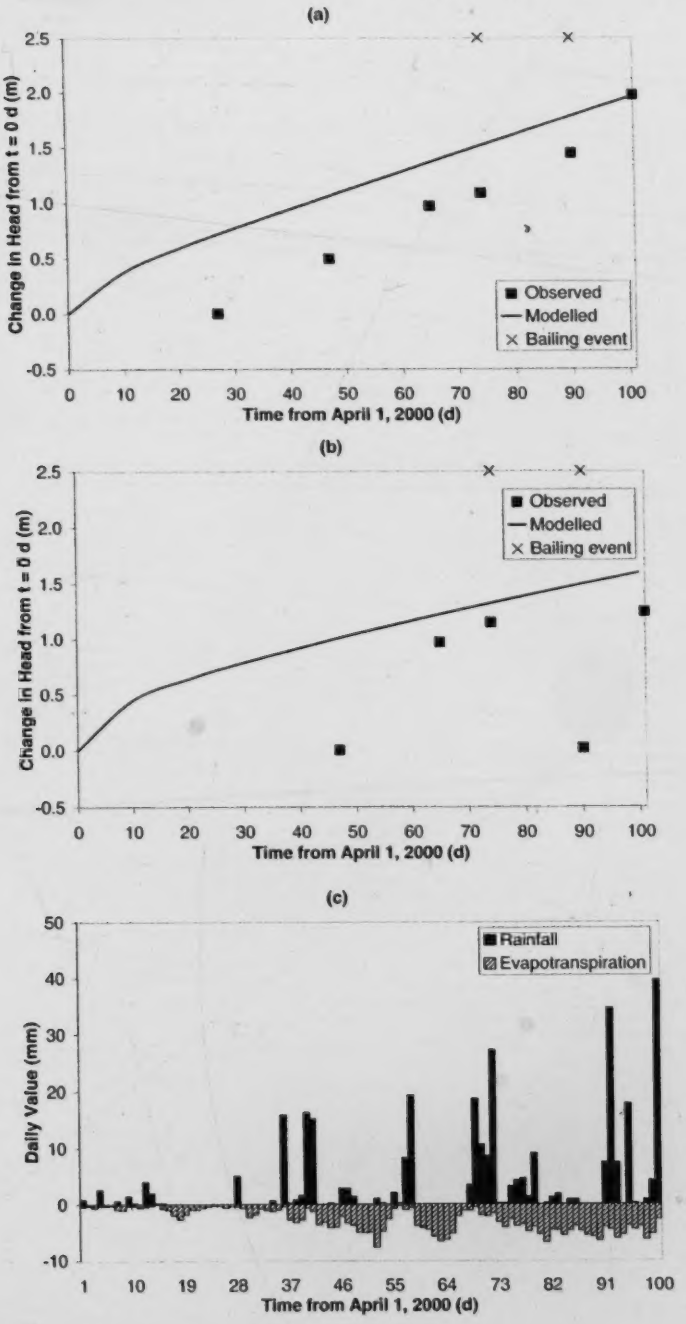

Figure 6-6 Observed and modelled heads during the period of net recharge for outer piezometers [(a) P99-1A, and (b) P99-4A], and (c) recorded rainfall and calculated evapotranspiration.

6.4.2.2 Period of Net Discharge

A key aspect of calibration during net discharge was implementing a time-varying top boundary flux, as opposed to the constant flux applied during the net recharge simulation. Over the duration of the dewatering period (116 d), the flux was applied in 10 even time increments of approximately 11.6 d each, decreasing by an order of magnitude over the duration of the simulation from -5 x 10^{-9} m/s to -5 x 10^{-10} m/s (Table 6-4). For the first 5 time increments, the flux decreased by -1 x 10^{-9} m/s at each increment, while for the last 5 increments, the flux decreased by -1 x 10^{-10} m/s. The rate decrease was essentially a trial and error approximation, but reflected the observation that the rate of water level decline decreased from approximately July to March at the GPRS (section 5.3). Also, the rate of evapotranspiration decreased from its maximum in July (approximately 6.5 mm/d, or 7.5 x 10^{-8} m/s) to a negligible value in November, reducing by at least an order of magnitude.

Precipitation and evapotranspiration are variable on diurnal, and shorter, timescales. Given the period of time between head observations at each piezometer (minimum of 5 days), it is not possible to evaluate the effect of changing the top boundary flux on a shorter timescale than the 11.6 d used for incremental flux changes in the model. Even if more observations were available, it would be impractical to change fluxes on a diurnal timescale for a simulation of this length.

In addition to layer K changes, another change made from the initially implemented material properties was to raise the S_s of the stiff clay till layer from 2.6 x 10^{-3} m^{-1} to 1 x 10^{-2} m^{-1} (Table 6-3). This value is approximately the upper limit for clay till (Grisak and Cherry 1975; de Marsily 1986; Shaver 1998). The change in S_s was implemented because drawdowns with the initial material properties (Table 6-1) were too large during the net discharge simulation. Conceptually, increasing S_s slows the layer's head change during dewatering

and evapotranspiration, allowing greater head perturbation in the higher K, lower S_s EPM fractured zone.

During the period of net discharge in the area of the horizontal well (both shallow and deeper observation wells), the decreases in modelled heads exceeded the decreases in observed heads (the only exception was P97-13B). The difference was generally greater for shallower wells. Figure 6-7 presents the results for the same shallow (P97-7A, P97-11A) and deeper (P97-4B, P97-13B) observation wells presented earlier. Overall, the form of the head decline was well represented by the model. The hydrographs are labelled with bailing events, when dewatering began and ended, and when a vacuum truck was used on site to help remove water from the areas undergoing dewatering.

Even with the improvements made by a time-variable boundary flux and a higher clay S_s, the model was still somewhat limited in its description of the response of the fractured area to declining head conditions. Soil moisture data (section 4.4.1) in the area of the horizontal well clearly indicated the importance of the contribution of fracture drainage to overall groundwater output. The EPM model, although better at describing the form of declining head than rising head conditions, was limited by describing the fracture drainage process in a porous medium framework.

During the period of net discharge in the raised pad area, modelled heads and observed heads were well matched for the duration of the simulation. Hydrographs for HP-W and HP-E are presented in Figure 6-8. Compared to observed heads in the area of the horizontal well (Figure 6-7), heads declined in a more linear fashion and without a large decrease near the beginning of the simulation when dewatering began. This suggests that the impact of dewatering was limited to areas within metres of extraction points. Observed heads at HP-E did show some impact to dewatering and the vacuum truck event (Figure 6-8), indicating its proximity to the metal culvert extraction point.

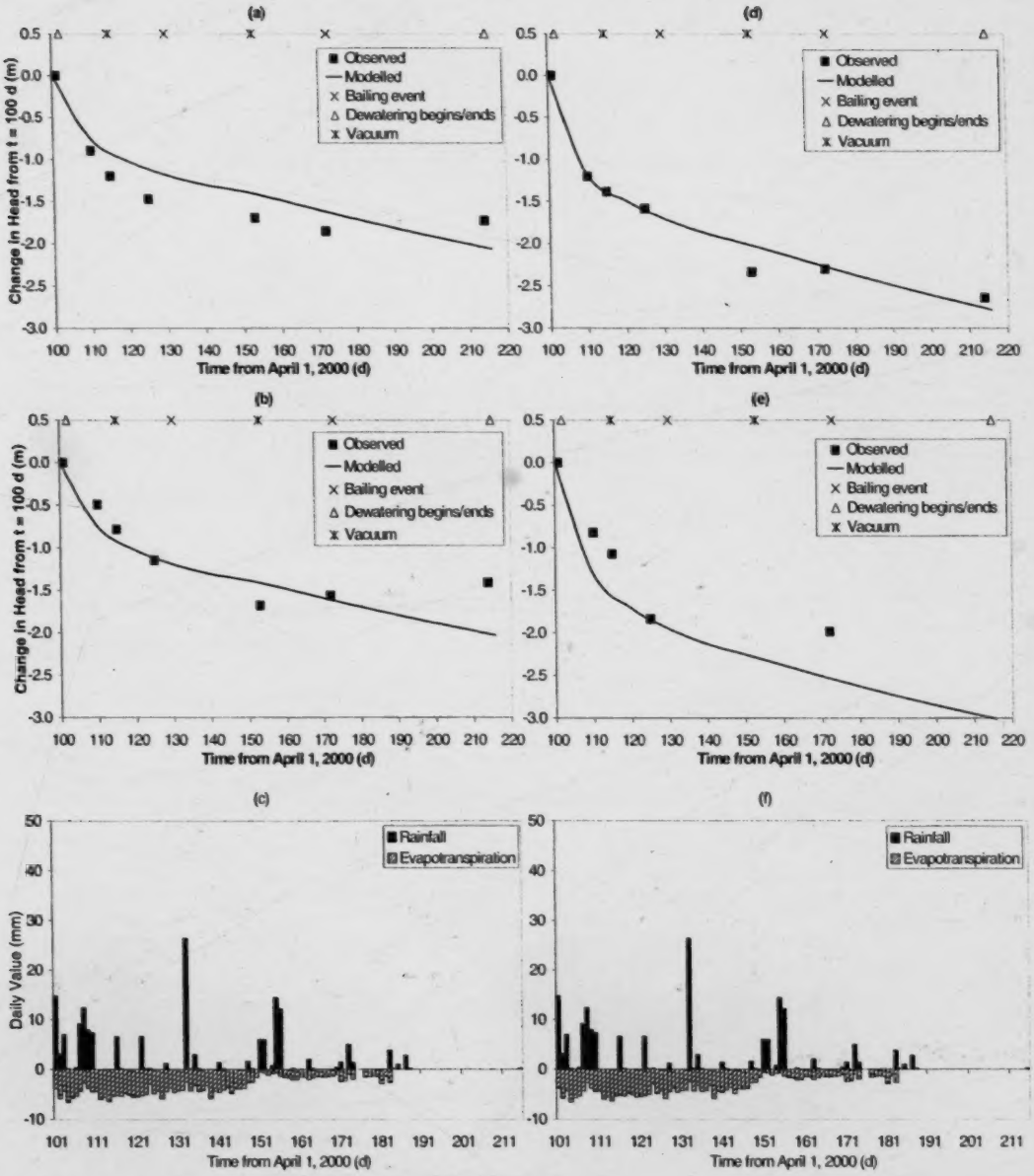

Figure 6-7 Observed and modelled heads during the period of net discharge for shallow piezometers near the horizontal well [(a) P97-7A, and (b) P97-11A], deeper piezometers near the horizontal well [(d) P97-4B, and (e) P97-13B], and (c) and (f), recorded rainfall and calculated evapotranspiration.

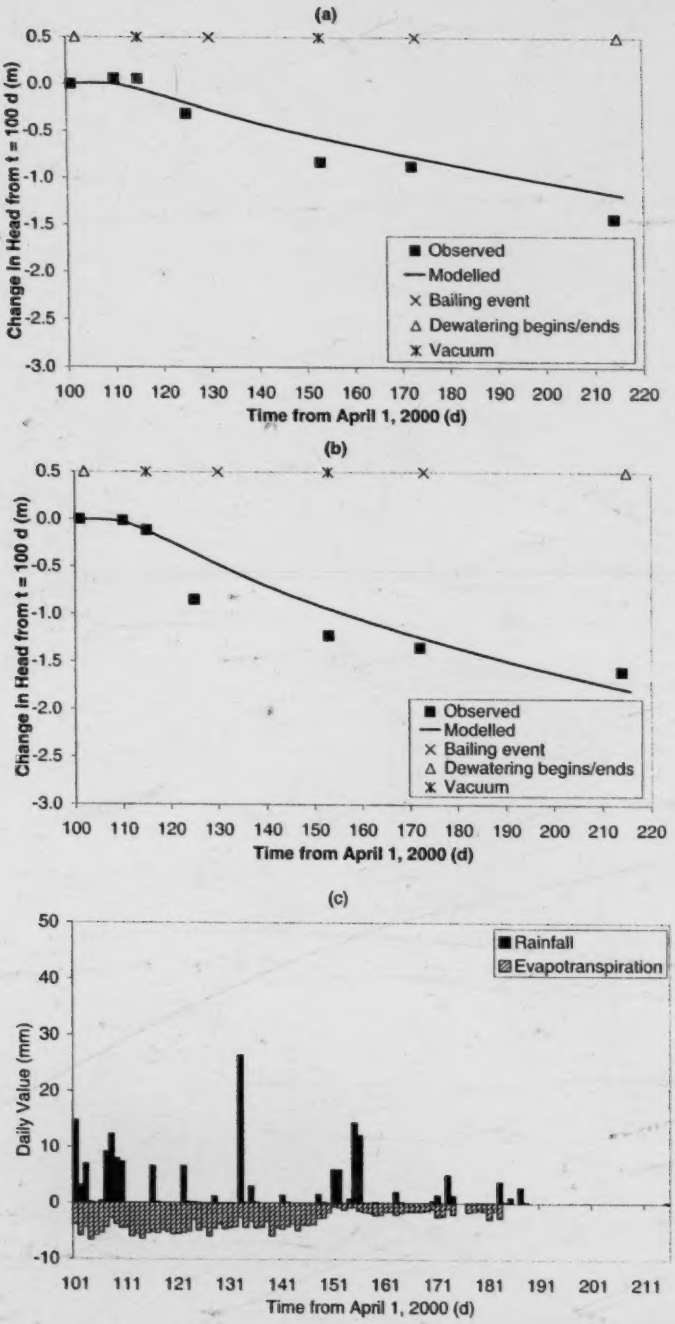

Figure 6-8 Observed and modelled heads during the period of net discharge for raised pad area piezometers [(a) HP-W, and (b) HP-E], and (c) recorded rainfall and calculated evapotranspiration.

Similar to the period of net recharge, outer wells were again difficult to evaluate during the period of net discharge because of variable observations. For example, observed heads at P99-1A and P99-6A initially rose and did not show a net decline until 20 to 30 days after the period of net discharge began. Figure 6-9 presents hydrographs for P99-2A and P99-4A during the period of net discharge. P99-2A displays a very good fit between modelled and observed heads. The total amount of drawdown simulated in outer areas was comparable to what was observed in the field, again confirming the localized impact of dewatering.

6.4.2.3 Additional Measures of Calibration

The hydrographs presented in the previous section were subjectively chosen to display characteristic responses for particular areas of the site. To remove this subjectivity from the evaluation of the calibration, scatterplots (Figure 6-10) of observed heads versus modelled heads at 23 different locations were created at:

- P97-1A, -4A, -7A, -11A, and -13A in shallow areas near the horizontal well;
- P97-1B, -4B, -7B, -11B, and -13B in deeper areas near the horizontal well;
- HP-W, HP-E and HP-N in the raised pad area;
- P99-1A, -2A, -4A, -6A, and -7 in shallow outer areas; and
- P99-1B, -4B, -5B, -5C and -6B in deeper outer areas.

The scatterplots were created at four different times during the calibration, corresponding to changes in the modelled stress periods (section 6.3.2.2):

- April 1, 2000, at the beginning of the calibration;
- July 10, 2000, at the end of the period of net recharge;
- November 2, 2000, at the end of the period of dewatering; and
- April 1, 2001, at the end of the winter decline period.

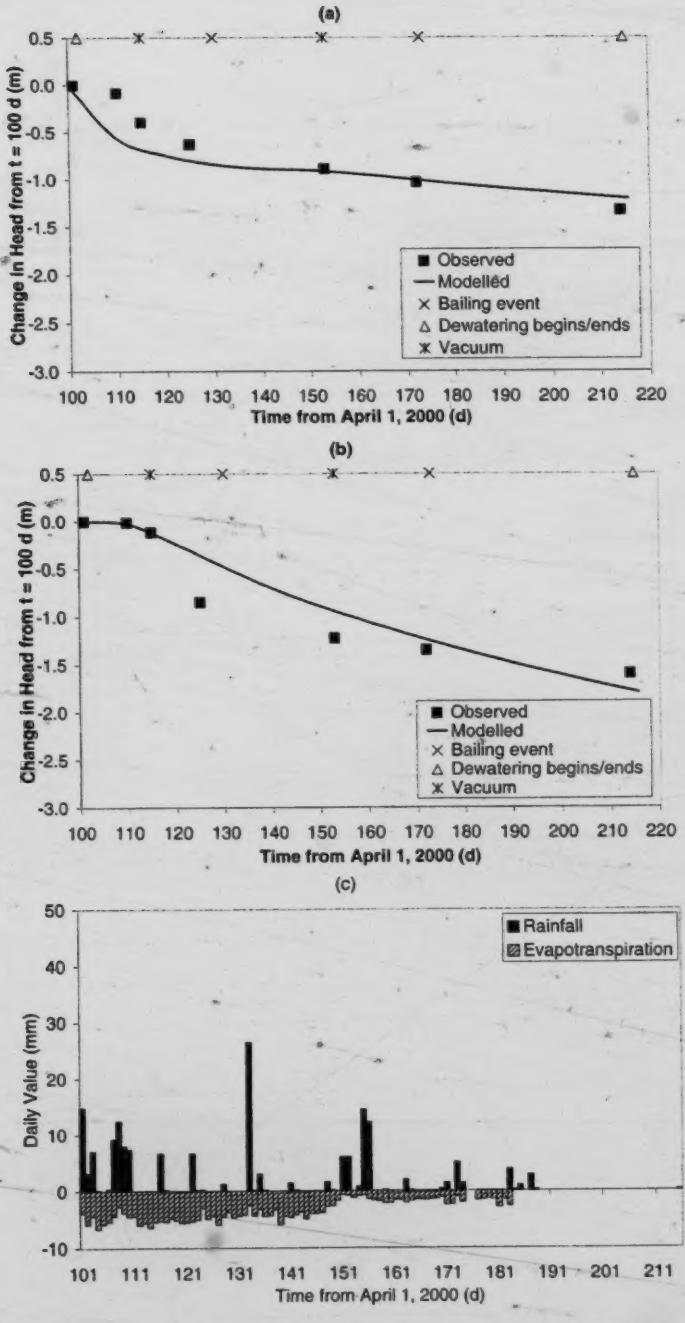

Figure 6-9 Observed and modelled heads during the period of net discharge for outer piezometers [(a) P99-2A, and (b) P99-4A], and (c) recorded rainfall and calculated evapotranspiration.

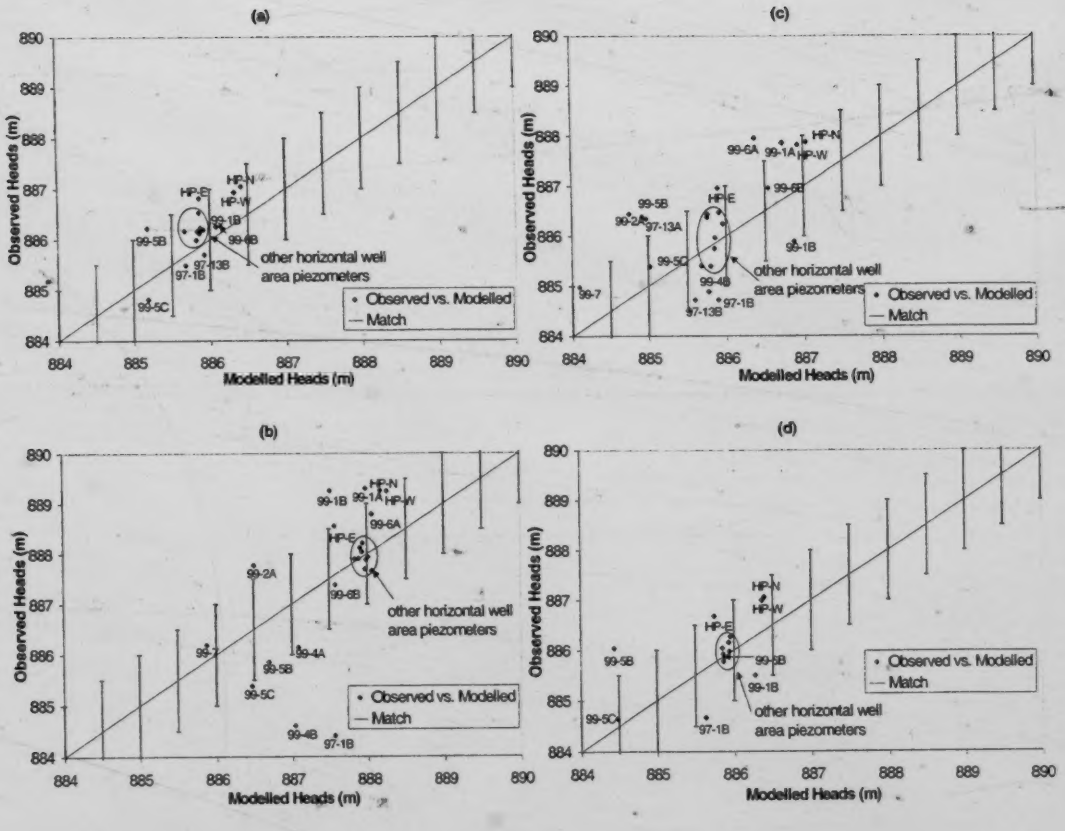

Figure 6-10 Scatterplots of observed heads versus modelled heads with ± 1 m error criteria indicated for (a) April 1, 2000, (b) July 10, 2000, (c) November 2, 2000 and (d) April 1, 2001.

The average calibration in each part of the site was quantified by the mean absolute error (MAE), which is the mean of the absolute value of the differences between observed and modelled heads (Anderson and Woessner 1992):

$$MAE = \frac{1}{n}\sum_{i=1}^{n}\left|(h_o - h_m)_i\right| \qquad (6\text{-}4)$$

where n is the number of calibration values, h_o is the observed head and h_m is the modelled head. MAE values for each of the four different evaluation times are presented in Table 6-5.

Time	MAE site overall (m)	MAE shallow horizontal well (m)	MAE deeper horizontal well (m)	MAE raised pad area (m)	MAE shallow outer (m)	MAE deeper outer (m)
April 1, 2000	0.42	0.38	0.27	0.74	No data	0.43
July 10, 2000	0.62	0.18	0.12	1.02	0.91	0.97
November 2, 2000	0.81	0.66	0.57	0.93	1.11	0.82
April 1, 2001	0.48	0.19	0.37	0.74	No data	0.64

Table 6-5 Mean absolute errors between observed and modelled heads at four different times during the calibration at 23 calibration points across the site.

Based on the average values reported in Table 6-5, the calibration criteria of ±1 m was only exceeded during two stress periods, in one area of the site each time. For all observation points considered at all times, 80% of modelled heads were within the 1 m calibration criteria to observed heads. For the same set of all points and times, more than 35% of modelled heads were within an even tighter error criteria of 0.3 m difference between modelled and observed heads.

Head residuals are randomly scattered (Figure 6-10), which is an indication of unbiased calibration (Anderson and Woessner 1992). If the residuals were to reveal a trend in certain areas of the site, parameter values or boundary conditions could be adjusted to remove the trend. A trend was evident, for example, in the raised pad area before additional recharge was simulated.

From Figure 6-10 and Table 6-5, it is apparent that the area near the horizontal well was most consistently closely calibrated to observed data. Arguably, given the potential of this area to act as a source zone and the abundance of head observations, it was most important to achieve good calibration in this area over other areas at the site. The time period in which calibration was the most difficult to achieve was the period from July to November 2000. This indicated the difficulty in modelling variable patterns of declining heads and responses to dewatering seen across the site using averaged fluxes and parameter estimates.

A more qualitative way of evaluating calibration is to compare contour plots of simulated and observed heads. Figure 6-11 presents the modelled head distribution on September 8, 2000 during the dewatering stress period, which can most readily be compared to the observed contour plot from September 1, 2000 (Figure 5-16), but in general to other plots as well (Figures 5-14 and 5-15).

As was found with observed contour plots, the modelled distribution (Figure 6-11) shows radially outward flow from the north part of the site and the raised pad area. The modelled head distribution also confirms that dewatering had a localized impact, with relatively steep drawdown cones developing near extraction points, but not propagating to beyond a few metres of influence (Figure 6-11). This compares favourably with the relatively steep gradients on the observed contour map (Figure 5-16). During dewatering, other than right near the extraction points, drawdown appears to be more significant in the EPM area than other surrounding areas (Figure 6-11).

The outer areas of the maps were more difficult to evaluate. The modelled head distribution shows that the Type II side boundaries have considerable influence on the flow direction (Figure 6-11). It is difficult to defend the modelled flow pattern in these outer areas due to the sparsity of observed data. However, the side boundary fluxes were conceptually necessary to simulate evapotranspiration and to help develop the radial flow pattern in the raised pad area. The influence

of the fluxes also propagated to the centre of the grid, helping to simulate horizontal flow due to the presence of sub-horizontal fractures in the area of the horizontal well.

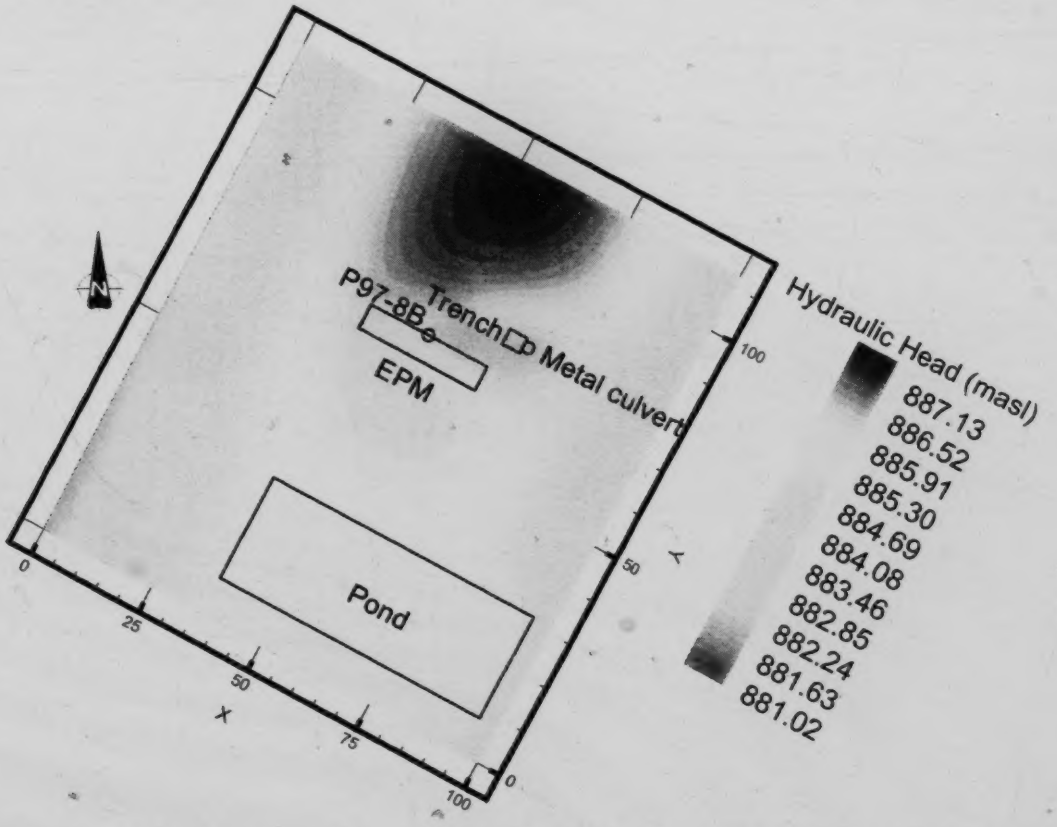

Figure 6-11 Plan view of the modelled hydraulic head distribution on September 8, 2000.

Velocities calculated by the model were difficult to compare to those calculated from field measured hydraulic heads (section 5.6.3). Field analysis assumed that flow was in a homogeneous environment represented by a single value of K, while model calculated velocities represented the results of the interactions of the layered flow system. Field calculated values also assumed that flow was aligned along the 2-D plane between measurement points, but the 3-D model invariably indicated a component of flow in the vertical direction as well.

An example of discrepancy between field-based and model calculated velocities occurred on May 18, 2000 at monitoring points HP-W and P97-10. Based on components in the x and y directions alone, horizontal velocity between these points was estimated by the model to be between 2.8×10^{-9} m/s and 8.2×10^{-9} m/s, while the lowest calculated field-based estimate between those two points was 1.1×10^{-7} m/s (Table 5-8). However, the model velocity has a strong vertical component, indicating the direction of velocity at HP-W and P97-10 to be downward 20° from vertical and downward 32° from vertical, respectively. Therefore, the model suggests that field-based horizontal velocity estimates may not be valid.

Model results at other times consistently suggested that the magnitudes of vertical fluxes were larger than horizontal fluxes in the calibrated flow system. This is consistent with field-based evidence that infiltrating water can be accounted for by vertical recharge and evapotranspiration (section 5.4). Also, other flow modelling studies in weathered tills (e.g., Edwards and Jones 1993, Gerber and Howard 2000) have shown the importance of characterizing and incorporating vertical fluxes to achieving calibration.

6.4.3 Verification

Model verification is the second half of a "split sampling" approach to calibration, where part of the historical field data set is used to calibrate the model and another part is used independently to verify the calibration (Konikow and Bredehoeft 1992). This is advantageous when relatively long data records are available for a site.

The verification scenario extended from the end of the calibration scenario, April 1, 2001, to November 2, 2001. The model endeavoured to match head observations during the period by altering Type II top boundary fluxes and internal stresses, both in terms of magnitude and timing of application, based on 2001 field data. The initial head distribution was from the end of the calibration

scenario. All other aspects of the calibration model design described in section 6.3.2 remained the same for the verification model.

For the top boundary fluxes, the intention was to implement the same ratio of calibrated flux to measured difference between precipitation and evapotranspiration, as was done for the calibration scenario. For the period of net recharge, this was not possible because calculated evapotranspiration exceeded precipitation, which would have led to the implementation of a negative flux and declining water levels, when water levels were actually rising. Evapotranspiration for the 2001 field season was calculated with the Hargreaves (1985) method, which was found to be a good approximation for reference evapotranspiration (section 4.3.2).

Therefore, during the period of net recharge in 2001, the same ratio of precipitation to calibrated flux as for the 2000 field season was used as the top boundary flux. The period of net recharge during 2001 was significantly drier, with only 44% of the precipitation of the similar period in 2000. Therefore, the top boundary flux during recharge was 2.8×10^{-9} m/s, with an additional 1.4×10^{-9} m/s applied to the raised pad area.

For the period of net discharge, it was possible to relate the same ratio of calibrated flux to measured difference between precipitation and evapotranspiration as for the calibrated model. Precipitation was much greater during this period in 2001 versus 2000 (236 mm to 164 mm), while evapotranspiration only increased slightly (312 mm versus 295 mm). Therefore, the implemented flux for 2001 was less negative than during the 2000 scenario. The flux was again divided into 10 equal time increments, beginning at -4.5×10^{-9} m/s, decreasing by -1×10^{-9} m/s for the first 5 time increments and then by -1×10^{-10} m/s for the last 5 time increments.

Field-measured heads indicated that the timing of water level rises and declines were different in 2000 and 2001. Therefore, the period of net recharge for the verification was defined to be from May 4 to August 12, while the period of net discharge was from August 12 to November 2. A top boundary flux of 0 was applied from April 1 to May 4 as a continuation of the winter portion of the calibration simulation.

In terms of internal stresses, a total of 48 m^3 of water was extracted during the 2001 dewatering: 39 m^3 from 4 piezometers in the area of the horizontal well (P97-4B, -8B, -10B and –12B) and 9 m^3 from the culvert and trench. As for the calibration scenario, these were implemented as time averaged fluxes during the dewatering period (June 7, 2001 to October 4, 2001), giving rates of:

- Culvert/trench (x = 70 m, y = 81 m, z = 886.4 to 889.4 m): -8.3×10^{-7} m^3/s;
- Each of P97-4B (x = 58 m, y = 70.5 m, z = 884.4 to 885.2 m), P97-8B (x = 50 m, y = 72 m, z = 884.7 to 885.5 m), P97-10B (x = 46 m, y = 73.5 m, z = 884.8 to 885.6 m) and P97-12B (x = 44 m, y = 70.5 m, z = 884.5 to 885.3 m): -9.6×10^{-7} m^3/s.

Representative hydrographs of observed and verification model heads are presented in Figures 6-12 and 6-13 for net recharge and discharge periods. The hydrographs represent some of the same monitoring points for which hydrographs were presented earlier.

For most areas of the site, the timing and the magnitude of the observed water level increase or decrease was well represented by the verification model until dewatering began (Figures 6-12 and 6-13). This validated the selection of a top boundary flux magnitude based on the ratio of measured precipitation, or the difference between precipitation and evapotranspiration, to the top boundary flux of the calibrated model.

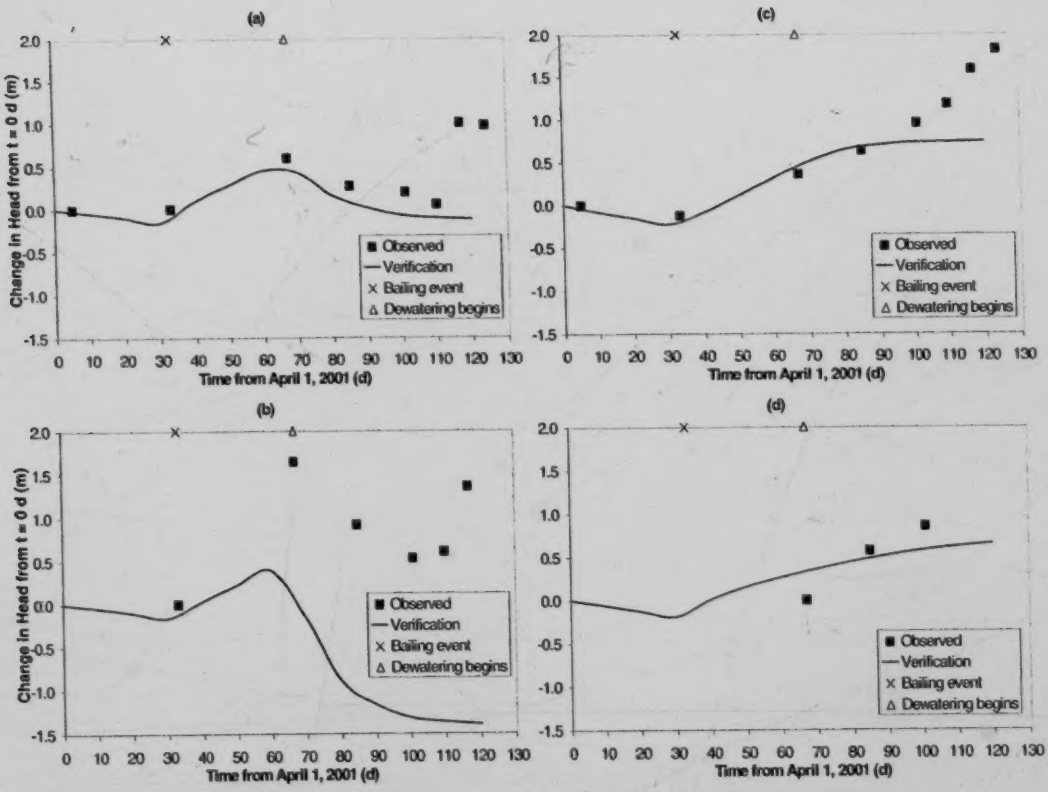

Figure 6-12 Observed and verification heads during the period of net recharge for (a) a shallow piezometer near the horizontal well (P97-7A), (b) a deeper piezometer near the horizontal well (P97-13B), (c) a raised pad area piezometer (HP-W) and (d) an outer piezometer (P99-4A).

The hydrographs for P97-13B (Figures 6-12b and 6-13b) exemplify the problems of modelling fracture flow processes with a continuum approach at this site. Observed heads display a faster and larger magnitude response to both recharge and discharge than the model can represent (Figures 6-12b and 6-13b). This was consistent for monitoring points with known or suspected fracture connection.

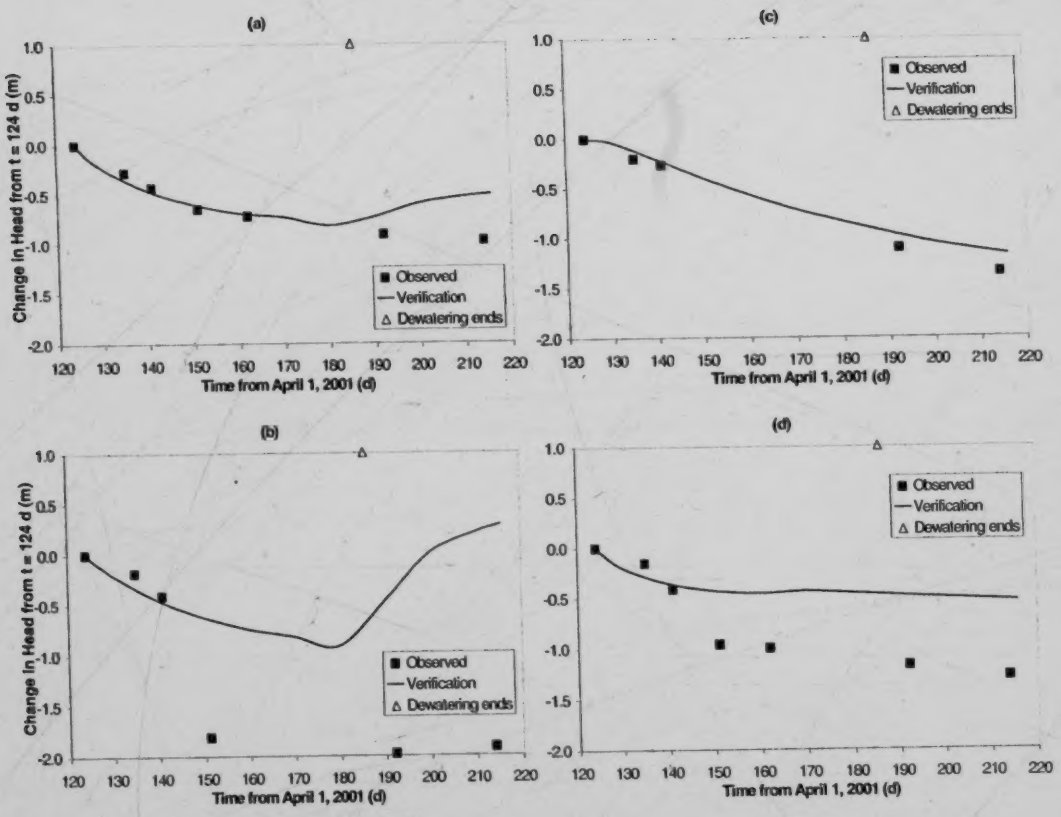

Figure 6-13 Observed and verification heads during the period of net decline for (a) a shallow piezometer near the horizontal well (P97-7A), (b) a deeper piezometer near the horizontal well (P97-13B), (c) a raised pad area piezometer (HP-W), and (d) an outer piezometer (P99-4A).

The modelled response to dewatering across the site is generally unsuitable, most notably at piezometers that are close to extraction points in the area of the horizontal well, where overall model drawdowns are at least 0.5 m too large (Figure 6-12b) and recovery after dewatering ends is unrealistic (Figure 6-13b). The effect is less noticeable in the raised pad area, although when dewatering begins, simulated heads do not continue to rise there (Figure 6-12c), even though recharge is being applied at the same rate from day 33 until day 124. At the higher rate of groundwater extraction during the verification scenario (almost 2.5 times the rate of the calibration scenario), the zone of influence of dewatering

extended to the raised pad area, which was not reflected in observed field data. Outer areas were again difficult to evaluate due to sparse observations.

The incorrect response to dewatering observed in the verification simulation emphasized the non-uniqueness of the calibrated model. Given that the calibrated model could not predict some future stresses appropriately, it is likely that the calibrated model contained errors compensating for the incorrect response to dewatering (Konikow and Bredehoeft 1992). Uncertainty made it difficult to judge which parameters or boundary conditions had the ability to compensate for errors in the model. The sensitivity analysis in the following section attempts to quantify this ability.

6.4.4 Sensitivity Analysis

The purpose of a sensitivity analysis is to systematically alter the porous medium parameters and boundary conditions of the calibrated simulation, within ranges justified by field or literature data, to quantify changes in predicted heads by each particular alteration (Anderson and Woessner 1992). As part of the analysis, the sensitivity to model design parameters, such as spatial and temporal discretization, can also be quantified.

In total, 14 different sensitivity simulations were performed. The parameter and boundary condition modifications are summarized in Table 6-6. For parameter and boundary condition estimates used in the calibration simulation, refer to sections 6.3 and 6.4.2.

Simulation	Description of Modifications
1	K of each layer increased by a factor of 10
2	K of each layer decreased by a factor of 10
3	K of EPM zone increased by a factor of 3.7
4	K of EPM zone decreased by a factor of 3.7
5	K of stiff clay till layer decreased by a factor of 60
6	Imparts a 10:1 ratio of vertical anisotropy ($K_v = 10\ K_h$)
7	Imparts a 10:1 ratio of horizontal anisotropy ($K_h = 10\ K_v$)
8	S_s of each layer increased by a factor of 2
9	S_s of each layer decreased by a factor of 2
10	Type II side fluxes are no-flow throughout the simulation
11	Type II side flux increased by a factor of 2.3 throughout the simulation
12	Type II south boundary flux implemented at same rate as side boundary flux throughout the simulation
13	Type II top boundary flux increased by a factor of 1.4 throughout the simulation
14	Type II top boundary flux decreased by a factor of 1.4 throughout the simulation

Table 6-6 Description of parameter and boundary condition modifications for the sensitivity analysis simulations.

Justifications for altering the parameter and boundary condition estimates in the sensitivity simulations were as follows:

- K estimates across the site ranged over more than 2 orders of magnitude (section 5.2). This was the range of variation allowed by the sensitivity simulations for each of the three layers in the system;

- The K of the EPM area was increased to the highest K calculated by bail test results in that area (2.6×10^{-6} m/s). The K was also decreased by the same factor (3.7) that it was increased from the calibrated value;
- The K of the stiff clay till layer was lowered to the lowest K calculated by bail tests at that depth (1.4×10^{-9} m/s). This was done to help determine whether the layer was better represented by a lower K reflecting the clay matrix or a higher K, indicative of secondary permeability effects;
- Vertical and horizontal anisotropy in K were introduced to simulate the effects of a medium dominated by either vertical (or sub-vertical) or horizontal (or sub-horizontal) permeability features. Evidence from different areas of the site showed both directions were important. Vertical fluxes dominated horizontal fluxes (section 5.7), suggesting vertically conductive fractures, while mapped fractures in the area of the horizontal well revealed sub-horizontal orientations (dip of 5° to 57°) (Frac Rite 1997).
- The S_s of each layer was either raised or lowered by a factor of 2 based on the ranges of S_s given for unconsolidated materials in Anderson and Woessner (1992);
- The Type II side boundary fluxes were either raised by a factor of 2.3, based on higher evapotranspirative water use at those boundaries, or made to be no-flow boundaries, representing the case of no significant flow across those boundaries. When the Type II south boundary was changed from no-flow, it was assumed that flow across that boundary was of the same magnitude as across the side boundaries; and,
- The Type II top boundary flux was assumed to have an uncertainty of a factor of approximately 3.5 based on the results of the WTF method (section 5.4), although this included the estimate from HP-S, which behaved anomalously throughout the study. Therefore, the top boundary flux was alternately increased and decreased by a factor of 1.4 from calibrated values in the sensitivity analysis for a total range of a factor of 2.

Sensitivity analysis results are presented by area, with the shallow and deeper monitoring points in the area of the horizontal well in Figure 6-14 and the raised pad and outer monitoring points in Figure 6-15. For the purposes of this analysis, no distinction was made between shallow and deeper outer monitoring points due to a lack of some observations at certain times of the year. Results are presented as average changes from calibrated values at three times during the calibration: July 10, 2000, November 2, 2000 and April 1, 2001. Error bars represent standard deviations.

In all areas of the site, the model is most sensitive to the most uncertain parameter, hydraulic conductivity (simulations 1, 2, 5, and 7 in particular, Figures 6-14 and 6-15). Given the observed heterogeneity of the site, it is not likely that more field-based K estimates would help to constrain the magnitude of K to less than its present uncertainty. The best approach to obtaining accurate model predictions is to keep modelled parameter values as close to measured values as possible (Hill et al. 1998). K values are also better constrained by the smaller uncertainty in the top boundary flux, given that the ratio of recharge to K is all that can be determined by the model (Sanford 2002).

The model is also sensitive to the distribution of K. Changes to K solely in the EPM area produced very small head deviations across the site (simulations 3 and 4, Figures 6-14 and 6-15). The decrease in clay till K produced head deviations greater than 1 m in all areas (simulation 5, Figures 6-14 and 6-15). This suggests that the clay till layer is better represented by a relatively high K, which suggests secondary permeability, rather than a lower K that is representative of the till matrix.

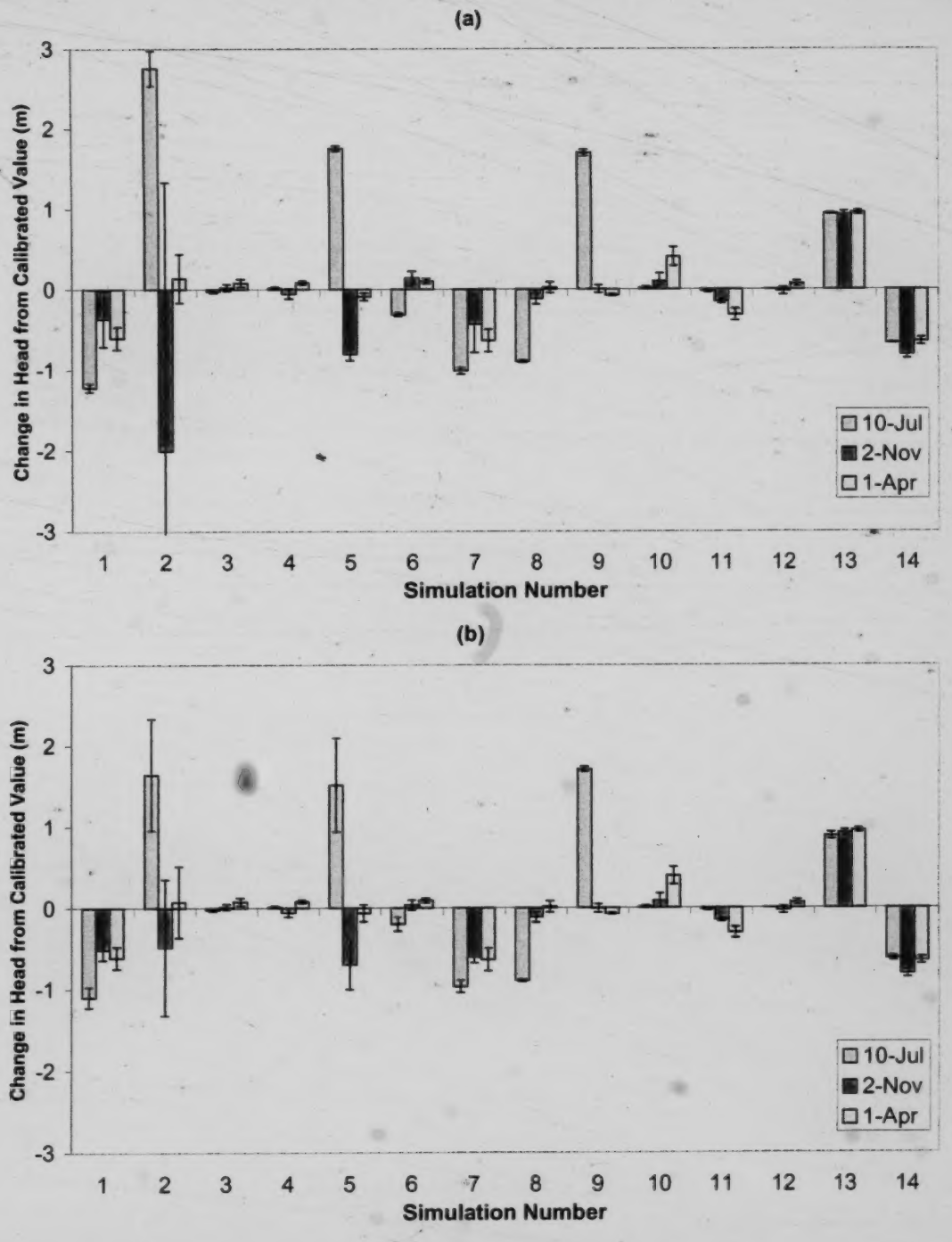

Figure 6-14 Sensitivity analysis results for (a) shallow and (b) deeper monitoring points in the area of the horizontal well on July 10, 2000, November 2, 2000 and April 1, 2001.

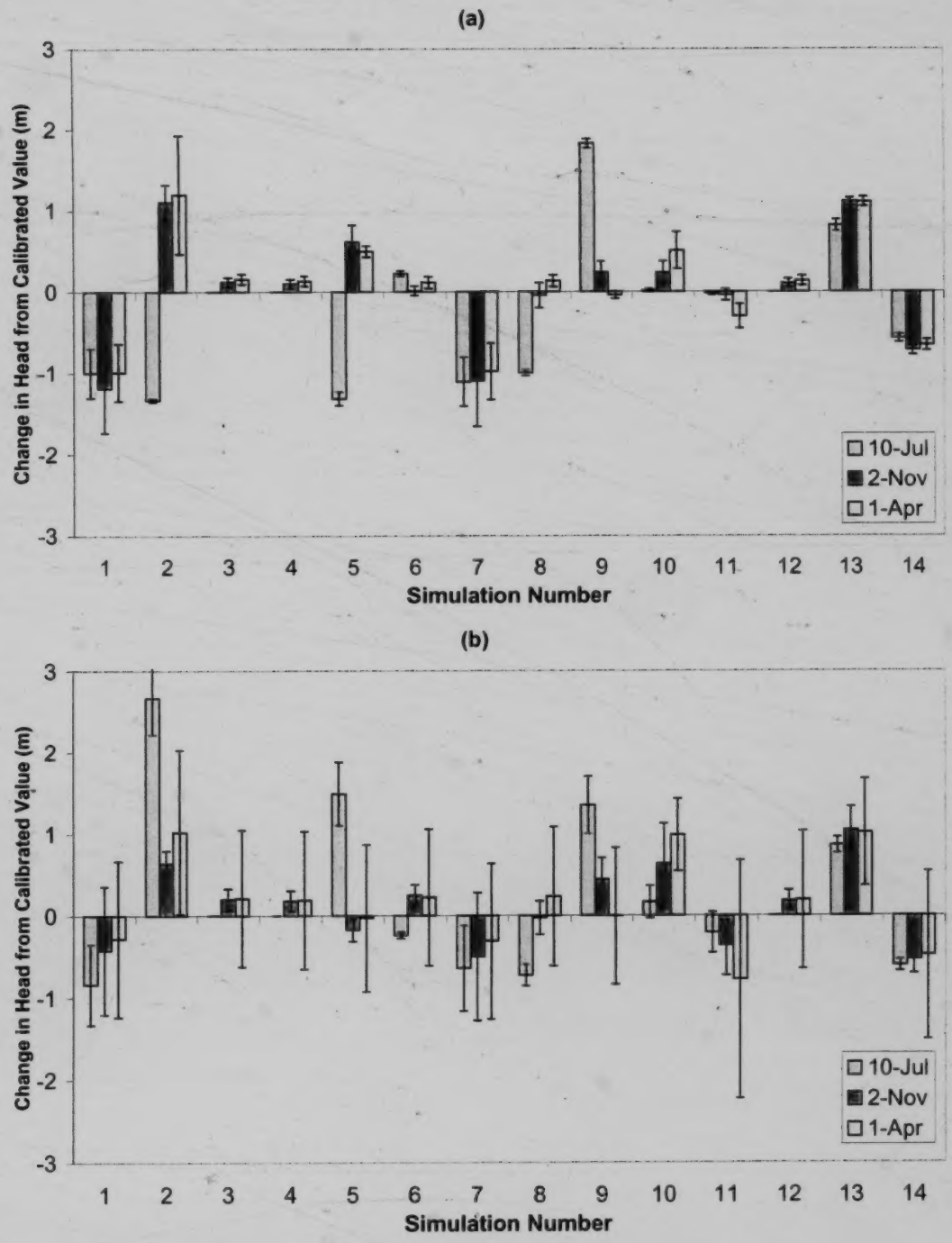

Figure 6-15 Sensitivity analysis results for (a) raised pad area and (b) outer piezometers on July 10, 2000, November 2, 2000 and April 1, 2001.

Although not very sensitive to vertical anisotropy, the model shows negative head deviations of more than 1 m in all areas when 10:1 horizontal anisotropy is introduced (simulations 6 and 7, Figures 6-14 and 6-15). This ratio might have been applicable to the area near the horizontal well with sub-horizontal fractures, but was probably not justifiable for the whole domain. In fact, greater horizontal flow in the area of the horizontal well may have improved calibration in that area of the site (section 6.4.2). For the rest of the site, vertical anisotropy was probably more realistic, representing vertically conductive fractures. Vertical anisotropy ratios typically range from 1 to 1000 in model application and are often determined during calibration (Anderson and Woessner 1992).

Changing the value of S_s produces head changes across the site that are similar in magnitude to the changes caused by K variations (simulations 8 and 9, Figures 6-14 and 6-15). Typically, most modelling efforts focus on the effects of the magnitude and distribution of K on modelled head distributions, due to the lack of measured S_s data and because many models are found to not be sensitive to typically small storage parameters (Anderson and Woessner 1992). Given the importance of modifying S_s to the calibration of this model (section 6.4.2.2), it is likely that the lack of information about the magnitude and distribution of S_s contributed almost as much error to the model as the estimation of K values. Therefore, K and S_s were the parameters most likely to have provided compensating errors (section 6.4.3) during calibration.

In general, the model is not sensitive to the Type II side or south boundaries (simulations 10-12, Figures 6-14 and 6-15), except for outer monitoring points (Figure 6-15b) that are close to the side boundaries. When the side boundary flux was increased by a factor of 2.3 (simulation 11), model output files show that the amount of water input to the domain by the Type I boundary nodes in the pond increased by a factor of 2.5. When the south boundary flux was implemented (simulation 12), the input of the Type I nodes increased by a factor of 5.8. Thereby, the Type I nodes became an inexhaustible supply of water, a

response of the system which cannot be confirmed by any of the field measurements undertaken for this project, and seemed unlikely.

Although showing variations of up to 1 m from calibrated heads in all areas, the model is not as sensitive to the Type II top boundary flux as it is to K and S_s (simulations 13 and 14, Figures 6-14 and 6-15). On average, each area responded in the same way to a change in the top boundary flux, which is not what was seen in the field. In reality, the recharge flux was a composite of several interacting processes that were highly variable across the site, such as rainfall-runoff, evapotranspiration under bare and vegetated conditions and infiltration into highly heterogeneous soils (Sanford 2002). The model was limited to describing site-wide response with a single flux value, other than the additional flux simulated in the raised pad area (section 6.4.2.1).

In addition to the parameter and boundary condition changes outlined in Table 6-6, the sensitivity to some aspects of model design was investigated:

- Element dimensions were alternately reduced in each of the coordinate directions to create a grid of up to 90 000 elements in some cases. Although simulation times with more elements were still practical, results were not different from the base case of 45 000 elements, and thus the relaxed discretization was used;
- The initial timestep was reduced from the base case of 60 s with no observable changes to simulation results. The adaptive timestepping procedure (Equation 6-3) was found to be efficient, especially when internal stresses were introduced; and,
- Time-variable pumping rates were investigated based on observations of dewatering system rates and performance. These simulations were found to have the same results as the base case, time-averaged dewatering simulations.

6.5 Summary and Conclusions

Trial and error calibration of a geologically simple (three layer) groundwater model of the GPRS was achieved primarily through modification of the timing and magnitude of the Type II top boundary flux (Table 6-4), a mixed-type boundary representing infiltration and evapotranspiration. Other modifications included significantly raising the S_s of the stiff clay till layer (Table 6-3), slightly lowering the K of all three layers (Table 6-3) and slightly reducing the Type II side boundary fluxes (Table 6-4). Dividing the model into three relevant stress periods, determined from field data, facilitated calibration.

The average calibration in each area of the site was quantified, without subjectivity, by calculating the mean absolute error, or mean absolute difference between simulated and observed heads. For the set of all modelled heads at all times, 80% were within the pre-established error criterion of 1 m difference, while more than 35% were within 0.3 m difference. Overall, the best calibration was in the area of the horizontal well, perhaps at the expense of calibration in other areas of the site where data were sparse.

Modelled head distributions confirmed that the influence of groundwater extraction does not extend beyond a few metres of the extraction point. More drawdown occurred in the EPM area near P97-8B than other surrounding areas. This confirmed the importance of transmissive fractures to the volume of water removed during dewatering.

Model calculated velocity vectors supported field data showing that vertical fluxes were more prevalent in the system than horizontal fluxes. Both the magnitude and direction of the velocity vectors tend to contradict the 2-D horizontal gradient and velocity estimates.

Verification showed that relating the calibrated Type II top boundary flux to measured precipitation and evapotranspiration was a satisfactory approach to

calibrating independent data sets, which reinforced confidence in the model design. However, unlikely responses to enhanced dewatering stresses in the area of the horizontal well revealed that the calibrated model likely had errors compensating for the incorrect response, most likely in the magnitude and distribution of K and S_s. This also confirmed the difficulty in representing fracture dewatering processes at this site with an equivalent porous medium, continuum approach.

A sensitivity analysis revealed that the model was most sensitive to the magnitude and distribution of the two most uncertain parameters, K and S_s. The compensation of the Type I nodes made the model relatively insensitive to the Type II side and south boundaries. Each area of the model responded uniformly to changes in the Type II top boundary flux, which emphasized the difficulty in fitting the variable responses seen across the site without zoning the top boundary flux.

CHAPTER 7

CONCLUSIONS

The physical hydrogeology of a decommissioned natural gas processing site impacted by processing chemicals was investigated. The site-scale groundwater flow regime was studied in greater detail than previous studies, as part of a multi-disciplinary remediation project. Although site-scale hydrogeological characterization was the main goal of this part of the project, it was anticipated that characterization techniques and interpreted flow characteristics could be used at other decommissioned upstream sites in Alberta, given the nominal similarities in processing chemicals and shallow stratigraphy between sites.

Site stratigraphy was found to be generally similar to till settings across the Western Glaciated Plains, although significant heterogeneity was found. Of hydrogeological importance was the distinction between weathered and unweathered sediments, where groundwater flow was active in the near-surface, weathered sediments. Due to the dryness of most of the deeply (6 m bgs) screened piezometers, flow was interpreted to be indeterminately, but probably rarely, active in the deeper, unweathered sediments.

Hydraulic conductivity testing was one of the keys to distinguishing zones of active and inactive groundwater flow. Active groundwater flow coincided with fractured material intervals. K decreased with depth, ranging from 1×10^{-9} m/s to 4×10^{-7} m/s, and the transition from weathered to unweathered till. Shallower piezometers had bail test responses characteristic of higher K fractured materials, while the majority of deeper piezometers did not. The highest K determined was in the fractured area near the horizontal well, where the most active groundwater flow was expected.

Soil moisture monitoring revealed the importance of fractures to the development of dual porosity flow. Soil moisture was temporally consistent in intervals

representing the till matrix, but was temporally variable in intervals that intersected fractures. In fractured zones, maximum volumetric moisture contents (35%) occurred during periods of water input, while minimum volumetric moisture contents (20%) occurred during periods of water output.

The water budget for 2000 consisted of one major component each of input and output: precipitation (494 mm) and evapotranspiration (545 to 575 mm), respectively. These vertical fluxes dominated the system, as has been found for several Alberta tills. This was also confirmed by recharge determinations (0.4 to 3 mm/d) with the water table fluctuation method, as incoming precipitation could be accounted for by recharge and evapotranspiration. Infiltrating water remained close to the surface for evapotranspiration by capillary rise.

Vertical flow dominated over horizontal flow. Horizontal hydraulic gradients (0.04 to 0.14) were relatively insignificant compared to upward vertical gradients (0 to 2.5). Given the lack of lateral hydraulic connection due to heterogeneity and the relatively low permeability, the most probable horizontal groundwater velocities do not exceed 5 m/y. Upward vertical gradients greater than 1 are strongly indicative of perched water table conditions.

Hydraulic heads generally decreased with depth, indicating the potential for recharge and perched water table conditions. Seasonal fluctuations dominated the local water level response. These fluctuations were attenuated with depth and generally did not occur at greater than 4 m bgs. The lack of these fluctuations and the continued dryness of deeper (> 6 m bgs) piezometers also suggested perched water table conditions and a low permeability boundary between weathered and unweathered till.

A numerical groundwater flow model was developed with FRAC3DVS to confirm the significant features of flow as interpreted from field measurements. In the development of the model, it was assumed that groundwater flow occurred under

saturated conditions, that there was no active groundwater flow below 6 m bgs, and that the fractured area near the horizontal well could be modelled as an equivalent porous medium (EPM).

Model calibration was achieved primarily through trial and error modification of the timing and magnitude of the Type II top boundary flux, again reinforcing the importance of vertical fluxes in the system. Other important modifications included raising the S_s of the clay till layer, to 1×10^{-2} m^{-1} from 2.6×10^{-3} m^{-1}, and decreasing the K of all three geologic layers toward their geometric means. For all models considered, 80% of modelled heads were within the pre-established criterion of difference of 1 m from observed heads. The best match between modelled and observed heads occurred in the heavily instrumented area near the horizontal well.

Uncertainty arose during calibration due to a lack of field-measured hydrological fluxes. Field-measured fluxes would better quantify and constrain the Type II boundary conditions. Some suggested flux measurements for this study might be:

- A precision lysimeter or pond evaporation pan to constrain evapotranspiration estimates.
- Seepage or flow meters to measure hydrologic fluxes. These might be useful in the pond to determine how the pond influenced system behaviour. They may also be useful off-site, such as in the stream in the gully to the east of the site to determine if streamflow could be correlated to groundwater behaviour on-site.

During model verification, unlikely responses to enhanced dewatering stresses in the area of the horizontal well revealed errors in the calibrated model. These errors were most likely in the magnitude and distribution of K and S_s, the parameters to which the model was most sensitive. This suggests that till

heterogeneity controlled groundwater flow characteristics more than the geologically simple model represented.

The verification results also suggest that the assumption that the fractured area near the horizontal well could be modelled as an EPM was a poor choice. EPM models have been successfully used where fracture spacing is very close (cm or less) (McKay et al. 1993) or in large-scale (regional) settings. This suggests that the induced fracture spacing (3 to 4 m) was too large in the area of the horizontal well or that the model scale was not of sufficient size to meaningfully average fracture flow parameters, as was the intention of the EPM approach (Harrison et al. 1992). For this field-scale model, the fractured area near the horizontal well might be better represented by either a discrete fracture or dual porosity approach.

It is obvious that fractures, both natural and hydraulically induced, are major controls on groundwater flow at the GPRS. Although the induced fractures are well described, the character and distribution of natural fractures at the GPRS is not well known. A recommendation for groundwater flow studies in tills is to describe fracture flow properties by several methods, even though it may be a difficult, time-consuming task. The lack of knowledge about fracture properties limits both site-specific characterization and possibilities of extending site-specific results to other similar sites.

REFERENCES

Allen, R.G., 2000a. REF-ET Reference Evapotranspiration Calculation Software Manual for FAO and ASCE Standardized Equations, Version 2.0 for Windows. Kimberly, ID, 76 pp.

Allen, R.G., 2000b. Using the FAO-56 dual crop coefficient method over an irrigated region as part of an evapotranspiration intercomparison study. Journal of Hydrology, 229: 27-41.

Allen, R.G., Pereira, L.S., Raes, D. and Smith, M., 1998. Crop evapotranspiration: Guidelines for computing crop water requirements. Irrigation and Drainage Paper 56, Food and Agricultural Organization of the United Nations, Rome, 300 pp.

Amatya, D.M., Skaggs, R.W. and Gregory, J.D., 1995. Comparison of methods for estimating REF-ET. Journal of Irrigation and Drainage Engineering, 121: 427-435.

Anderson, M.P. and Woessner, W.W., 1992. Applied Groundwater Modeling: Simulation of Flow and Advective Transport. Academic Press, Inc., San Diego, 381 pp.

Artemis Consulting, 1997. Assessment Report for the Facility at [the Gas Plant Remediation Site]. Prepared for Imperial Oil Resources Ltd., April 1997.

Barbour, S.L., 1998. Nineteenth Canadian Geotechnical Colloquium: The soil-water characteristic curve: a historical perspective. Canadian Geotechnical Journal, 35: 873-894.

Bedient, P.B., Rifai, H.S., and Newell, C.J., 1994. Ground Water Contamination: Transport and Remediation. Prentice-Hall, Englewood Cliffs, 541 pp.

Bentley, L.R., Gharibi, M., and Lunn, S.R.D., 2001. Time-lapse electrical resistivity monitoring of groundwater remediation. In: Proceedings of the 2nd Joint CGS-IAH Groundwater Specialty Conference, Calgary, pp. 944-951.

Beyazgul, M., Kayam, Y., and Engelsman, F., 2000. Estimation methods for crop water requirements in the Gediz Basin of Western Turkey. Journal of Hydrology 229: 19-26.

Bouwer, H., 1989. The Bouwer and Rice slug test - An update. Ground Water, 27(3): 304-309.

Bouwer, H. and Rice, R.C., 1976. A slug test for determining hydraulic conductivity of unconfined aquifers with completely or partially penetrating wells. Water Resources Research, 12(3): 423-428.

Bowles, M.W., 1998. The Trench and Gate groundwater remediation system. Master of Science thesis, University of Calgary.

Bowles, M.W., Bentley, L.R., Hoyne, B. and Thomas, D.A., 2000. In situ ground water remediation using the trench and gate system. Ground Water, 38(2): 172-181.

Boydell, A.N., Bayrock, L.A., and Reimchen, T.H.F., 1974. Surficial geology of Rocky Mountain House (NTS 83B). Research Council of Alberta, Edmonton, map, scale 1: 250 000.

Braatne, J.H., 1999. Biological aspects of hybrid poplar cultivation on floodplains in western North America – a review. U.S. Environmental Protection Agency, Document no. 910-R-99-002, Seattle.

Bradbury, K.R. and Muldoon, M.A., 1990. Hydraulic conductivity determinations in unlithified glacial and fluvial materials. In: D.M. Nielsen and A.I. Johnson (Editors), Ground Water and Vadose Zone Monitoring. American Society for Testing and Materials, Philadelphia, pp. 138-151.

Briggs, D. et al., 1993. Fundamentals of Physical Geography. Copp Clark Pittman, Toronto, 692 pp.

Buol, S.W., Hole, F.D., McCracken, R.J., and Southard, R.J., 1997. Soil Genesis and Classification, 4th ed. Iowa State University Press, Ames, 527 pp.

Butler, J.J., 1998. The Design, Performance and Analysis of Slug Tests. Lewis Publishers, Boston, 252 pp.

Buttle, J.M., 1989. Soil moisture and groundwater responses to snowmelt on a drumlin sideslope. Journal of Hydrology, 105: 335-355.

Campbell Scientific, 1994. Tripod-based weather station installation manual, models CM6, CM10, CM6/10K. Campbell Scientific Inc., Logan.

Cherry, J.A., 1989. Hydrogeologic contaminant behaviour in fractured and unfractured clayey deposits in Canada. In: Kobus and Kinzelbach (Editors), Contaminant Transport in Groundwater. Balkema, Rotterdam, pp. 11-19.

Clark, W.E., 1967. Computing the barometric efficiency of a well. Journal of the Hydraulics Division, American Society of Civil Engineers, 93(HY4): 93-98.

CPN Company, 1985. 503 DR Hydroprobe Moisture Depth Gauge operating manual. CPN Company, Martinez, CA., 34 pp.

CPN Company, 1993. Nuclear gauge radiation safety training manual. CPN Company, Martinez, CA., 26 pp.

Craig, R.F., 1992, Soil Mechanics, 5th ed. Chapman and Hall, London, 427 pp.

Cravens, S. J., and Ruedisili, L.C., 1987. Water movement in till of east-central South Dakota: Ground Water, 25(5): 555-561.

D'Astous, A.Y., Ruland, W.W., Bruce, J.R.G., Cherry, J.A. and Gillham, R.W., 1989. Fracture effects in the shallow groundwater zone in weathered Sarnia-area clay. Canadian Geotechnical Journal, 26: 43-56.

Davis, D.R. and Rasmussen, T.C., 1993. A comparison of linear regression with Clark's method for estimating barometric efficiency of confined aquifers. Water Resources Research, 29(6): 1849-1854.

Dawson, K.J. and Istok, J.D., 1991. Aquifer Testing: Design and Analysis of Pumping and Slug Tests. Lewis Publishers, Inc., Chelsea, 344 pp.

Day, R.W., 2001. Soil Testing Manual. McGraw-Hill, Toronto, 618 pp.

de Marsily, G., 1986. Quantitative Hydrogeology: Groundwater Hydrology for Engineers. Academic Press Inc., Toronto, 440 pp.

de Vries, J.J. and Simmers, I., 2002. Groundwater recharge: an overview of processes and challenges. Hydrogeology Journal, 10: 5-17.

Design Analysis Associates, Inc. H-310 Submersible Pressure Transducer Owner's Manual. Document no. H310000, Design Analysis Associates Inc., Logan.

Deutsch, C.V., and Journel, A. G., 1992. GSLIB: Geostatistical Software Library and User's Guide. Oxford University Press, New York, 339 pp.

Dingman, S.L., 1994. Physical Hydrology. Prentice-Hall Inc., Englewood Cliffs, 575 pp.

Domenico, P.A., and Schwartz, F.W., 1990. Physical and Chemical Hydrogeology. John Wiley and Sons, Toronto, 824 pp.

Doorenbos, J. and Pruitt, W.O., 1977. Guidelines for predicting crop water requirements. Irrigation and Drainage Paper 24, Food and Agriculture Organization of the United Nations, Rome, 156 pp.

Dzikowski, P.A., 1990. Agroclimatic Atlas of Alberta. Conservation and Development Branch, Alberta Agriculture, Edmonton.

Edwards, K.B. and Jones, L.C., 1993. Modeling pumping tests in weathered glacial till. Journal of Hydrology, 150: 41-60.

Fenton, M.M., 1984. Quaternary stratigraphy of the Canadian Prairies. In: R.J. Fulton (Editor), Quaternary Stratigraphy of Canada – A Canadian Contribution to IGCP Project 24. Geological Survey of Canada Paper 84-10, Calgary, pp. 57-68.

Fetter, C.W., 1994. Applied Hydrogeology. Maxwell Macmillan Canada, Toronto, 691 pp.

Forsyth, P.A., 1991. A control volume finite element approach to NAPL groundwater contamination. Journal of Scientific and Statistical Computing, 12(5): 1029-1057.

Forsyth, P.A. and Sammon, P.H., 1986. Practical considerations for adaptive implicit methods in reservoir simulation. Journal of Computational Physics, 62: 265-281.

Frac Rite Environmental Ltd., 1997. Horizontal Fracturing Project, [Gas Plant Remediation Site]. Document no. 97FR01, prepared for Imperial Oil Resources Ltd., November 1997.

Frank, U. and Barkley, N., 1995. Remediation of low permeability subsurface formations by fracturing enhancement of soil vapor extraction. Journal of Hazardous Materials, 40: 191-201.

Fredericia, J., 1990. Saturated hydraulic conductivity of clayey tills and the role of fractures. Nordic Hydrology, 21: 119-132.

Fredlund, D.G. and Rahardjo, H., 1993. Soil Mechanics for Unsaturated Soils. John Wiley and Sons, Toronto, 517 pp.

Fredlund, D.G. and Xing, A., 1994. Equations for the soil-water characteristic curve. Canadian Geotechnical Journal, 31: 521-532.

Fredlund, D.G., Xing, A. and Huang, S., 1994. Predicting the permeability function for unsaturated soils using the soil-water characteristic curve. Canadian Geotechnical Journal, 31: 553-546.

Freeze, R.A., 2000. The Environmental Pendulum: A Quest for the Truth About Toxic Chemicals, Human Health and Environmental Protection. University of California Press, Berkeley, 309 pp.

Freeze, R.A. and Cherry, J.A., 1979. Groundwater. Prentice-Hall, Inc., Englewood Cliffs, NJ, 604 pp.

Furbish, D.J., 1991. The response of water level in a well to a time series of atmospheric loading under confined conditions. Water Resources Research, 27(4): 557-568.

Gardner, W.H., 1986. 21: Water Content, Methods of Soil Analysis, Part I. Physical and Mineralogical Methods, Agronomy Monograph no. 9, 2nd ed., pp. 493-544.

Gelhar, L.W., 1993. Stochastic Subsurface Hydrology. Prentice Hall, Englewood Cliffs, 390 pp.

Gerber, R.E., Boyce, J.I. and Howard, K.W.F., 2001. Evaluation of heterogeneity and field-scale groundwater flow regime in a leaky till aquitard. Hydrogeology Journal, 9: 60-78.

Gerber, R.E. and Howard, K., 2000. Recharge through a regional till aquitard: three dimensional flow model water balance approach. Ground Water, 38(3): 410-422.

Gillham, R.W., 1984. The capillary fringe and its effect on water-table response. Journal of Hydrology, 67: 307-324.

Glass, D. (Editor), 1997. Lexicon of Canadian Stratigraphy Volume 4, Including Eastern British Columbia, Alberta, Saskatchewan and Southern Manitoba. Canadian Society of Petroleum Geologists, Calgary.

Golden Software Inc., 1999. Surfer 7 User's Guide. Golden Software Inc., Golden, CO.

Goovaerts, P. and Chiang, C.N., 1993. Temporal persistence of spatial patterns for minerizable nitrogen and selected soil properties. Soil Science Society of America Journal, 57: 372-381.

Grisak, G.E., 1975. The fracture porosity of glacial till. Canadian Journal of Earth Sciences, 12: 513-515.

Grisak, G.E., and Cherry, J.A., 1975. Hydrogeologic characteristics and response of fractured till and clay confining a shallow aquifer. Canadian Geotechnical Journal, 12: 23-43.

Grisak, G.E., Cherry, J.A., Vonhof, J.A., and Blumele, J.P., 1976. Hydrogeologic and hydrochemical properties of fractured till in the Interior Plains region. In: R.F. Legget (Editor), Glacial Till: An Inter-Disciplinary Study. The Royal Society of Canada Special Publication No. 12, Ottawa, pp. 304-335.

Hare, P.W. and Morse, R.E., 1997. Water-level fluctuations due to barometric pressure changes in an isolated portion of an unconfined aquifer. Ground Water, 35(4): 667-671.

Hargreaves, G.H. and Samani, Z.A., 1985. Reference crop evapotranspiration from temperature. Applied Engineering in Agriculture, 1(2): 96-99.

Harrison, B., Sudicky, E.A. and Cherry, J.A., 1992. Numerical analysis of solute migration through fractured clayey deposits into underlying aquifers. Water Resources Research, 28(2): 515-526.

Hatfield, J.L. and Allen, R.G., 1996. Evapotranspiration estimates under deficient water supplies. Journal of Irrigation and Drainage Engineering, 122(5): 301-308.

Healy, R.W. and Cook, P.G., 2002. Using groundwater levels to estimate recharge. Hydrogeology Journal, 10: 91-109.

Heath, R.C., 1988. Hydrogeologic setting of regions. In: W. Back, J.S. Rosenshein, and P.R. Seaber (Editors), Hydrogeology, v. O-2, The Geology of North America, Geological Society of America, Boulder, pp. 15-35.

Hendrickx, J.M.H., Wierenga, P.J., Nash, M.S. and Nielsen, D.R., 1986. Boundary location from texture, soil moisture and infiltration data. Soil Science Society of America Journal, 50: 1515-1520.

Hendry, M.J., 1982. Hydraulic conductivity of a glacial till in Alberta. Ground Water, 20(2): 162-169.

Hendry, M.J., 1988. Hydrogeology of clay till in a prairie region of Canada. Ground Water, 26(5): 607-614.

Hill, M.C., Cooley, R.L., and Pollock, D.W., 1998. A controlled experiment in ground water flow model calibration. Ground Water, 36(3): 520-535.

Hillel, D., 1982. Introduction to Soil Physics. Academic Press, Toronto, 364 pp.

Holter, M., 1973. Quaternary Stratigraphy of Central Alberta. Alberta Research Council Open File Report 1973-24, Edmonton, 29 pp.

Husain, M.M., Cherry, J.A., Fidler, S. and Frape, S.K., 1998. On the long term hydraulic gradient in the thick clayey aquitard in the Sarnia region, Ontario. Canadian Geotechnical Journal, 35: 986-1003.

Huyakorn, P.S. and Pinder, G.F., 1983. Computational Methods in Subsurface Flow. Academic Press, Toronto, 473 pp.

Huyakorn, P.S., Thomas, S.D., and Thompson, B.M., 1984. Techniques for making finite elements competitive in modeling flow in variably saturated porous media. Water Resources Research, 20(8): 1099-1115.

HydroSolve Inc., 1996. AQTESOLV for Windows User's Guide. HydroSolve, Inc., Reston, VA.

Ingebritsen, S.E., and Sanford, W.E., 1998. Groundwater in Geologic Processes. Cambridge University Press, Cambridge, 339 pp.

Jacob, C.E., 1940. On the flow of water in an elastic artesian aquifer. Transactions American Geophysical Union, 21: 574-586.

Jensen, M.E., Burman, R.D. and Allen, R.G., 1990. Evapotranspiration and irrigation water requirements. Engineering Practice Manual 70, American Society of Civil Engineers, New York, 332 pp.

Kachanoski, R.G. and de Jong, E., 1988. Scale dependence and the temporal persistence of spatial patterns of soil water storage. Water Resources Research, 24: 85-91.

Keller, C.K., van der Kamp, G. and Cherry, J.A., 1986. Fracture permeability and groundwater flow in clayey till near Saskatoon, Saskatchewan. Canadian Geotechnical Journal, 23: 229-240.

Keller, C.K., van der Kamp, G. and Cherry, J.A., 1988. Hydrogeology of two Saskatchewan tills, I. Fractures, bulk permeability and spatial variability of downward flow. Journal of Hydrology, 101: 97-121.

Keller, C.K., van der Kamp, G. and Cherry, J.A., 1989. A multiscale study of the permeability of a thick clayey till. Water Resources Research, 25(11): 2299-2317.

Kitanidis, P., 1997. Introduction to Geostatistics – Applications in Hydrogeology. Cambridge University Press, Cambridge, 249 pp.

Kite, G.W., and Droogers, P., 2000. Comparing evapotranspiration estimates from satellites, hydrological models and field data. Journal of Hydrology, 229: 3-18.

Komex International Ltd., 2000a. Site Characterization and Piezometer Installation Program: [Gas Plant Remediation Site]. Report to Imperial Oil Resources, April 2000, C45790400.

Komex International Ltd., 2000b. Enhanced Bioventing of Alkanolamine/Glycol Contamination Using Hydraulic Fractures. Report to Imperial Oil Resources, April 2000, C45790401.

Komex International Ltd., 2000c. Soil and Groundwater Investigation at [Gas Plant Remediation Site]. Report to Imperial Oil Resources, October 2000, C45790501.

Komex International Ltd., 2002. 2001 Soil Quality Investigation at [Gas Plant Remediation Site]. Report to Imperial Oil Resources, April 2002, C45790607.

Konikow, L.F., and Bredehoeft, J.D., 1992. Ground-water models cannot be validated. Advances in Water Resources, 15: 75-83.

Kruseman, G.P., and de Ridder, N.A., 1990. Analysis and Evaluation of Pumping Test Data, 2nd ed. Publication 47, International Institute for Land Reclamation and Improvement, Wageningen, 377 pp.

Lennox, D.H., Maathuis, H. and Pederson, D., 1988. Region 13, Western Glaciated Plains. In: W. Back, J.S. Rosenhein and P.R. Seaber (Editors), The Geology of North America: Hydrogeology. Geological Society of America, Boulder, CO, pp. 115-128.

Lerner, D.N., Issar, A.S. and Simmers, I. (Editors), 1990. Groundwater recharge: A guide to understanding and estimating natural recharge. International Contributions to Hydrogeology, 8. Verlag Heinz Heise, Hannover, 345 pp.

Lide, D.R. (Editor), 1999. CRC Handbook of Chemistry and Physics. CRC Press, New York.

McAneney, K.J. and Itier, B., 1996. Operational limits to the Priestley-Taylor formula. Irrigation Science, 17: 37-43.

McKay, L.D., Cherry, J.A. and Gillham, R.W., 1993. Field experiments in fractured clay till 1. Hydraulic conductivity and fracture aperture. Water Resources Research, 29(4): 1149-1162.

Meyboom, P., 1966. Unsteady groundwater flow near a willow ring in hummocky moraine. Journal of Hydrology, 4: 38-62.

Mrklas, O., 2002. Ethanolamine and Glycol Biodegradation: From Detection to Remediation. Ph.D. thesis, University of Calgary.

Mrklas, O., Lunn, S., and Chu, A., 2001. Laboratory investigations of aerobic and anaerobic monoethanolamine biodegradation. In: Proceedings of the 2nd Joint CGS-IAH Groundwater Specialty Conference, Calgary, pp. 1194-1200.

Nyer, E.K., 1996. Practical remediation technologies. Ground Water Monitoring and Remediation (Fall 1996): 54-57.

Parlange, M.B., and Katul, G.G., 1992. Estimation of diurnal variation of potential evaporation from a wet bare soil surface. Journal of Hydrology, 132: 71-89.

Pawluk, S., and Bayrock, L.A., 1969. Some characteristics and physical properties of Alberta tills. Bulletin 26, Research Council of Alberta, Edmonton, 72 pp.

Penman, H.L., 1948. Natural evaporation from open water, bare soil and grass. Proceedings of the Royal Society of London, A193: 120-146.

Pettapiece, W.W., 1986. Physiographic Subdivisions of Alberta. Agriculture Canada, Ottawa, map, scale 1: 1 500 000.

Poeter, E.P. and Hill, M.C., 1996. Unrealistic parameter estimates in inverse modelling: a problem or a benefit for model calibration? In: K. Kovar and P. Van der Heijde (Editors), Calibration and Reliability in Groundwater Modelling. International Association of Hydrological Sciences Publication No. 237, Oxfordshire, pp. 277-285.

Priestley, C.H.B. and Taylor, R.J., 1972. On the assessment of surface heat flux and evaporation using large-scale parameters. Monthly Weather Review, 100: 81-92.

Prothero, D.R., and Schwab, F., 1996. Sedimentary Geology. W.H. Freeman and Company, New York, 575 pp.

Pupp, C., Stein, R., and Grove, G., 1989. Groundwater Quality in Alberta: Hydrogeology, Quality Concerns, Management. National Hydrology Research Institute Contribution No. 89051, Saskatoon, 113 pp.

Rasmussen, T.C. and Crawford, L.A., 1997. Identifying and removing barometric pressure effects in confined and unconfined aquifers. Ground Water, 35(3): 502-511.

Remenda, V.H., van der Kamp, G., and Cherry, J.A., 1996. Use of vertical profiles of $\delta^{18}O$ to constrain estimates of hydraulic conductivity in a thick, unfractured aquitard. Water Resources Research, 32: 2979-2987.

Reynolds, W.D. and Elrick, D.E., 1986. A method for simultaneous measurement in the vadose zone of field-saturated hydraulic conductivity, sorptivity and the conductivity-pressure head relationship. Ground Water Monitoring Review (Winter 1986): 84-95.

Rodvang, S.J. and Simpkins, W.W., 2001. Agricultural contaminants in Quaternary aquitards: A review of occurrence and fate in North America. Hydrogeology Journal, 9: 44-59.

Rowe, R.K. and Booker, J.R., 1990. Contaminant migration through fractured till into an underlying aquifer. Canadian Geotechnical Journal, 27: 484-495.

Rudolph, D.L., Cherry, J.A., and Farvolden, R.N., 1991. Groundwater flow and solute transport in fractured lacustrine clay near Mexico City. Water Resources Research, 27: 2187-2201.

Ruland, W.W., Cherry, J.A. and Feenstra, S., 1991. The depth of fractures and active ground-water flow in a clayey till plain in southwestern Ontario. Ground Water, 29(3): 405-417.

Sanford, W., 2002. Recharge and groundwater models: an overview. Hydrogeology Journal, 10: 110-120.

Scanlon, B.R., Healy, R.W. and Cook, P.G., 2002. Choosing appropriate techniques for quantifying groundwater recharge. Hydrogeology Journal, 10: 18-39.

Schwartz, F.W., Crowe, A.S., Hendry, M.J., and Chorley, D.W., 1987. A case study to assess the potential for saline soil development due to irrigation. Journal of Hydrology, 91: 1-27.

Shaver, R.B., 1998. The determination of glacial till specific storage in North Dakota. Ground Water, 36(4): 552-557.

Shaw, R.J. and Hendry, M.J., 1998. Hydrogeology of a thick clay till and Cretaceous clay sequence, Saskatchewan, Canada. Canadian Geotechnical Journal, 35: 1041-1052.

Shetsen, I., 1990. Quaternary geology of central Alberta. Alberta Research Council, Edmonton, map, scale 1: 500 000.

Simpkins, W.W., and Bradbury, K.R., 1992. Groundwater flow, velocity, and age in a thick, fine-grained till unit in southeastern Wisconsin. Journal of Hydrology, 132: 283-319.

SoilCover, 1997. SoilCover User's Manual – Version 4.0. Unsaturated Soils Group, University of Saskatchewan, Saskatoon.

Soil Moisture Equipment Corporation. Operating instructions for the cat. no. 1600 5 Bar Pressure Plate Extractor, Santa Barbara, CA.

Sorensen, J.A., Gallagher, J.R., Chollak, D. and Harju, J.A., 1999. Remediation strategies for soils contaminated with amine-based gas sweetening wastes. In: SPE/EPA Exploration and Production Environmental Conference. Society of Petroleum Engineers, Inc., Austin, Texas.

Sorensen, J.A., Hawthorne, S.B., Gallagher, J.R., Thompson. J.S., and Harju, J.A., 1997. Assessment of the subsurface environmental fate of amines used by the gas industry. In: SPE/EPA Exploration and Production Environmental Conference. Society of Petroleum Engineers, Inc., Dallas, Texas.

Steiner, J.L., Howell, T.A., and Schneider, A.D., 1991. Lysimetric evaluation of daily potential evapotranspiration models for grain sorghum. Agronomy Journal, 83: 240-247.

Sudicky, E.A., and McLaren, R.G., 1992. The Laplace transform Galerkin technique for large-scale simulation of mass transport in discretely-fractured porous formations. Water Resources Research, 28(2): 499-514.

Suthersan, S.S., 1997. Remediation Engineering: Design Concepts. CRC Press Inc., Boca Raton, 384 pp.

Therrien, R. and Sudicky, E.A., 1996. Three-dimensional analysis of variably-saturated flow and solute transport in discretely-fractured porous media. Journal of Contaminant Hydrology, 23: 1-44.

Therrien, R., Sudicky, E.A., and McLaren, R.G., 2001a. FRAC3DVS Input/Output User's Guide. Groundwater Simulations Group, Waterloo, 79 pp.

Therrien, R., Sudicky, E.A., and McLaren, R.G., 2001b. FRAC3DVS Mathematical Theory and Verification. Groundwater Simulations Group, Waterloo, 32 pp.

Therrien, R., Sudicky, E.A. and McLaren, R.G., 2001c. FRAC3DVS Version 4b. Groundwater Simulations Group, Waterloo.

Therrien, R., Sudicky, E.A. and McLaren, R.G., 2001d. NP Version 4b. Groundwater Simulations Group, Waterloo.

Thomas, D., 1999. Characterization of water fluxes at a trench and gate groundwater remediation site. Master of Science thesis, University of Calgary.

Tindall, J.A. and Kunkel, J.R., 1999. Unsaturated Zone Hydrology for Scientists and Engineers. Prentice-Hall, Inc., Upper Saddle River, 624 pp.

Tokarsky, O., 1971. Hydrogeology of the Rocky Mountain House Area, Alberta. 71-3, Research Council of Alberta, Edmonton.

van der Kamp, G., 2001. Methods for determining the in situ hydraulic conductivity of shallow aquitards- an overview. Hydrogeology Journal, 9: 5-16.

van der Kamp, G., and Keller, C.K., 1993. Casing leakage in monitoring wells: detection, confirmation and prevention. Ground Water Monitoring and Remediation, 13: 136-141.

van Genuchten, M.T., 1980. A closed-form equation for predicting the hydraulic conductivity of unsaturated soils. Soil Science Society of America Journal, 44: 892-898.

Van Pelt, R.S. and Wierenga, P.J., 2001. Temporal stability of spatially measured soil matric potential probability density function. Soil Science Society of America Journal, 65: 668-677.

Ward, C.H., Cherry, J.A., and Scalf, M.R. (Editors), 1997. Subsurface Restoration. Sleeping Bear Press Inc., Chelsea, 500 pp.

Weeks, E.P., 1979. Barometric fluctuations in wells tapping deep unconfined aquifers. Water Resources Research, 15(5): 1167-1176.

White, J.C., 1997. Soil characterization and evaporation estimates at a groundwater remediation site in southwestern Alberta, Canada. Bachelor of Science thesis, Department of Geology and Geophysics, University of Calgary.

Williams, R.E., and Farvolden, R.N., 1967. The influence of joints on the movement of groundwater through glacial till. Journal of Hydrology, 5: 163-170.

Wilson, G.W., Fredlund, D.G. and Barbour, S.L., 1994. Coupled soil-atmosphere modelling for soil evaporation. Canadian Geotechnical Journal, 31: 151-161.

Wong, R.C.K. and Alfaro, M.C., 2001. Fracturing in low-permeability soils for remediation of contaminated ground. Canadian Geotechnical Journal, 38: 316-327.

Wright, J.L., 1982. New evapotranspiration crop coefficients. Journal of Irrigation and Drainage Division, ASCE, 108: 57-74.

Wright, J.L., 1996. Derivation of alfalfa and grass reference evapotranspiration. In: C.R. Camp, E.J. Sadler and R.E. Yoder (Editors), Evapotranspiration and Irrigation Scheduling. ASAE, San Antonio, pp. 133-140.

Zaltsberg, E., 1985. Estimation of hydrogeologic parameters and groundwater-balance components based on fluctuations in the water table. Canadian Journal of Earth Sciences, 22: 1803-1812.

Page 189 has been removed because Appendix A, Collected Data and Model Input Files, will not be included with the microfilmed copy of the thesis. Data can be obtained from the author or his supervisor:

- Trevor Butterfield: butter@darcy.eas.ualberta.ca
- Dr. Carl Mendoza: carl.mendoza@ualberta.ca

APPENDIX B

EVAPOTRANSPIRATION CALCULATION METHODS

B.1 Reference Evapotranspiration Calculation Methods

Based on the results of an expert consultation in May 1990, the Food and Agriculture Organization of the United Nations' Penman-Monteith (FAO-56 PM) method is the sole recommended method for calculating ET_o (Allen et al. 1998). For this study, ET_o was calculated and compared for four methods, although only the ET_o from the FAO-56 PM method was used to calculate ET_c.

In the FAO-56 PM method, ET_o is the evapotranspiration that occurs under given meteorological conditions for a standardized reference crop. This allows determination of the evaporative demand of the atmosphere without referring to crop type or management practices (Allen et al. 1998). Thus, ET_o can be compared among sites and between seasons because it refers to the same reference surface (Jensen et al. 1990). A specific crop was chosen as a reference surface over a free water surface because it incorporates the biological and physical processes involved in evapotranspiration from cropped surfaces. The properties of the reference surface are (Allen et al. 1998):

- Extensive surface of well-watered, actively growing, green grass that completely shades the ground;
- Assumed crop height of 0.12 m;
- Fixed surface resistance of 70 s/m. Implies a moderately dry surface resulting from weekly irrigation frequency; and
- Albedo of 0.23.

B.1.1 Temperature-Based Method

The temperature-based method chosen to calculate ET_o was the empirical Hargreaves (1985) method. This method is the sole temperature-based method that has shown reasonable ET_o results with a global validity (Allen et al. 1998):

$$ET_o = 0.0023(T_{max} - T_{min})^{0.5}(T_{mean} + 17.8)R_a \quad \text{(B-1)}$$

where T_{max} is the maximum daily air temperature (°C), T_{min} is the minimum daily air temperature (°C), T_{mean} is the mean daily air temperature ($(T_{max}+ T_{min})/2$, °C), and R_a is extraterrestrial radiation (mm/d):

$$R_a = \frac{24\,(60)}{\pi} G_{sc} d_r [\omega_s \sin(\gamma)\sin(\delta) + \cos(\gamma)\cos(\delta)\sin(\omega_s)] \quad \text{(B-2)}$$

where G_{sc} is the solar constant (8.2×10^{-2} MJ/m^2/d), d_r is the inverse relative distance Earth-Sun, ω_s is the sunset hour angle (rad), γ is the latitude (rad), and δ is the solar declination (rad). To calculate d_r, ω_s, and δ:

$$d_r = 1 + 0.033 \cos\left(\frac{2\pi}{365} J\right) \quad \text{(B-3)}$$

$$\omega_s = \frac{\pi}{2} - \arccos[-\tan(\gamma)\tan(\delta)] \quad \text{(B-4)}$$

$$\delta = 0.4093 \sin\left(\frac{2\pi}{365} J - 1.39\right) \quad \text{(B-5)}$$

where J is the number of the day in the year, i.e. the Julian day (1-365 or 366).

B.1.2 Radiation-Based Method

The radiation-based method chosen to calculate ET_o was the semi-empirical Priestley-Taylor (1972) method. The method has produced reasonable results in humid regions (McAneney and Itier 1996):

$$ET_o = 1.26 \frac{\Delta}{\Delta + \gamma} \frac{R_n - G}{\lambda} \tag{B-6}$$

where Δ is the slope of the vapour pressure curve (kPa/°C), γ is the psychrometric constant (kPa/°C), R_n is the net radiation (MJ/m^2/d), G is the soil heat flux density (MJ/m^2/d), and λ is the latent heat of vaporization (MJ/kg).

B.1.3 Penman-Combination Methods

The Penman-combination methods are based on the original derivation by Penman (1948). Two methods were chosen to examine how ET_o might vary within the same category. The two methods chosen were the FAO-56 PM method (Allen et al. 1998), the recommended method, and the Kimberly-Penman method (Wright 1982), which was chosen to show how ET_o might vary with a different wind function. The original Penman (1948) equation is:

$$ET_o = \left(\frac{\Delta}{\Delta + \gamma} (R_n - G) + K_w \frac{\gamma}{\Delta + \gamma} (a_w + b_w u_2)(e_s - e_a) \right) / \lambda \tag{B-7}$$

where K_w is a unit constant (6.43 mm/d or 0.268 mm/hr), a_w and b_w are empirical wind coefficients (a_w = 1.0 and b_w = 0.537), u_2 is the wind speed at 2 m (m/s), e_s is the saturation vapour pressure (kPa), and e_a is the actual vapour pressure (kPa). All other variables are as defined in equation B-6. The FAO-56 PM equation (Allen et al. 1998) is:

$$ET_o = \frac{0.408\,\Delta(R_n - G) + \gamma \frac{900}{T+273} u_2 (e_s - e_a)}{\Delta + \gamma(1 + 0.34\,u_2)} \quad \text{(B-8)}$$

where T is the mean daily air temperature at 2 m height (°C). All other variables are as defined in equations B-6 and B-7. The Kimberly-Penman method (Wright 1982) uses the original form of the Penman (1948) equation (Equation B-7) with wind coefficients for grass that vary with the time of year. The method originally used an alfalfa reference crop, but was subsequently modified to a grass reference crop (Wright 1996):

$$a_w = 0.3 + 0.58 \exp\left(\left[-\left(\frac{J-170}{45}\right)^2\right]\right) \quad \text{(B-9)}$$

$$b_w = 0.32 + 0.54 \exp\left(\left[-\left(\frac{J-170}{45}\right)^2\right]\right) \quad \text{(B-10)}$$

where J is the Julian day (1-365 or 366).

All ET_o calculations were performed with the REF-ET Reference Evapotranspiration Calculator Version 2.0 for Windows (Allen 2000a). REF-ET can calculate ET_o for the methods outlined by Jensen et al. (1990) and Allen et al. (1998), which encompass the methods used for this study.

Daily meteorological data from April 1 to September 30, 2000 were imported into REF-ET in ASCII format from existing, formatted spreadsheets. Other data were input manually or were calculated within REF-ET from the user-supplied data. These included:

- Latitude, input as 53.5°N for the calculation of R_a in the Hargreaves (1985) method;
- Net radiation, estimated from solar radiation as follows (Allen et al. 1998):

$$R_n = R_{ns} - R_{nl} \tag{B-11}$$

where R_n is the net radiation, R_{ns} is the incoming net shortwave radiation and R_{nl} is the outgoing net longwave radiation (all in $MJ/m^2/d$). R_{ns} is expressed as:

$$R_{ns} = (1-\alpha)R_s \tag{B-12}$$

where α is the albedo (0.23 for FAO-56 PM) and R_s is the incoming solar radiation ($MJ/m^2/d$). R_{nl} is calculated by:

$$R_{nl} = \sigma\left[\frac{T_{max}^{\ 4} + T_{min}^{\ 4}}{2}\right](0.34 - 0.14\sqrt{e_a})\left(1.35\frac{R_s}{R_{so}} - 0.35\right) \tag{B-13}$$

where σ is the Stefan-Boltzmann constant (4.9×10^{-9} $MJ/K^4/m^2/d$), T_{max} is the maximum absolute temperature in the 24 hour period (K), T_{min} is the minimum absolute temperature in the 24 hour period (K), e_a is the actual vapour pressure (kPa), and R_{so} is the calculated clear-sky radiation ($MJ/m^2/d$). For the Kimberly Penman method, R_n is calculated with a variable albedo and other variable coefficients (Wright 1982);

- The magnitude of the soil heat flux under a fully vegetated surface is small over long periods (Allen et al. 1998). Therefore, G was taken as 0 in the FAO-56 PM and Priestley-Taylor calculations. In the Kimberly Penman method, the soil heat flux is measured from changes in daily air temperature and a soil specific heat coefficient (Wright 1982);

- All other data can be derived from the user-input values. The reader is referred to Allen (2000a) for details.

B.2 Actual Evapotranspiration Calculation Methods

B.2.1 Crop Coefficient Method

Step 1: Selection of Single or Dual Crop Coefficient Method

The dual crop coefficient method was chosen over the single crop coefficient method because it results in ET_c calculations that better reflect day-to-day variations in surface wetness, whereas the single crop coefficient method expresses only a time-averaged ET_c (Allen et al. 1998). The dual crop coefficient approach describes the effects of transpiration (K_{cb}) and evaporation (K_e) (Equation 4-2) separately.

There are essentially three properties of vegetation which influence transpiration, and hence the value of K_{cb} (Allen et al. 1998):

- Crop height, which influences aerodynamic resistance and the turbulent transfer of vapour to the atmosphere;
- Albedo, determined by the fraction of vegetation covering the ground and the wetness of the vegetation, which influences the amount of energy available for transpiration; and
- Canopy resistance, affected by leaf area, age and condition, which influences the surface resistance.

Evaporation, and the value of K_e, depends on the availability of water at the soil surface. When water is readily available, evaporation occurs at the potential rate. When water is not readily available, soil factors become more important.

Three stages have been described for the evaporation of water from soil based on the availability of water (Hillel 1982, Wilson et al. 1994):

- Stage I drying, where the soil surface is at or near saturation and evaporation is determined by climatic conditions;
- Stage II drying, where the soil moisture content is reduced and evaporation is determined by both the conductive properties of the soil and climatic conditions; and
- Stage III drying, where soil moisture distribution becomes discontinuous and evaporation is a diffusive process.

Step 2: Selection of vegetation and growth stage lengths

The selection of representative vegetation for the GPRS was difficult because over 20 herbaceous and tree species have been identified on-site (C. Vanwyngaarden, University of Calgary, pers.com.) and their spatial distributions have not been mapped. Also, most documented empirical crop coefficients are for agricultural crops, not for natural or non-pristine vegetation. Foxtail barley was chosen as the representative site vegetation because there was information available on general growing stages and crop coefficients in Allen et al. (1998).

Step 3: Construct locally adjusted K_{cb} curves

Although information on K_{cb} for initial stage, mid-season and end of season was available in the literature for foxtail barley, several adjustments were made to the K_{cb} values to take into account local conditions. In general, a reduction of the K_{cb} in comparison to cropped situations was expected because natural vegetation is not likely to have as much leaf area or be covering as much of the ground as planted crops (Allen et al. 1998). Adjustments were also made to K_{cb} values based on differences in climate from the reference "subhumid" climate with a minimum daily relative humidity of 45% and a mean daily windspeed of 2 m/s.

More humid climates and lower values of windspeed reduce the crop coefficient (Allen et al. 1998).

Therefore, the estimates for K_{cb} for foxtail barley throughout the 2000 field season were as follows:

- $K_{cb\ ini}$, the basal crop coefficient at the start of the growing season (April), was taken to be 0, meaning that initially there is no transpiration component to ET_c;
- $K_{cb\ mid}$, the basal crop coefficient while the crop is developing, was estimated based on the approximated height and fraction of ground covered by the foxtail barley:

$$K_{cb\ mid} = K_{cb,\ h}\, fh \qquad \text{(B-14)}$$

where $K_{cb,\ h}$ is the basal crop coefficient determined for non-pristine vegetation based on it's height, h ($K_{cb,\ h}$ = 1.0 + 0.1h) and f is the fraction of ground covered by the vegetation (Allen et al. 1998); and

- $K_{cb\ end}$, the basal crop coefficient near plant harvest or senescence, was estimated to be 0.25 based on the suggested value (Doorenbos and Pruitt 1977).

Step 4: Determine daily K_e values for evaporation

K_e is determined as the minimum of two expressions (Allen et al. 1998):

$$K_e = K_r(K_{c\,max} - K_{cb}) \leq f_{ew} K_{c\,max} \qquad \text{(B-15)}$$

where K_e and K_{cb} are as previously defined, K_r is the evaporation reduction coefficient, which depends on the cumulative amount of water evaporated from the topsoil, $K_{c\ max}$ is the maximum value of K_c, which is determined by energy

available at the surface, and f_{ew} is the fraction of soil exposed and wetted, from which most evaporation occurs. $K_{c\,max}$ may be expressed by (Allen et al. 1998):

$$K_{c\,max} = \max\left(\left\{ 1.2 + [0.04(u_2 - 2) - 0.004(RH_{min} - 45)] \left(\frac{h}{3} \right)^{0.3} \right\}, \{K_{cb} + 0.05\} \right) \quad \text{(B-16)}$$

where RH_{min} is the minimum daily relative humidity (%), h is the mean maximum plant height during any stage of the season (m) and all other variables are as defined before. This equation suggests that K_{cb} may be expected to increase by 0.05 following a wetting event. The 1.2 factor in the equation represents increased aerodynamic roughness during growth and reduced albedo due to soil wetting, which both increase evaporation (Allen et al. 1998).

K_r, which determines the stage of drying during evaporation, may be expressed by two equations depending on the evaporable water available in the soil (Allen et al. 1998):

$$K_r = 1, \text{ when } D_{e,i-1} \leq REW \quad \text{(B-17)}$$

and

$$K_r = \frac{TEW - D_{e,i-1}}{TEW - REW}, \text{ when } D_{e,i-1} > REW \quad \text{(B-18)}$$

where $D_{e,\,i-1}$ is the cumulative depth of evaporation at the end of the previous day (mm), REW (readily evaporable water) is the cumulative depth of evaporation at the end of stage 1 drying (mm) and TEW (total evaporable water) is the maximum depth of evaporation from the soil surface (mm). REW and TEW can be estimated based on the soil texture classification (Allen et al. 1998):

$$TEW = 1000\,(\theta_{FC} - 0.5\theta_{WP})Z_e \quad \text{(B-19)}$$

where θ_{FC} is the volumetric soil moisture content at field capacity, θ_{WP} is the volumetric soil moisture content at the wilting point, and Z_e is the depth of soil that is subject to drying by evaporation (generally 0.1 m to 0.15 m). Because soil at the GPRS is composed of approximately 70% silt and clay (Wong and Alfaro 2001), it was classified as silt loam with the following ranges for evaporation properties (Table B-1) (Allen et al. 1998):

Parameter	θ_{FC} (m^3/m^3)	θ_{WP} (m^3/m^3)	REW (mm)	TEW (mm)
Value	0.22-0.36	0.09-0.21	8-11	18-25

Table B-1 Soil water evaporation characteristics for silt loam.

The value of f_{ew} may be represented by (Allen et al. 1998):

$$f_{ew} = \min(1 - f_c, f_w) \tag{B-20}$$

where $1\text{-}f_c$ represents average soil fraction not covered by vegetation and f_w represents the soil fraction wetted by irrigation or precipitation. At the GPRS, there was no irrigation and f_w for precipitation was assumed to be 1. f_c was estimated based on elapsed time from the beginning of the field season in April 2000 and ranged from 0.1 to 0.5.

To complete the calculation of K_r, a daily water balance calculation must be made to find the cumulative depth of evaporation for the day (Allen et al. 1998):

$$D_{e,i} = D_{e,i-1} - (P_i - RO_i) - \frac{I_i}{f_w} + \frac{E_i}{f_{ew}} + T_{ew,i} + DP_{e,i} \tag{B-21}$$

where $D_{e,\,i}$ is the cumulative depth of evaporation following wetting on day i (mm), P_i is the precipitation on day i (mm), RO_i is the runoff on day i (mm), I_i is the irrigation depth on day i (mm), E_i is the evaporation on day i (i.e., $E_i = K_e ET_o$)

(mm), $T_{ew,\,i}$ is the depth of transpiration from the exposed and wetted fraction of the soil surface (mm), and $DP_{e,\,i}$ is the deep percolation loss from the topsoil layer on day i (mm).

To simplify the calculations, several assumptions were made. I_i was known to be 0. RO_i and $DP_{e,\,i}$ are probably not 0, but were assumed to be based on lack of information to the contrary. $T_{ew,\,i}$ is normally 0 except for very shallow rooted crops and was assumed to be 0 in this study.

Step 5: Calculate K_c and ET_c

Once all the components have been calculated as outlined in the above steps, Equations 4-1 and 4-2 can calculate K_c and ET_c. ET_c was determined for bare soil and foxtail barley conditions for the period of April 1 to September 30, 2000.